Universidade de Aveiro
Departamento de Electrónica, Telecomunicações e Informática,
2016

Tiago Miguel Valente Varum

Agregados 2D de Antenas Microstrip não Uniformes para Aplicações Sem Fios

Nonuniform 2D Microstrip Antenna Arrays for Wireless Applications

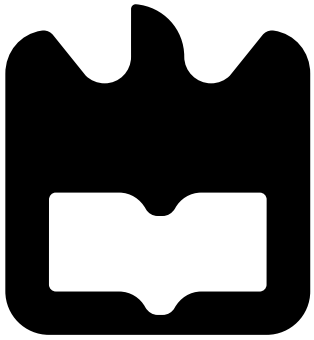

Universidade de Aveiro
Departamento de Electrónica, Telecomunicações e Informática,
2016

Tiago Miguel Valente Varum

Agregados 2D de Antenas Microstrip Não Uniformes para Aplicações Sem Fios

Nonuniform 2D Microstrip Antenna Arrays for Wireless Applications

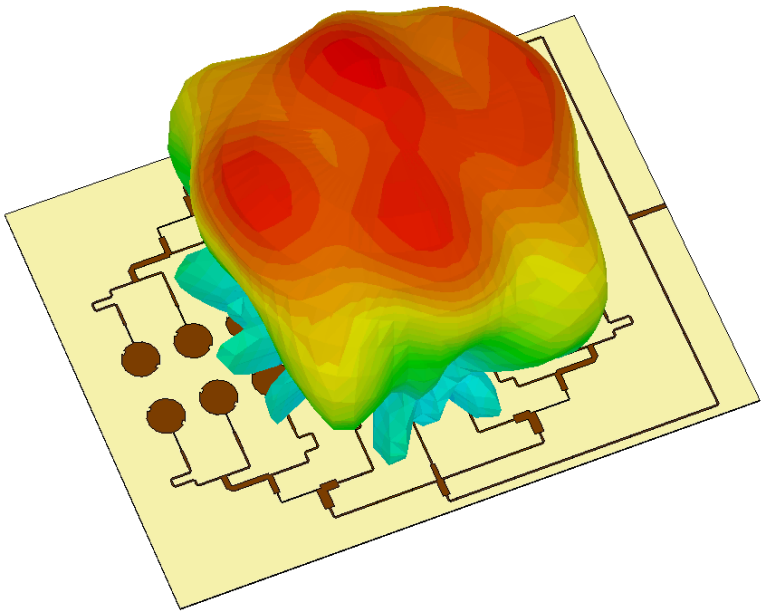

Tiago Miguel Valente Varum

Agregados 2D de Antenas Microstrip Não Uniformes para Aplicações Sem Fios

Nonuniform 2D Microstrip Antenna Arrays for Wireless Applications

Tese apresentada à Universidade de Aveiro para cumprimento dos requisitos necessários à obtenção do grau de Doutor em Engenharia Electrotécnica, realizada sob a orientação científica do Professor Doutor João Nuno Pimentel da Silva Matos, Professor Associado do Departamento de Electrónica, Telecomunicações e Informática da Universidade de Aveiro e do Professor Pedro Renato Tavares Pinho, Professor Adjunto no Departamento de Engenharia de Electrónica e Telecomunicações e de Computadores do Instituto Superior de Engenharia de Lisboa.

Dedico este trabalho à minha irmã, e à minha mãe, pela exemplo e força que sempre me demonstraram, e pelo incondicional e incansável apoio.

"Believe in yourself and there will come a day when others will have no choice but to believe with you."
(Cynthia Kersey)

o júri / the jury

presidente / president

Doutor Vitor José Babau Torres
Professor Catedrático da Universidade de Aveiro

vogais / examiners committee

Doutor Glauco Fontgalland
Professor Catedrático da Universidade Federal de Campina Grande, Brasil

Doutor Nuno Miguel Gonçalves Borges de Carvalho
Professor Catedrático da Universidade de Aveiro

Doutor Rafael Ferreira da Silva Caldeirinha
Professor Coordenador da Escola Superior de Tecnologia e Gestão de Leiria

Doutor Henrique Manuel de Castro Faria Salgado
Professor Associado da Faculdade de Engenharia da Universidade do Porto

Doutor João Nuno Pimentel Silva Matos
Professor Associado da Universidade de Aveiro (orientador)

agradecimentos / acknowledgements

Em primeiro lugar gostaria de agradecer, na pessoa da mais jovem da família, a Maria Leonor, a toda minha família começando pelos meus pais, pelo exemplo, preocupação, e paciência em todo o percurso da minha vida que me conduziu até aqui.

Em segundo lugar, e também muito importante para aqui chegar, aos meus orientadores. O professor João N. Matos e o professor Pedro Pinho foram fundamentais, mantendo-me motivado nos momentos mais desanimadores, procurando sempre ajudar-me na melhor condução deste percurso. Agradeço-lhes a paciência, a partilha de conhecimento, e por sempre acreditarem em mim.

Gostaria igualmente de agradecer à Universidade de Aveiro, Departamento de Electrónica, Telecomunicações e Informática, e principalmente um enorme agradecimento ao Instituto de Telecomunicações, que ao longo destes anos me acolheu, me proporcionou as melhores condições que um aluno de doutoramento pode ter, os melhores apoios técnicos, os melhores serviços, um enorme muito obrigado.

A todos os meus companheiros e amigos, principalmente no grupo de radio systems, com os quais convivi ao longo destes anos pela amizade, pela partilha, pela motivação.

Nas pessoas do João e do Ruben, gostaria de agradecer a todos os meus amigos, que sempre me motivaram, sempre se orgulharam de mim, sempre me deram força. Ao Wall Street English de Aveiro, na pessoa da professora Iolanda, agradeço toda a amizade e ensino.

palavras-chave

Antenas Microstrip, Agregado Planar de Antenas, Agregados Não Uniformes, Comunicações Dedicadas de Curto Alcance, Comunicações Sem-Fios em Espaços Desportivos, Antenas Inteligentes

Resumo

As comunicações sem fios têm sofrido, ao longo das ultimas décadas, um enorme progresso em consequência do aumento exponencial da procura de dispositivos móveis, estando hoje em dia cada vez mais presentes na vida das pessoas. Esta presença reflete-se através do uso de um elevado número de aplicações das quais se tornam cada vez mais dependentes.

As antenas, nas suas mais diversificadas formas, são elementos cruciais no estabelecimento deste tipo de comunicações. Cada aplicação envolve um conjunto de características específicas, pelo que a melhoria das comunicações sem fios está relacionada com a adequação da antena usada.

Muitas aplicações necessitam de antenas com diagramas de radiação com formatos próprios (em termos de larguras de feixe, níveis de lobos secundários, direção, etc..), sejam eles estáticos ou dinâmicos (antenas adaptativas), implicando na maioria dos casos o uso de agregados de antenas para fazer face a tais condições.

Nesta tese são abordadas várias técnicas de desenho de antenas constituídas por agregados planares, com alimentação não uniforme dos seus elementos. Um conjunto de algoritmos de estimação dos ângulos de chegada e de formação de feixe são também apresentados e analisados com vista à sua aplicação em agregados de antenas adaptativas, com formação de feixe dinâmico. Um vasto e diversificado conjunto de agregados com diferentes requisitos de radiação, destinados a diferentes aplicações foram desenvolvidos. Estes agregados têm grande aplicabilidade nos atuais tópicos de investigação em antenas, tais como as comunicações veiculares, Wi-Fi em espaços desportivos e *smart* antenas.

keywords

Microstrip Antennas, Planar Antenna Array, Nonuniform Arrays, Dedicated Short Range Communications, Wi-Fi in Sports Arenas, Smart Antennas

Abstract

Wireless communications have undergone over the last decades a tremendous progress as a consequence of the exponential growth in demand for mobile devices, and nowadays are more and more involved in people's lives. This presence is reflected through the use of a large number of applications of which they become increasingly dependent on.

The antenna, in its most different forms, are crucial elements in the establishment this type of communication. Each application involves a number of specific characteristics, whereby, the improvement of wireless communications is related to the appropriateness of the used antenna.

Many applications require antennas with radiation pattern with its particular shapes (in terms of beamwidth, side lobes levels, direction, etc ..), static or dynamic (adaptive antennas), involving in most cases the use antenna arrays to meet to such constraints.

In this thesis, a number of techniques to synthesize antennas consisting of planar arrays with nonuniform excitation of their elements, are addressed. A group of the direction of arrival and beamforming estimation algorithms are also presented and analyzed, in order to enable their application in adaptive antenna array with dynamic beamforming. A vast and diversified set of arrays with different radiation requirements, and for different applications were developed. These arrays have great applicability in current research topics in antennas, such as vehicle communications, Wi-Fi in sports venues and smart antennas.

Table of Contents

List of Figures

List of Tables

List of Acronyms

AF Array Factor

AFN Array Feed Network

AP Access Point

AR Axial Ratio

BST Barium Strontium Titanate

CEN Comité Européen de Normalisation / European Committee for Standardization

DSP Digital Signal Processor

DSRC Dedicated Short Range Communications

EIRP Effective Isotropic Radiated Power

ETC Electronic Toll Collection

FDTD Finite Difference Time Domain

FEM Finite Element Method

FNBW First Null Beam Width

FTM Fourier Transform Method

GPS Global Positioning System

GSC Generalized Sidelobe Canceller

HPBW Half Power Beam Width

ISM Industrial, Scientific and Medical

ITS Intelligent Transport Systems

LAN Local Area Network

LCMV Linearly Constrained Minimum Variance

LHCP Left Hand Circular Polarization

LMS Least Mean Square

MMIC monolithic microwave integrated circuit

MEMS micro-electromechanical systems

MoM Method of Moments

MSC Multiple Side Lobe Canceller

OBU On Board Unit

PS Phase Shifter

RHCP Right Hand Circular Polarization

RLS Recursive Least Squares

RSU Road Side Unit

RTTT Road Transport and Traffic Telematics

SLL Side Lobe Level

SNR Signal-to-Noise Ratio

SOI Signal-Of-Interest

SNOI Signal-Not-Of-Interest

V2I Vehicle-to-Infrastructure

V2V Vehicle-to-Vehicle

WLAN Wireless Local Area Network

Chapter 1

Introduction

1.1 Motivation

Maxwell (1831-1879), H. Hertz (1857-1894), and Marconi (1874-1937) played a key role in the idealization and conception of what revolutionized worldwide communications, the wireless communications. Since then and principally in recent decades, these communications keep on with great development, and widely deployed in people's lives.

These communications avoid, as a main benefit, the unnecessary use of wires to its establishment, since the electromagnetic waves are propagated in the free space, providing a greater flexibility and mobility regarding the wired communications. In addition, a larger coverage of communications is allowed at a lower cost than using cable connections, reaching rural areas, remote places on the planet, or even some locations in space.

We look around us today and wireless communications are widespread, almost present everywhere, and people in many situations already depend on them and on the infinitude of applications that they provide.

The main challenges of the wireless communications are related to the fading of the signal, due to the multipath fading effects, path loss attenuation, or shadowing by obstacles. Another challenge is the interference provided by the unguided communication medium, between transmitters and/or receivers, or even both. The cost and efficiency as well as the need for security mechanisms are also important aspects.

Currently there is a broad group of wireless technology systems, with own standards and specific characteristics, that enable communication at different ranges of distances, from the centimeters to thousands of kilometers.

There are a several examples of widely known wireless systems. The wireless LANs (local area network wireless) systems that are designed to connect mobile and portable devices (smartphones, laptops, printers etc.) in a LAN, within a building or a confined place. The cellular network systems that cover a zone divided by cells, with fixed base stations, and the users through their mobile phones can communicate with each other anywhere. There are also broadcast systems (TV or radio), satellite systems, sensor networks, etc. The application of this type of communication systems ranges from transportation, (land, maritime or aerial), military, weather forecast, satellite applications (point-to-point communication, GPS, etc), wireless power transfer, smart homes, and other private and public places, etc .. almost everywhere.

Each application has its individual characteristics and constraints in the way the commu-

nication is accomplished, particularly regarding to the radiation shape, and in most of wireless systems the use of antenna arrays is indispensable. The antenna is therefore a crucial element in any wireless communication system.

To meet the objectives, regarding to the radiation shape suitable to each wireless application, including to obtain higher gains and directivity, specific beamwidths (typically narrow), reduced sidelobes, or to steer the main lobe, it is common to use nonuniform antenna arrays, because several of these parameters cannot be reached together using individual radiating elements or even just with uniform antenna arrays.

As is widely known, there are five main aspects in the design of antenna arrays, which affect the way how they transmit or receive electromagnetic waves. They are illustrated in the Fig.(1.1), and are:

- Number of array elements and the arrangement of the elements in the array,
- Distance between elements,
- The single element (radiation shape),
- The amplitude of excitation of each array element,
- The phase of excitation of each array element,

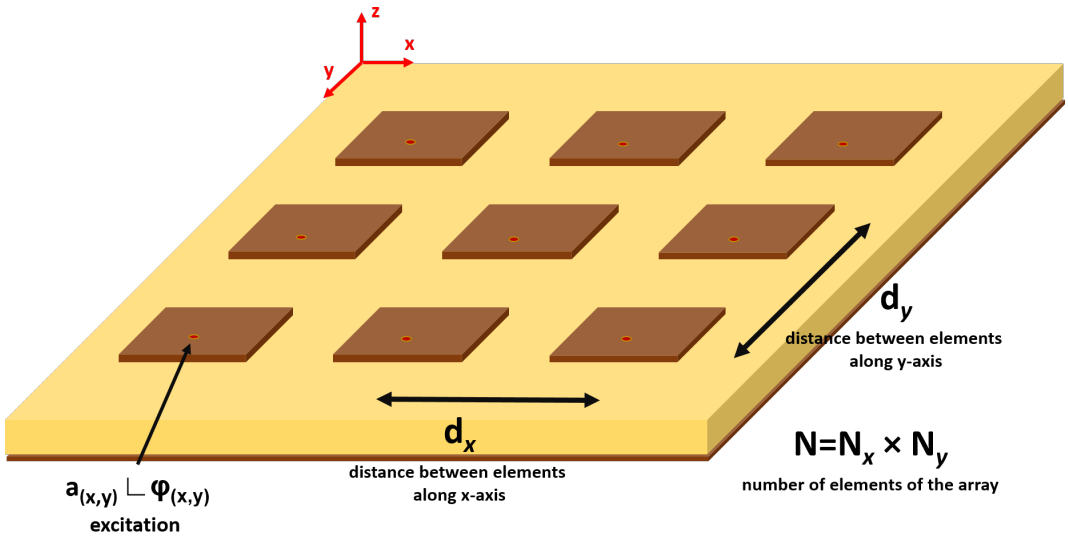

Figure 1.1: Antenna Array

The feeding of each element of the array can be fixed, implemented by array feeding networks properly designed and providing a static radiation pattern, or may be dynamic, ie frequently adjusted, modifying the shape of radiation pattern according to the constraints imposed at each moment. In this case the array is a *smart antenna*.

How much better an antenna fulfills the requirements of each particular system, whether in terms of radiation characteristics, but also in terms of usage conditions such as the local, the available space, weight supported, etc, better will be the communication, and also the reliability and durability of the system.

1.2 Background and Objectives

This PhD thesis happens after a MSc's dissertation entitled *"Antena para comunicações DSRC"* held under the supervision of the same supervisors, at this university, and in the course of a collaboration of the Instituto de Telecomunicações (host institution) and Brisa Inovação e Tecnologia company, one of the main Portuguese operators of transport infrastructures.

The initial purpose at the beginning of the doctoral program, was the development of an adaptive antenna for satellite communications, whose beamforming would be made fully electronic, since such lack in the state of the art has been identified in this kind of antennas. In this sense at first, the search for state of the art on adaptive antennas was made. The steering of the adaptive antenna radiation pattern is more suitable with electronic adaptive beamforming than with mechanical rotation that has serious physical limitations, as a slow tracking, more wear and a bulky apparatus. The main obstacle in developing an antenna array with electronic beamforming is the difficulty to design an efficient feed network in terms of amplitude and phase that can control every element of the array. There are some hybrid solutions (using electronic steering in elevation angles and mechanical steering for azimuth angles), or just mechanical, to steer the array radiation pattern.

Moreover, the objective was not just to design an antenna with a fully electronic beamforming, but also fulfilling acceptable cost needs (reduced), and keeping a compact design and volume, which does not seem easy given the need for feed network circuits, using amplifiers/attenuators and phase shifters that correspond to these requirements.

An adaptive antenna is, in its genesis, an antenna that autonomously steers (and adjusts) its radiation shape, depending on the environment in which it is inserted. Therefore, it should be able to estimate the directions of the incident signals that reach it, and then the ability to adapt its radiation pattern. This is accomplished using signal processing capabilities, applying DOA, and beamforming algorithms. Thus, various algorithms of DOA and Beamforming were analyzed, which are described in Chapter 5 of this thesis.

With the aim to idealize a suitable structure for the array feeding network to enable a completely electronic beam steering, the options in terms of phase shifters technologies, that allow to find the desired phase shifts as well as to comply with the limitations in terms of volume, cost, simplicity, etc., were studied. This component is one of the main difficulties in such structure, and one of the more costly components. A brief summary about recent phase shifters technologies is provided in a section of the chapter 5 of this thesis. It was concluded that the technology using the composite material BST (Barium Strontium Titanate) was promising, and in first analysis it corresponds to the expected objectives. A number of meetings with members from the Department of Materials and Ceramics Engineering (DEMAC) of Universidade de Aveiro were held in order to evaluate the possibility of fabrication and characterization of such type of composite materials. However, over the time, it was realized that a major limitation would be the placement process (because it is done at high temperatures) over the substrates typically used in microwaves, besides other associated costs.

Parallel to these studies, I kept trying to obtain a scholarship from FCT (Portuguese national funding agency). However, I've never been selected. To have funding support, I was collaborating and developing research work for some other research projects, especially emphasizing one that was maintained with the BRISA company. In this context, several antenna arrays (mainly) for vehicular communications (for DSRC band) were investigated and designed, and the work recognized through a number of scientific publications. This group of antennas can be seen in Chapter 3 of this thesis.

Collaboration also with WAVECOM company was preserved to find a directive antenna for each Wi-Fi band, in order to cover each of a huge number of sectors wherein a stadium has been divided. This was accomplished at the time of an important international final of a sports competition held in Portugal, and in order to cover a sports stadium with a modern Wi-Fi network with large capacity. An important requirement was the cost and simplicity of the prototype since, naturally, several tens/hundreds of antennas (sectors) would be necessary for this coverage. These solutions are proposed and described in chapter 4 of this thesis.

More recently, I started a collaboration with a BEACON European research project, also referred to in Chapter 5, since the objective of the project is related to the initial aim of this thesis, although using photonic phase shifter.

However, and given the range of the work performed and scientifically recognized, in the different applications of wireless communications, almost all involving the common characteristic of being planar antennas arrays using nonuniform excitation, it was considered to redirect the overall objective of the PhD Thesis as the combination of all the sub-targets that have been overcome along this journey, which are summarized in the three following points.

- Analysis of direction of arrival and beamforming estimation algorithms for planar antenna arrays.
- Development of planar antenna arrays with low cost, weight, and volume, suitable for vehicular communications systems.
- Development of low-cost planar antennas, suitable for Wi-Fi networks with sectoral coverage in sports venues.

1.3 Thesis Organization

This thesis is structured into six chapters, and the content of each one was carefully selected to be more easily understandable, individually and globally, which are described below.

Chapter 1 affords the motivation that led to select the topic addressed in this thesis, wireless communications, and all its relevance in the present and in the future, reporting the trajectory regarding to the PhD over the last few years to get here, and presenting the objectives taken as well as the main contributions achieved.

Chapter 2 provides a theoretical overview of the main aspects used throughout the thesis, subdivided into three major sections, the first on fundamental parameters of antennas, which are important to understand and analyze an antenna. Another group is on microstrip antennas, the type of antennas adopted and currently one of the most used in wireless communications. Finally, the last section is on antenna arrays, describing important aspects of analysis and design, as well as a number of known feed distributions.

Chapter 3 is devoted to the application of wireless communications in vehicular technology (transport sector), designing a number of antennas/antenna arrays for different devices and conceptions, of a dedicated short range communication system, a hot topic currently under strong attention and exploration.

Chapter 4 is dedicated to the development of two antennas arrays to cover a defined sector and suitable for placement of Wi-Fi networks in sports stadiums. The development of these directive arrays with reduced sidelobes, using a planar structure, and with low cost substrates (promoting mass production) are presented as the main advantages.

Chapter 5 deals with the topic of adaptive antennas, also known as smart antennas. In this chapter a number of estimation algorithms of directions of arrival and beamforming, important for such antennas, are implemented (using Matlab) and applied to planar antenna arrays, as well as a detailed analysis of these algorithms is provided. Moreover, some discussion relating to phase shifters and with a contribution to a research project associated with this topic are addressed.

Chapter 6 comprises the most important conclusions taken from this PhD thesis, summarizes each topic addressed, and presents some future research subjects.

1.4 Main Contributions

This PhD work allowed relevant scientific contributions, accepted and published, both in recognized international journals **[J]** and international conferences **[C]**, supporting and covering the topics addressed in the different chapters, and which were taken into consideration and referenced along the thesis. An invitation to perform a book chapter **[Ch1]** about the main results taken in Chapter 5 of this thesis, regarding the direction of arrival and beamforming estimation algorithms, and their analysis made, was received. The chapter was submitted (the proposal), accepted, and will be part of a book about beamforming, to be edited later.

Book Chapters

[Ch1] T. Varum, J. N. Matos, P. Pinho, "Detect and Pointing algorithms performance for a 2D Adaptive Antenna Array", Beamforming, InTech (2017), ISBN 978-953-51-5229-3 (under submission - provisionally accepted)

Papers in International Journals

[J1] T. Varum, J. N. Matos, P. Pinho, R. Abreu, A. Oliveira, J.A. Alves, "Microstrip Antenna Array for Multiband Dedicated Short Range Communications", *Microwave and Optical Technology Letters*, Vol.53, No.12, pp.2794 - 2796, December, 2011

[J2] T. Varum, J. N. Matos, P. Pinho and R. Abreu, "Nonuniform Broadband Circularly Polarized Antenna Array for Vehicular Communications," in *IEEE Transactions on Vehicular Technology*, vol.65, no.9, pp.7219 - 7227, Sept. 2016.

[J3] T. Varum, J. N. Matos, P. Pinho, "Non-Uniform Microstrip Antenna Array for DSRC in Single-Lane Structures", Sensors 2016, No.12, 2101

[J4] T. Varum, J. N. Matos, P. Pinho, R. Abreu, "Printed nonuniform antenna array for WI-FI sectorized communications", *Microwave and Optical Technology Letters*, Vol.57, No.9, pp.2037 - 2041, September 2015

[J5] T. Varum, J. N. Matos, P. Pinho, "Detect and pointing algorithm's performance for a planar smart antenna array: a review", *Applied Computational Electromagnetics Society Journal*, Vol.30, No.8, pp. 824 - 837, August 2015

[J6] T. Varum, J. N. Matos, P. Pinho, "Direction of Arrival Estimation Analysis Using a 2D Antenna Array", *Procedia Technology*, Vol.17 , No.1, pp. 617 - 624 , November 2014

Papers in Conferences

[C1] T. Varum, J. N. Matos, P. Pinho, "Printed antenna for On-Board Unit of a DSRC System", *IEEE International Symposium on Antennas and Propagation USNC/URSI National Radio Science Meeting*, Spokane, United States, Vol., pp. 457 - 460, July, 2011

[C2] T. Varum, J. N. Matos, P. Pinho, "Omnidirectional Circularly Polarized Antenna for DSRC Systems", *IEEE International Symposium on Antennas and Propagation USNC /URSI National Radio Science Meeting*, Chicago , United States, Vol. 1, pp. 1 - 2, July, 2012

[C3] T. Varum, J. N. Matos, P. Pinho, A. Oliveira, "Printed Antenna for DSRC Systems with Omnidirectional Circular Polarization", *15th International IEEE Conference on Intelligent Transportation Systems*, Anchorage, United States, Vol. 1, pp. 475-478, September, 2012

[C4] T. Varum, J. N. Matos, P. Pinho, R. Abreu, "Microstrip antenna for vehicular communications with improved axial ratio band", *IEEE EUROCON - International Conference on Computer as a Tool (EUROCON), and CONFTELE*, Lisbon, Portugal , Vol. , pp. 1 - 4, April, 2011

[C5] T. Varum, J. N. Matos, P. Pinho, R. Abreu, "The impact of different power dividers used in a non-uniform planar antenna array", *IEEE International Symposium on Antennas and Propagation USNC/URSI National Radio Science Meeting*, Memphis, United States, Vol. 1, pp. 1690 - 1691, July 2014

[C6] T. Varum, J. N. Matos, P. Pinho, R. Abreu, "Non-uniform microstrip antenna array for Rx DSRC communications", *IEEE International Symposium on Antennas and Propagation USNC/URSI National Radio Science Meeting*, Memphis, United States, Vol. 1, pp. 1071 - 1072, July 2014

[C7] T. Varum, J. N. Matos, P. Pinho, "Microstrip antenna array for a new tolling approach in highways access", *10th Conference on Telecommunications Conftele* , Aveiro , Portugal , Vol. 1, pp. 1 - 4, September, 2015

[C8] T. Varum, J. N. Matos, P. Pinho, "Non-uniform microstrip antenna array for tolling using a single access lane", *IEEE International Symposium on Antennas and Propagation USNC/URSI National Radio Science Meeting*, Fajardo , Puerto Rico , Vol. 1, pp.1-4 , July , 2016

[C9] T. Varum, J. N. Matos, P. Pinho, R. Abreu, "Non-uniform printed antenna array for wireless communications in sports arenas", *European Conference on Antennas and Propagation (EuCAP)*, Lisbon , Portugal , Vol. 1 , pp. 1 - 4 , April 2015

[C10] T. Varum, J. N. Matos, P. Pinho, V. C. Duarte, "Circularly polarized microstrip antenna array for the Ka-band", *IEEE International Symposium on Antennas and Propagation USNC/URSI National Radio Science Meeting*, Vancouver, Canada, Vol. 1, pp. 1864 - 1865, July 2015

Chapter 2

Fundamental concepts of Antennas and Antenna Arrays

Wireless communications (unguided) involve the use of antennas. An antenna is therefore, the crucial component in wireless communications that, in transmission, receives the coming power from a radio circuit (guided wave) and sends it into space (free-space wave). In reception, collects the energy of electromagnetic waves from space and delivers it to a radio receiver.

Nowadays the antennas are present everywhere, such as the homes, vehicles, aviation, satellites, sensors, mobile devices, etc, with numerous different applications. The quality of a wireless communication system depends highly on the capability of its antenna be able to send/receive the electromagnetic waves. The antennas can be divided into several categories, such as wire, reflector, microstrip, horn, among some others.

In many situations, it is also necessary resort to several antennas, arranged in a specific configuration to form an antenna array. The antennas can also be classified in terms of their radiation pattern: omnidirectional or directional, and with higher or smaller side lobes. Although there are a wide variety of antenna types and shapes, its principle of operation is identical.

This chapter presents a general theoretical description of concepts used in the next chapters, such as the fundamental antenna parameters, important notions on antenna arrays and nonuniform excitation techniques, as well as an introduction to microstrip antennas.

2.1 Antenna Parameters

The selection of the antenna to use is an important step in the design of a particular wireless telecommunication system, since it (and its characteristics) affects all the communication.

To choose the antenna that best fits a particular application within a certain radio circuit, fundamental aspects of antennas should be understood and taken into account, such as its radiation fields and their patterns, polarization, directivity and gain, bandwidth, impedance, etc. In this section some of these parameters are presented.

2.1.1 Polarization

The polarization is an important parameter in the design of an antenna for any communications system, because it has impact in the quality of communication and might even prevent it. By definition, the polarization of an antenna is the polarization of the electromagnetic waves it radiates, and describes the way the magnitude and orientation of the electric field vector E changes as a function of time, at a location z in space [1, 2, 3].

For an antenna, in the far field region, an electromagnetic wave radiated through it can be considered a plane wave, with equal electric field amplitude and propagating through a radial direction.

Considering the total electric field vector $\mathbf{E}$ expressed in (2.1), which is a vector phasor function of the space coordinates, the instantaneous total time-harmonic vector field *E(x,y,z,t)* of a plane wave traveling along the positive z-direction is given by (2.2).

$$\mathbf{E} = [\mathbf{E_x}(x, y, z) + \mathbf{E_y}(x, y, z)]\ e^{-jkz} \tag{2.1}$$

$$E(x, y, z, t) = \Re\left\{\mathbf{E}(x, y, z)\ e^{jwt}\right\} \tag{2.2}$$

The electric field lies in the xoy plane and is a vector function of the space coordinates and the time. In terms of electric field components, (2.1) can be expressed as [1]:

$$E(z, t) = E_x(z, t)\hat{\mathbf{x}} + E_y(z, t)\ \hat{\mathbf{y}} \tag{2.3}$$

$$E_x(z, t) = \Re\left\{\mathbf{E_x}\ e^{jwt}\right\}\ \ldots\ E_x = E_1\ e^{j(wt-kz+\delta_x)} \tag{2.4}$$

$$E_y(z, t) = \Re\left\{\mathbf{E_y}\ e^{jwt}\right\}\ \ldots\ E_y = E_2\ e^{j(wt-kz+\delta_y)} \tag{2.5}$$

with $E_x(z, t)$ and $E_y(z, t)$, representing the instantaneous components, calculated through (2.4) and (2.5), E_1 and E_2 being the amplitudes of each component, and δ_x e δ_y, the correspondent phases.

Setting $\delta = \delta_y - \delta_x$ as the time-phase difference between the two components, the total instantaneous electric field can be rewritten as (2.6) [2].

$$E(z, t) = E_1 \cos(wt - kz)\hat{\mathbf{x}} + E_2 \cos(wt - kz + \delta)\ \hat{\mathbf{y}} \tag{2.6}$$

Using the equation (2.6) at $z = 0$, manipulating it, it is possible to get the following relationship as function of the two components of electric field. This equation describes the polarization ellipse, which allows to characterize the polarization of the antenna [2].

$$aE_x^2 - bE_xE_y + cE_y^2 = 1 \tag{2.7}$$

$$a = \frac{1}{E_1^2 \sin^2(\delta)}\ b = \frac{2\cos(\delta)}{E_1E_2 \sin^2(\delta)}\ c = \frac{1}{E_2^2 \sin^2(\delta)} \tag{2.8}$$

An ellipse, as shown in Fig.(2.1), may be characterized by the relationship between their axes, given by the axial ratio (AR) (2.9), and the angle τ between its major axis (OA) and the x-axis.

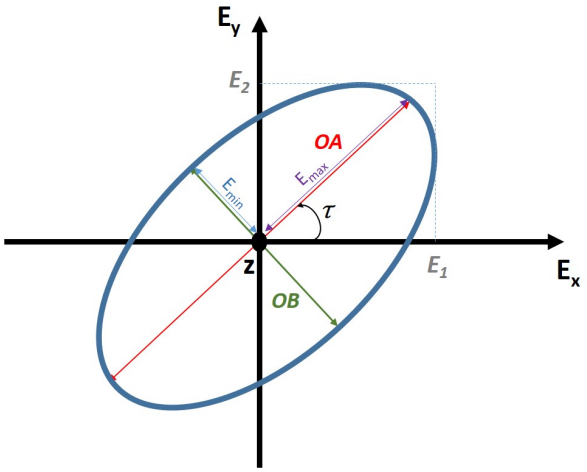

Figure 2.1: Polarization ellipse

$$AR = \frac{E_{max}}{E_{min}} = \frac{major\ axis}{minor\ axis} = \frac{OA}{OB} \qquad 1 \leq AR \leq \infty \tag{2.9}$$

$$OA = \left[\frac{1}{2}\left\{E_1^2 + E_2^2 + \left[E_1^4 + E_2^4 + 2E_1^2E_2^2\cos(2\delta)\right]^{\frac{1}{2}}\right\}\right]^{\frac{1}{2}} \tag{2.10}$$

$$OB = \left[\frac{1}{2}\left\{E_1^2 + E_2^2 - \left[E_1^4 + E_2^4 + 2E_1^2E_2^2\cos(2\delta)\right]^{\frac{1}{2}}\right\}\right]^{\frac{1}{2}} \tag{2.11}$$

$$\tau = \frac{1}{2}\tan^{-1}\left(\frac{2E_1E_2}{E_1^2 - E_2^2}\cos(\delta)\right) \tag{2.12}$$

Based on the previous theory, a plane wave may have three types of polarization: elliptical, linear or circular. In the general case, the figure that the electric field vector traces in time is an ellipse, and therefore is referred to as elliptically polarized plane wave.

However, there are two particular cases:

(a) when one of the axes of the ellipse is or tends to zero, the figure drawn by the electric field vector is a line, and the plane wave is referred to as *linearly polarized.*

(b) when the two axes of the ellipse have an equal magnitude and are offset 90°, the ellipse becomes a circle, and the polarization is referred to as *circularly polarized.*

these cases are the most desired in antenna design, and will be explored below.

Linear Polarization

An antenna is linearly polarized [1, 4], when the variation of the time-harmonic electric field vector of a plane wave it generates, over the time, at a given point in space, is oriented in a straight line, as illustrated in Fig.(2.2).

This implies that:

i. Either the electric field vector has only one component,

- E_1=0, linear polarized in y-direction, see Figs.(2.2a) and (2.2b)
- E_2=0, linear polarized in x-direction, see Figs.(2.2c) and (2.2d)

ii. or the time-phase between the two components complies with the following condition:

$$\delta = \delta_y - \delta_x = n\pi, \qquad n = 0, 1, 2, ... \tag{2.13}$$

iii. if δ=0 and $E_1 = E_2$, the wave is linear polarized with τ=45 degrees

iv. In these cases the AR=∞

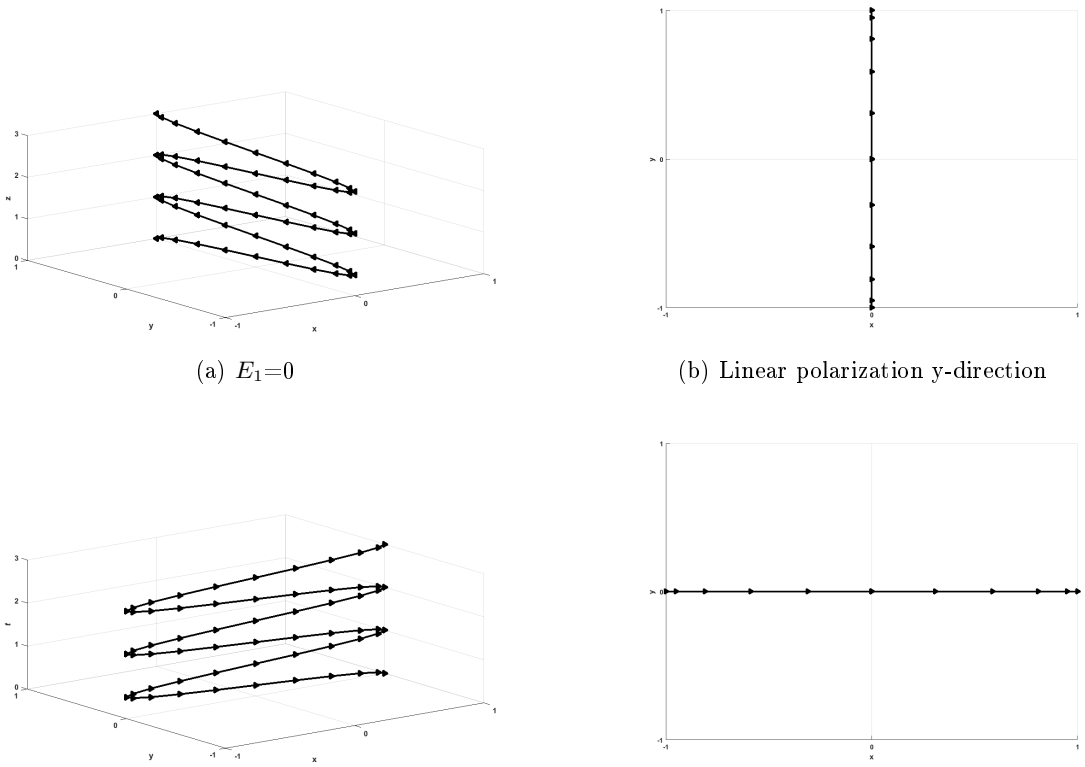

(a) E_1=0

(b) Linear polarization y-direction

(c) E_2=0

(d) Linear polarization x-direction

Figure 2.2: Linearly polarized electromagnetic waves as function of t for a fixed position

Circular Polarization

An antenna is circularly polarized when the variation of the time-harmonic electric field vector of a plane wave it generates, over the time, at a given point in space, is oriented in a circle, as illustrated in Figs.(2.3a) and (2.3b).

This implies that:

i. the two components of electric field have the same magnitude, $E_1 = E_2$,

ii. the time-phase between the two components complies with the following condition:

$$\delta = \delta_y - \delta_x = \begin{cases} \frac{\pi}{2} + 2n\pi & n = 0, 1, 2, ... \quad LHCP \\ -\frac{\pi}{2} + 2n\pi & n = 0, 1, 2, ... \quad RHCP \end{cases} \tag{2.14}$$

iii. In these cases the AR=1

The rotation of the electric field can have two possible directions, left or right. If one put the left hand thumb according to the direction of propagation and the fingers to bend toward the electric field direction, it is because the electromagnetic wave is rotating to the left, so it has left polarization. If this happens using the right hand, the wave has right polarization.

In the case of circular polarization it becomes left hand circular polarization (LHCP) or right hand circular polarization (RHCP).

The Fig.(2.3) shows several graphs of electric field expression (2.6), for different cases. In the left side it is possible to observe the variation in the electric field over a period of time, for a z fixed position, while on the right side is shown the trace of the electric field vector in time, relating it to the polarization ellipse.

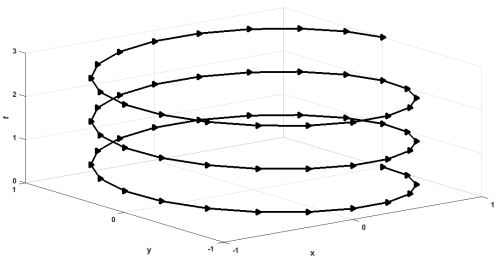

(a) E_1=E_2, δ=$\frac{\pi}{2}$

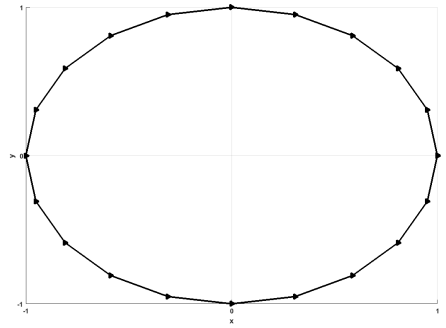

(b) Circular polarization

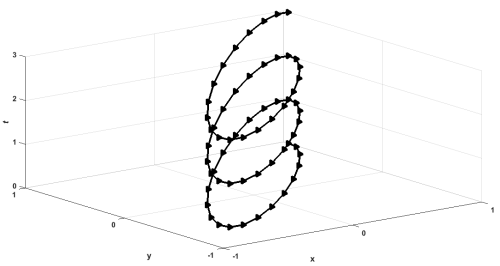

(c) E_1=E_2, δ=$\frac{\pi}{10}$

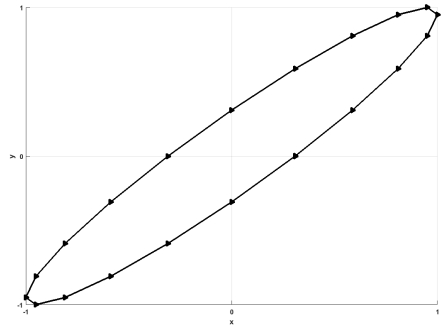

(d) Elliptical polarization, $\tau = 45^o$

Figure 2.3: Circular and elliptical electromagnetic waves as function of t for a fixed position

2.1.2 Radiation Pattern

According to IEEE Standard definitions for antennas [5], the concept radiation pattern, or also antenna pattern is:

"A graphical representation of the radiation properties of the antenna as a function of space coordinates. In the usual case the radiation pattern is determined in the far-field region and is represented as a function of directional coordinates. Radiation properties include power flux density, field strength, phase, and polarization."

The radiation patterns usually represent the field or power, usually normalized to its maximum. These diagrams are commonly presented using a spherical coordinate system, as shown in Fig.(2.4), and can be classified by the directionality as isotropic, omnidirectional or directional.

A radiation pattern is isotropic when radiation is equal in all directions. This represents only a hypothetical case, and is taken as reference in directivity classification. The omnidirectional radiation patterns are those which have a directive radiation along one radiation plane, while in the orthogonal plane, it has an equal radiation in all directions. Finally, the directional radiation patterns, represent those which the radiation is mainly focused in one direction.

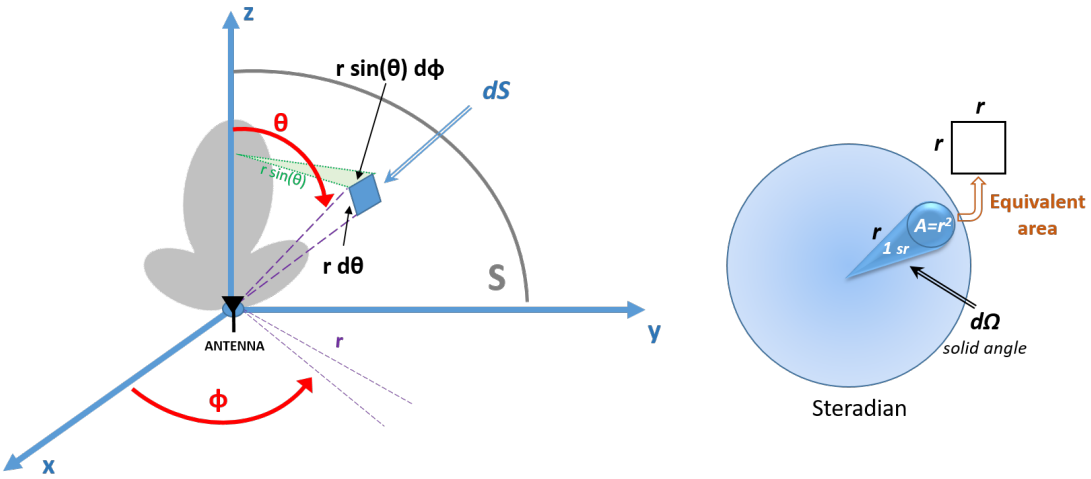

Figure 2.4: Spherical coordinate system

To completely analyze the radiation characteristics of an antenna, a three-dimensional radiation pattern can be used, or more commonly, using two planar radiation patterns (two dimensional) with both main planes of radiation.

These planes, representing two planar patterns, are obtained by cutting the spatial radiation pattern (3D), and are usually named by the horizontal and vertical planes, or also E and H planes.

The horizontal plane of radiation has the antenna radiation as function of ϕ angle, for a fixed value of θ, (usually $\theta = 90^o$), while the vertical plane represents the radiation characteristic as a function of the angle θ, for a fixed value of ϕ, (usually 0^o or 90^o).

Through correct analysis of the radiation pattern, a group of parameters can be taken, representing the radiation characteristics of an antenna, such as the level of side lobes, and the widths of main lobe. These main characteristics are discussed below.

2.1.3 Radiation Intensity

To define the radiation intensity, first assume a steradian (sr) as the unit of a solid angle. As shown in the Fig.(2.4), a sr is a solid angle with the center of a sphere S of radius r subtended by a spherical surface which has an area that is equal to the area of a square of side r [1]. Since the area of a sphere is equal to $4\pi r^2$, and the area of the spherical surface and the square is r^2, so there are 4π sr in a sphere of radius r.

Considering the instantaneous Poynting vector $\mathscr{P}$, the vector that quantifies the power associated to an electromagnetic wave, for time-harmonic fields, the time-average vector power density is the integration of $\mathscr{P}$ over a period T and dividing by T,

$$\mathbf{P}_{avg} = \frac{1}{T}\oint_T \mathscr{P}\, dt \quad = \frac{1}{T}\oint_T E \times H\, dt \ldots = \frac{1}{2}\Re[\mathbf{E}\times\mathbf{H}^*] \quad (W/m^2) \tag{2.15}$$

the total time-average power radiated by the antenna is obtained by integrating $\mathbf{P}_{avg}$ over the surface S,

$$P_{rad} = \oint_S \mathbf{P}_{avg}\cdot\, dS \quad = \oint \frac{1}{2}\Re[\mathbf{E}\times\mathbf{H}^*]\, dS \tag{2.16}$$

As the surface S under analysis is a sphere of radius r, then the area $dS = r^2\sin\theta\, d\theta\, d\phi$ (see Fig.(2.4)) and,

$$P_{rad} = \int_0^{2\pi}\int_0^{\pi} \mathbf{P}_{avg}\cdot r^2\sin\theta\, d\theta\, d\phi \tag{2.17}$$

An antenna radiation intensity (U) is defined as the radiated power per solid angle [1, 5]. This far-field parameter is the result of the multiplication of the radiation density $\mathbf{P}_{avg}$ by the square of the distance,

$$U(\theta,\phi) = r^2\mathbf{P}_{avg} \qquad (W/unit\ solid\ angle) \tag{2.18}$$

Considering $d\Omega = \frac{dS}{r^2} = \sin\theta\, d\theta\, d\phi$, as the element of solid angle and eq.(2.18), the eq.(2.17) becomes,

$$P_{rad} = \oint_\Omega U(\theta,\phi)\, d\Omega \tag{2.19}$$

Finally, the average radiation intensity U_{avg} can be determined by dividing the total radiated power by 4π,

$$U_{avg} = \frac{P_{rad}}{4\pi} \tag{2.20}$$

2.1.4 Directivity

The directivity (D) is an antenna parameter that allows to describe how an antenna directs the energy in a certain direction. Through [1, 5], the directivity of an antenna is defined as the ratio between the radiation intensity in a given direction and the average radiation intensity in all directions, and is given by:

$$D(\theta,\phi) = \frac{U(\theta,\phi)}{U_0} = \frac{4\pi U(\theta,\phi)}{P_{rad}} \tag{2.21}$$

The values of D can range between zero and a maximum value D_{max}. The directivity of an isotropic antenna is unitary, since it radiates equally in all directions.

Usually the directivity of an antenna is expressed in decibel logarithmic units:

$$D(dB) = 10\log_{10}(D(\theta,\phi)) \tag{2.22}$$

2.1.5 Gain

The definition of gain (G) and directivity are similar, differing only in terms of power. While in a given direction the directivity is the ratio between the radiation intensity $U(\theta, \phi)$ and the total radiated power P_{rad} divided by 4π, the gain is defined as the ratio of the radiation intensity $U(\theta, \phi)$ and total input power at the antenna P_{in} divided by 4π [1, 5].

To calculate the gain of an antenna in a certain direction, the proportion of dissipated power at the antenna through ohmic losses is accounted.

In the ideal antenna, lossless, is assumed that $P_{in} = P_{rad}$, whereby the gain coincides with directivity. If there are losses, the radiated power is always less than the power delivered to the antenna terminals, $P_{rad} \leq P_{in}$, which is the reason why usually gain is lower than the directivity.

$$G(\theta, \phi) = \frac{4\pi U(\theta, \phi)}{P_{in}} \tag{2.23}$$

therefore, through eqs.(2.21) and (2.23), it is possible to relate these two antenna measures by introducing a new definition of radiation efficiency (η_r).

$$P_{rad} = \eta_r P_{in} \tag{2.24}$$

The gain is also usually expressed in decibels (dB), so

$$G(dB) = 10 \log_{10}(G(\theta, \phi)) \tag{2.25}$$

2.1.6 Efficiency

The total power radiated by an antenna does not correspond to the total power delivered at its terminals, because there are a number of associated losses (mismatch, transmission lines, antenna losses, etc..), which affect the overall efficiency of the antenna.

Considering P_{in} as the power delivered to the antenna terminals, this value is divided into two components, one is concerning to the ohmic losses and the other is radiated by the antenna.

Through the eq.(2.24), the antenna radiation efficiency can be written as,

$$\eta_r = \frac{P_{rad}}{P_{in}} \quad = \frac{P_{rad}}{P_{rad} + P_{ohm}} \tag{2.26}$$

The radiation efficiency is typically close to 100%, the reason why most antennas gain and directivity have similar values. The radiation efficiency can also be written as the multiplication of two elements: conduction efficiency (η_c) and dielectric efficiency (η_d),

$$\eta_r = \eta_c \cdot \eta_d \tag{2.27}$$

The total efficiency (η_{total}) of an antenna includes not only the radiation efficiency (η_r) (dielectric and conducting) but also losses due to impedance (η_m) and to polarization(η_p) mismatch.

$$\eta_{total} = \eta_r \cdot \eta_m \cdot \eta_p \tag{2.28}$$

The mismatch impedance efficiency, assuming a characteristic impedance Z_c of the line, and Z_{in} of the antenna input impedance, can be written

$$\eta_m = 1 - |\Gamma|^2 \qquad |\Gamma| = \frac{Z_{in} - Z_c}{Z_{in} + Z_c} \tag{2.29}$$

2.1.7 Bandwidth

The antenna bandwidth Δf is considered the range of frequencies around the central frequency (f_0), in which the antenna keeps an acceptable performance in one or more of its parameters. The parameters normally considered are the input impedance matching, polarization, sidelobe levels, gain, etc.

$$f_0 - \Delta f/2 < f < f_0 + \Delta f/2 \tag{2.30}$$

The antenna bandwidth often corresponds to the impedance bandwidth, describing the bandwidth where the antenna presents a good impedance matching, and is usually expressed as a percentage of the central frequency.

When given the requirements, it is expected that the antenna fulfills more than one constraint, ex: good input impedance matching and circular polarization, the antenna bandwidth is assumed the interception of all individual bandwidths of the various parameters considered.

2.2 Microstrip Antennas

Microstrip antennas have been widely used over the last years and will have a great applicability in the future as a result of their characteristics suitable, especially to the frequency band of microwaves. Their applications are diverse and range from aircraft, military, vehicular, and mobile wireless communications, to applications in satellite communication.

A microstrip antenna, as shown in Fig.(2.5), consists of a dielectric material (substrate) which is covered on both sides with conductive metallic layers and one side completely filled, operating as ground plane, and the opposite side partially filled, operating as a radiating element [1, 6].

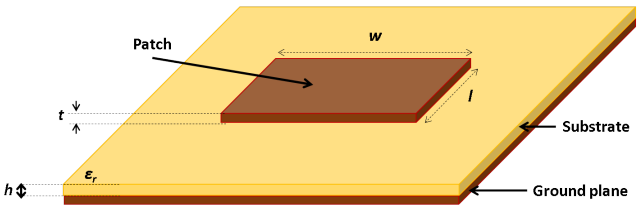

Figure 2.5: Microstrip antenna

The main positive characteristics of this type of antennas include low profile, light weight, low cost, ease of manufacture and to install, and compatibility with circuits and microwave components. The microstrip antennas also have the advantage of being a versatile type of antennas in their properties, such as polarization, impedance, frequency of resonance, and in the construction of antenna arrays.

The principal disadvantage of using such antennas is the limited bandwidth, even though several techniques are already available in order to increase the bandwidth of microstrip antennas. Moreover this kind of antennas is unable to deal with very high powers, and also presents lower efficiencies due to the substrate losses. A microstrip antenna can have a variety of shapes according to technical constraints, and are presented next.

2.2.1 Substrate, Antenna shapes, and Feed techniques

The selection of the dielectric substrate to use is an important step in the design of a microstrip antenna, which significantly influences its performance. The substrate has as primary purpose to support the patch, ensuring its separation from the ground plane. Depending on its characteristics, the structure may change their properties predominantly for radiation or transmission [6].

A variety of substrates of different materials and with a vast range of prices (between other characteristics) can currently be found in the market according to the application requirements (cost, patch size, bandwidth, thermal stability, etc.). The best choice must be weighed. A dielectric substrate has as main characteristics the thickness h, its dielectric constant ϵ_r, and the loss tangent $\tan\delta$.

The dielectric constant, also known as relative permittivity of the material, ϵ_r, represents how much the electric field is slowed as it propagates into the material, relating to propagation in a vacuum. This parameter varies with frequency and temperature, and significantly affects the size and bandwidth of the antenna, as we will see ahead. Thicker substrates with low dielectric constant promote radiation (antennas), in contrast, substrates with higher dielectric constant with thin thicknesses are suitable for energy transmission (transmission lines).

In a microstrip structure, four types of waves are typically generated, propagating on it: spatial waves, guided waves, surface waves and leaky waves, which are illustrated in Fig.(2.6)[7].

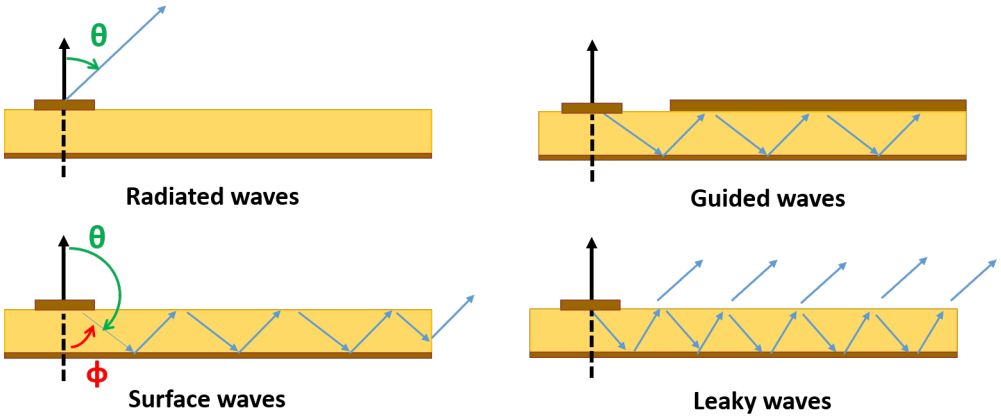

Figure 2.6: Waves propagating on a microstrip structure

- **Spatial waves** are the desired when a microstrip structure acts as an antenna. These waves are sent to the space according to an angle

$$0 < \theta < \pi/2 \tag{2.31}$$

- **Guided waves** are propagated when there are two conductive surfaces on both sides of the substrate, as shown in Fig.(2.6). In this case, the structure behaves as a waveguide and these are the predominant waves when the microstrip structure is used as a transmission line.

- **Surface waves** are waves radiated toward the substrate with an angle

$$\pi/2 < \theta < (\pi - \phi) \qquad \phi = \sin^{-1}(1/\sqrt{\epsilon_r}) \tag{2.32}$$

Such waves will propagate between the substrate and the ground plane, as shown in Fig.(2.6), being reflected successively, both with total reflections. This type of waves, thus remains trapped within the dielectric substrate contributing to reduce radiated energy (in the case of structure operating as an antenna), resulting in a deterioration of the antenna's efficiency.

- **Leaky waves** are identical to surface waves, however in this case the angle of incidence is,

$$(\pi - \phi) < \theta < \pi \qquad \phi = \sin^{-1}(1/\sqrt{\epsilon_r}) \tag{2.33}$$

such waves do not allow a total reflection at the top of substrate, whereby a part of the energy is reflected back toward the ground plane while the other part is radiated.

The radiating element, also named 'patch', may have different shapes, either rectangular or square, circular or elliptical, triangular, pentagonal, ring, or simply a strip in the case of monopole antennas. Beyond that, many other variants can be obtained to improve or to achieve new features. The most popular, and also the better documented in literature, are rectangular and circular patches, which will be the ones addressed here.

There are several possibilities to feed a microstrip antenna. The three most used techniques will be addressed: coaxial probe feed, Microstrip line feed, and aperture coupled feed [6, 7].

- **Coaxial-Probe Feed**: This method, as shown in Fig.(2.7), consists of placing a coaxial connector (typically 50-ohms) with its exterior part soldered in the back of the ground plane, and the inner conductor passing through the substrate, soldering the patch at a given point, allowing a correct impedance matching.

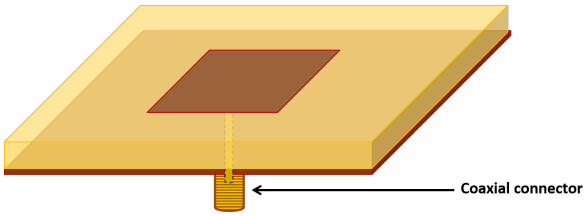

Figure 2.7: Microstrip antenna with coaxial-probe feed

Since the feeding is made in a plane opposite to the radiation plane, such feeding method does not degrade the radiation pattern and the choice of substrate used in the antenna does not depend on the feeding method. This method requires, however, a care when using thick substrates due to the necessary length of the inner conductor, which will introduce a higher inductance and can create matching problems.

- **Microstrip-Line Feed**: This method, as shown in Fig.(2.8), consists of directly feeding the microstrip patch antenna with a microstrip transmission line that connects the patch in one side and, therefore, in the same plane of the antenna.

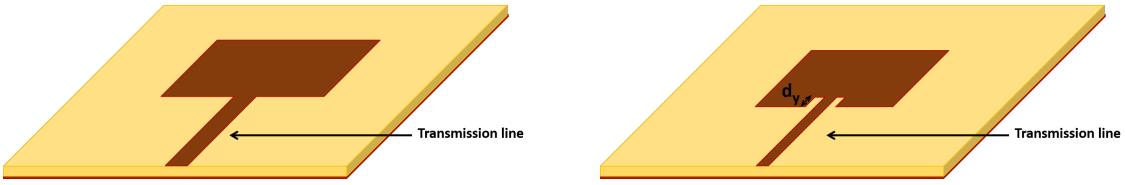

(a) microstrip line feed (b) recessed microstrip line feed

Figure 2.8: Microstrip antenna with microstrip-line feed

Considering the higher impedance at the ends of a microstrip patch, typically 150, 200Ω, the adoption of this method often requires the additional use of a quarter-wavelength transformer to convert this input impedance to the usual 50Ω, or to use an additional technique that consists of making a reentrance in microstrip patch in order to connect the patch at a point where the input impedance is 50Ω.

This method permits the manufacture of the feeding lines in the same plane as the radiating elements, which makes for an easy fabrication with reduced costs. However, the transmission lines introduce losses and increase the chances of degradation the antenna characteristics. Moreover, using this feeding technique it is necessary a trade-off in the choice of the substrate, in order to the substrate does not harm the antenna radiation and also enabling a good transmission in feeding lines.

- **Aperture Coupled Feed**: This feeding method, as illustrated in Fig.(2.9), uses two substrate layers (with identical or different characteristics, ϵ_r, h) and consists of placing the patch element on top of the substrate 1 (ϵ_{r1}, h_1), which is in the upper side of the ground plane. On the bottom of the substrate 2 (ϵ_{r2}, h_2), which is placed below the ground plane, the feeding line is created.

  The excitation of the antenna is made through coupling by creating a slot in the ground plane, as shown in Fig.(2.9). This method avoids the use of solder connections and, since the transmission lines are in different planes, the degradation of antenna radiation pattern through of lines is prevented.

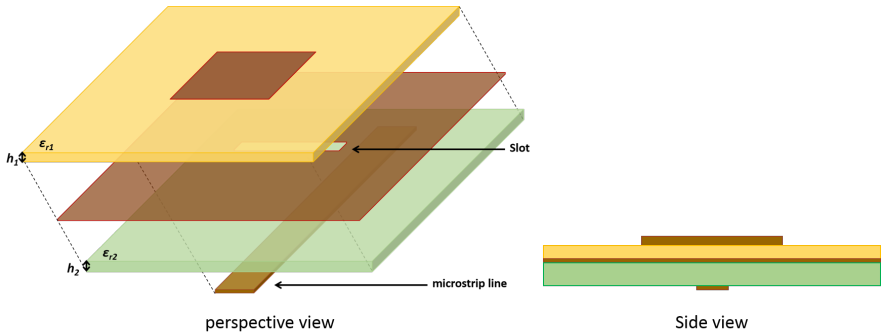

Figure 2.9: Microstrip antenna with aperture coupled feed

The aperture coupling method also allows to choose different substrates both for feeding and for the antenna, that best ensure these characteristics. In addition, this technique allows for higher bandwidths.

2.2.2 Analysis and Design of Microstrip Antennas

Analyzing a microstrip structure is necessary to take into account that it is not a homogeneous structure and, therefore, approximate methods of analysis are needed.

There are some reported methods that allow to analyze microstrip structures, in particular the microstrip antennas, simplifying the design as well as enabling to understand its main parameters, such as operating frequency, input impedance, radiation pattern, etc. The most usual methods of analysis are the transmission line method, the cavity method, and some methods that use more complex integral equations called full wave methods [1, 6].

The transmission line method is simple and provides the physical parameters of the antenna, although it is not very accurate, and has some lack of generalizability to be applied to other patch's shapes.

The cavity method estimates the physical parameters of the antenna with an accuracy higher than the transmission line method, but with an increased complexity as well. Both methods have problems regarding the coupling modulation. However, they provide a reasonable approximation to the physical principles of operation of the antenna.

There are also some full wave methods, which are based on numerical methods to solve the Maxwell's equations applied to the microstrip structure: Moment Method, Finite-Difference Time-Domain (FDTD) Method and Finite-Element Method (FEM). These methods are more accurate, versatile, and applicable to various types of structures, however the complexity is high, requiring a large computational load and they are therefore especially used by most electromagnetic simulators used in antenna simulation.

By its simplicity, the method studied, used, and presented here is the transmission line method [1, 6, 7, 8, 9].

Rectangular Patch

A microstrip patch antenna can be modeled by two $W \times h$ radiating slots separated by a low impedance characteristic Z_c transmission line with length L, as shown in Fig.(2.10).

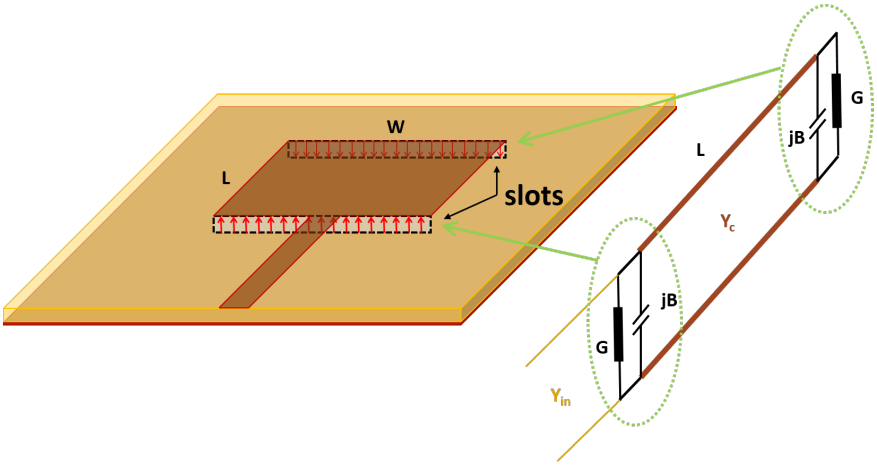

Figure 2.10: Microstrip patch antenna and its equivalent circuit model

The slots represent a very high impedance terminations from both sides of the transmission line, and each slot is described by an admittance $Y = G + jB$.

As the dimensions of the microstrip patch are finite, at its boundaries the fields will leave out of the structure, propagating in two different mediums, the dielectric substrate and the air. This property is illustrated in the Fig.(2.11), and is called fringing effects.

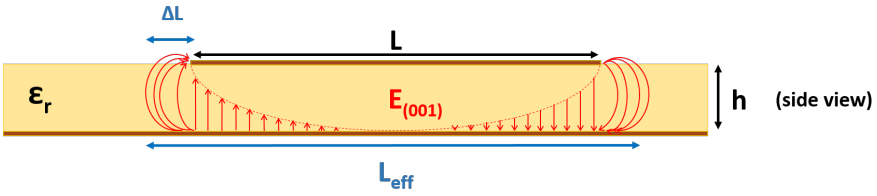

Figure 2.11: Fringing effects on a microstrip structure

These effects are reflected in the electrical dimensions of the structure which becomes slightly higher, affecting the resonance frequency of the antenna.

To take into account of such effects, this method also introduces the terms of effective dielectric constant (ϵ_{eff}), and effective length (L_{eff}).

- **Effective dielectric constant (ϵ_{eff})**: This concept was introduced to account for the fringing effects of waves propagating in two dielectric mediums, in which part of the electric field is in air and a part is in the dielectric substrate.

  The effective dielectric constant of microstrip structure is lower than the relative dielectric constant since a fraction of the fields are in air ($\epsilon_{r_{air}} = 1$). Moreover, it is a function of the relative dielectric constant of the substrate, increasing with the width of microstrip (W), and can be calculated through the equation (2.34).

$$\epsilon_{eff} = \frac{\epsilon_r + 1}{2} + \frac{\epsilon_r - 1}{2}\left[1 + \frac{12h}{W}\right]^{-1/2} \tag{2.34}$$

- **Effective Length (L_{eff})**: The physical length (L) is near the half wavelength, which inverses the direction of the electric field in the slots. Since the electric field can be divided into vertical and horizontal components, the vertical components are annulled while the horizontal components (parallel to the ground plane) are added in phase, resulting in a maximum radiation normal to the patch.

  Due to the fringing effects, the electric size of the microstrip antenna, referred as effective length, is greater than the physical size (L), including also a ΔL extension, function of the effective dielectric constant (ϵ_{eff}), the substrate thickness (h), and width of the patch (W).

$$\Delta L = 0.412h\frac{(\epsilon_{eff} + 0.3)(\frac{W}{h} + 0.264)}{(\epsilon_{eff} - 0.258)(\frac{W}{h} + 0.8)} \tag{2.35}$$

$$L_{eff} = L + 2\Delta L \tag{2.36}$$

The resonance frequency of the dominant mode (TM_{010}) of the antenna can be determined taking into account the fringing effects by

$$L_{eff} = \frac{\lambda_g}{2} \qquad f_r = \frac{c}{2L_{eff}\sqrt{\epsilon_{eff}}} \tag{2.37}$$

and the patch width (W) can be determined by [1]

$$W = \frac{c}{2f_r}\sqrt{\frac{2}{\epsilon_r + 1}} \tag{2.38}$$

The typical procedure of designing a microstrip patch antenna involves the use of the substrate parameters (ϵ_r and h) and the desired operating frequency (f_r), applying the equations (2.34) to (2.38), to determine the dimensions L and W antenna.

Through the equivalent circuit of a microstrip patch antenna of Fig.(2.10), each slot is represented by an admittance $Y = G + jB$, and for slot with width (W) [1, 8, 9]:

$$G = \frac{W}{120\lambda_0}[1 - \frac{(k_0 h)^2}{24}] \qquad \frac{h}{\lambda_0} < \frac{1}{10} \tag{2.39}$$

$$B = \frac{W}{120\lambda_0}[1 - 0.636\ln(k_0 h)] \qquad \frac{h}{\lambda_0} < \frac{1}{10} \tag{2.40}$$

The input admittance (Y_{in}) [1, 9], taking account of the two slots, is

$$Y_{in} = 2G \tag{2.41}$$

And the input impedance is real and,

$$Z_{in} = \frac{1}{Y_{in}} = R_{in} \tag{2.42}$$

This is an approximation because the mutual coupling between the two slots are not taken into account. It is important to note the dependence of Z_{in} to the width of the patch W.

Circular Patch

The circular shape is also commonly used to design a microstrip patch. In this structure, as shown in Fig.(2.12), the resonance frequency is defined by the radius of the structure (r), which is the single dimension of the patch.

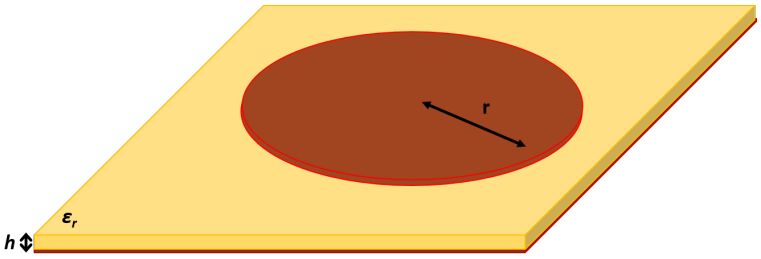

Figure 2.12: Circular Microstrip Patch Antenna

Through [1, 7], using the method of the cavity is achieved the following equations which enable the calculation of the dimensions of the circular patch, through the characteristics of the substrate and the resonant frequency (using h in cm, and f_r in Hz).

$$r = \frac{F}{\left\{1 + \frac{2h}{\pi\epsilon_r F}\left[\ln\left(\frac{\pi F}{2h}\right) + 1.7726\right]\right\}^{1/2}} \tag{2.43}$$

$$F = \frac{8.791 \times 10^9}{f_r\sqrt{\epsilon_r}} \tag{2.44}$$

2.2.3 Circular Polarization in Microstrip Antennas

In its regular configuration, a circular or rectangular microstrip antenna radiates linearly polarized waves. Nonetheless, one of the good benefits of microstrip antennas is its versatility to produce other types of polarization.

The circular polarization in a microstrip patch element (circular or square) can be easily achieved mainly using two approaches [1, 7]:

- **Using dual feed:** This technique consists of excite the two orthogonal modes by feeding the microstrip element in two orthogonal points with equal amplitude but with phase shift of 90° between them.

  By feeding the patch using microstrip lines, the structure becomes identical to the Fig.(2.13a), wherein the 90° phase shift is achieved with the addition of a section of quarter-wavelength microstrip line. Depending on the location of the phase shift, the LHCP or RHCP can be achieved.

  The arrangement to feed the two points of the patch with an equal amplitude and the desired phase shift, is accomplished either through a simple T-shaped power divider or using a hybrid power divider, which already has two delayed 90° outputs in its essence. This technique is, from the two presented, that which has wider circular polarization bandwidths.

- **Using single feed and creating physical asymmetries in the patch:** Producing small perturbations that cause asymmetry in the microstrip structure is an alternative technique to generating circular polarization in the patch element, since it allows to excite two orthogonal modes, and the perturbation lets to achieve an equal amplitude and 90° offset between the two modes.

  Fig.(2.13b) displays the most common perturbations of microstrip patches reported in the literature [1, 7], which consist of truncating the corners, creating a slot in the element, etc. Alternatively it is possible to generate circular polarization feeding the patches in its diagonal. The main disadvantage of this technique is its reduced circular polarization bandwidth.

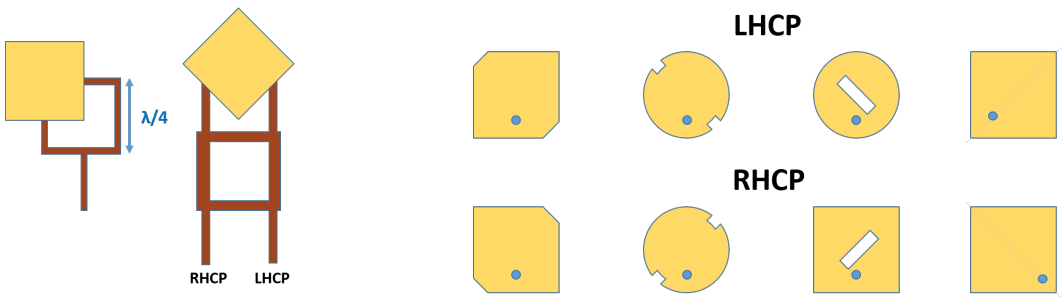

(a) Dual feed (b) Single Feed

Figure 2.13: Techniques to generate circular polarization in microstrip antennas

2.3 Antenna arrays

Usually the antennas as individual elements do not meet to the requirements of a number of applications of wireless communications, which often require specific radiation shapes (in terms of beamwidth, direction of maximum and nulls, sidelobes, etc..), characteristics that are hard to find using the standard antennas. To accomplish those requirements, is needed to group several antennas in a structure called antenna array.

An antenna array consists of a number of antennas placed in certain physical arrangement, and feed with a specific excitation in order to achieve a particular radiation pattern. This antenna configuration provides a vast number of benefits, including the possibility to obtain higher gains and directivities using simple radiating elements, which is important for long distance communications, as well as shaping the radiation pattern. Antenna arrays, by the processing of its received signals from its individual elements, and with a careful excitation of each element, allows to construct the increasingly used phased arrays and adaptive antennas, that improves several aspects of today's wireless communications, as multipath diversity gain, spatial filtering, interferences suppression, and steer the main lobe without moving the physically antenna.

In an antenna array, there are five main parameters that affect its radiation characteristics, which are selected according to the requirements, and changing them it is possible to shape the radiation pattern [1]:

- The number of elements and their geometric arrangement in the array, which may be linear, rectangular/square, circular, etc.
- The distance between the elements.
- The radiation pattern of each single array element used.
- The amplitude of excitation of each array element.
- The phase of excitation of each array element.

2.3.1 Array Factor

A generic array with identical elements and uniformly distributed according to a given configuration, can be characterized in a closed-form expression, function of the array geometry and of the excitation of its elements, called array factor (AF).

Two-Element Array

In the simplest example, consider an array of two elements, as shown in the Fig.(2.14). Each array element consists of an Hertzian dipole, placed along the z-axis (parallel to the y-axis), separated by a distance d, and feed by currents of equal amplitude I_0 and a phase difference of α, respectively $I_1 = I_0$ and $I_2 = I_0 e^{j\alpha}$.

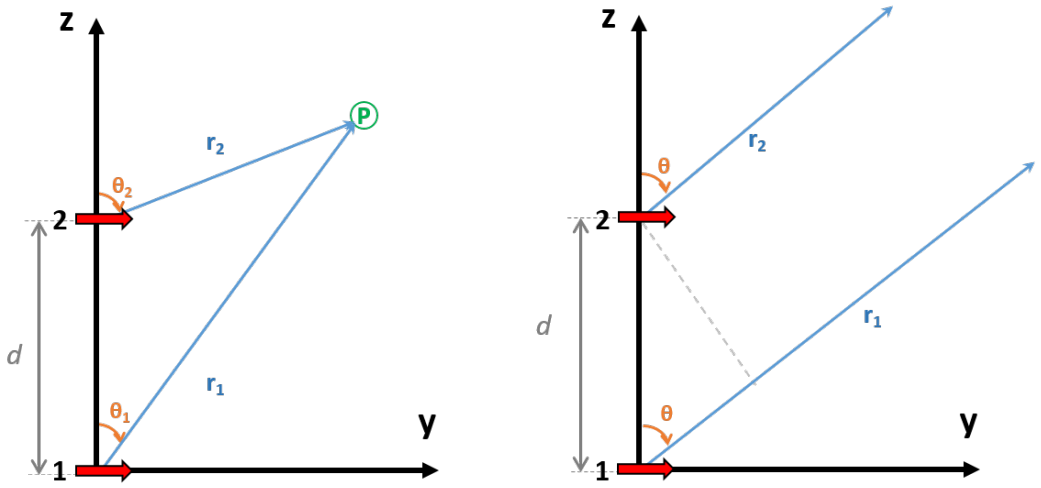

(a) generic local (P) observation (b) far-field observation

Figure 2.14: Two Hertzian dipole antenna array

According to Fig.(2.14a), the total electric field at a observation point P is the vector sum of the contributions from each element, expressed by the eq.(2.45).

$$\mathbf{E}_t = \mathbf{E}_1 + \mathbf{E}_2 = j\frac{\eta\beta\ell e^{-j\beta r_1}}{4\pi r_1}\,|\cos\theta_1|\,I_1\;\mathbf{a}_{\theta_1} + j\frac{\eta\beta\ell e^{-j\beta r_2}}{4\pi r_2}\,|\cos\theta_2|\,I_2\;\mathbf{a}_{\theta_2} \tag{2.45}$$

In a region sufficiently away from the antenna, guarantying the far field condition, the fields from each dipole can be considered nearly parallel, as illustrated in Fig.(2.14b), and therefore, the electric field vectors have the same direction, whereby some approximations can be made.

Far field approximations:

$$\theta = \theta_1 \approx \theta_2 \qquad 1/r = 1/r_1 \approx 1/r_2 \qquad e^{-j\beta r} = e^{-j\beta r_1},\; e^{-j\beta r_2} = e^{-j\beta(r - d\cos\theta)}$$

Thus, eq.(2.45) can be simplified,

$$\mathbf{E}_t = \left[j\frac{\eta\beta\ell e^{-j\beta r}}{4\pi r}\,|\cos\theta|\,I_0 + j\frac{\eta\beta\ell e^{-j\beta r}}{4\pi r}e^{j\beta d\cos\theta}\,|\cos\theta|\,I_0 e^{j\alpha}\right]\;\mathbf{a}_\theta \tag{2.46}$$

$$\mathbf{E}_t = \left[j\frac{\eta\beta\ell e^{-j\beta r}}{4\pi r}\,|\cos\theta|\,(I_0 + e^{j\beta d\cos\theta} I_0 e^{j\alpha})\right]\;\mathbf{a}_\theta \tag{2.47}$$

$$\mathbf{E}_t = \left[\underbrace{j\frac{\eta\beta I_0\ell e^{-j\beta r}}{4\pi r}\,|\cos\theta|}_{Element\ \ Factor}\underbrace{(1 + e^{j(\beta d\cos\theta+\alpha)})}_{Array\ \ Factor}\right]\;\mathbf{a}_\theta \tag{2.48}$$

Through eq.(2.48), it is possible to realize that the total electric field created by the array of two dipoles in far field, is equal to the electric field produced by one dipole (Element Factor) multiplied by a factor, known as array factor. This is one important property of the antenna array theory.

This example can be generalized to an array of N elements.

N-Element Linear Array

Considering the general case of N identical elements positioned along the z-axis, and spaced by distance d, creating a linear antenna array, as shown in Fig.(2.17).

Assuming also that the array is a uniform, which means that all elements are feed with equal amplitude and a progressive phase variation α, whereby $I_1 = I_0$, $I_2 = I_0 e^{j\alpha}$, $I_3 = I_0 e^{j2\alpha}$, ..., $I_N = I_0 e^{j(N-1)\alpha}$.

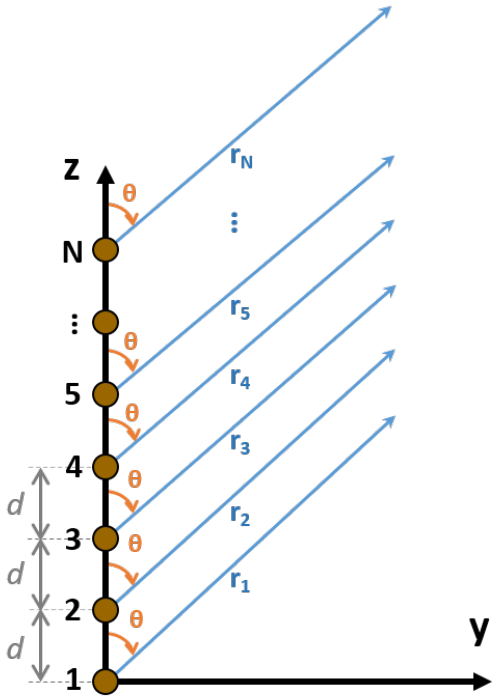

Figure 2.15: N-element uniform linear array

Applying the concepts referred in the aforementioned case a general formula for the array factor is obtained, given by [1]

$$AF = [1 + e^{j(\beta d \cos\theta + \alpha)} + e^{j2(\beta d \cos\theta + \alpha)} + e^{j3(\beta d \cos\theta + \alpha)} + \ldots + e^{j(N-1)[\beta d \cos\theta + \alpha]}] \tag{2.49}$$

This equation may also be simplified as a sum of exponentials [1],

$$\psi = \beta d \cos\theta + \alpha \tag{2.50}$$

$$AF = \sum_{n=1}^{N} e^{j(n-1)\psi} \tag{2.51}$$

Alternatively, with some mathematical management, the array factor can be expressed in a compact formula,

$$AF = e^{j(N-1)\frac{\psi}{2}} \left[\frac{\sin\frac{N\psi}{2}}{\sin\frac{\psi}{2}} \right] \tag{2.52}$$

When the reference point of the array is its physical center, the simplified expression for the array factor is given by eq.(2.53), and the eq.(2.54) represent the normalized array factor (in order to the maximum value be unitary).

$$AF = \frac{\sin\frac{N\psi}{2}}{\sin\frac{\psi}{2}} \tag{2.53}$$

$$AF_n = \frac{1}{N}\frac{\sin\frac{N\psi}{2}}{\sin\frac{\psi}{2}} \tag{2.54}$$

Some significant properties about the array factor of a uniform linear array:

Maximum - The principal maximum of the array factor, which also corresponds to the maximum of radiation (also known as main lobe), is one of the most important characteristics of the array factor, and therefore, of the antenna array.

The maximum is $AF_{max} = N$, and happens for $\psi = 0$,

$$\beta d\cos\theta_{max} + \alpha = \pm 2m\pi \quad \Rightarrow \quad \theta_{max} = \cos^{-1}(-\frac{\pm 2m\pi - \alpha}{\beta d}) \quad m = 0, 1, 2\ldots \tag{2.55}$$

The location of the maximum depends on the phase between elements α, but is independent of the number N elements. This fact is one of the fundamental principles adjacent to phased arrays theory, wherein it is possible to steer the position of the main lobe for a direction θ_x, applying a progressive phase shift between elements $\alpha_x = -\beta d\cos(\theta_x)$.

Antenna arrays can be classified according to the direction of its main lobe, as broadside array, or end-fire array.

- Broadside Array - The direction of the main lobe is normal to the array axis, ie, $\psi = 0,\ \theta = \pi/2 \Rightarrow \alpha = 0$.
- End-Fire Array - The direction of the main lobe is along the array axis, ie, $\psi = 0,\ \theta = 0$ or $\theta = \pi \Rightarrow \alpha = -\beta d$ or $\alpha = \beta d$.

Nulls - The nulls of the array factor represents the locals in which the $AF = 0$, ie,

$$AF = 0 \Rightarrow \sin(\frac{N\psi}{2}) = 0 \Rightarrow \frac{N\psi}{2} = \pm n\pi \tag{2.56}$$

$$\theta_{null} = \cos^{-1}(-\frac{\pm\frac{2n\pi}{N} - \alpha}{\beta d}) \quad n = 0, 1, 2, \ldots, n \neq N, 2N, 3N, \ldots \tag{2.57}$$

Side Lobes - The side lobes are the local maximums of the array factor. They are located between two consecutive nulls, near the points which the AF numerator reaches its maximum, ie,

$$\sin(\frac{N\psi}{2}) \cong \pm 1 \Leftrightarrow \frac{N\psi}{2} \approx \pm\frac{(1+2k)\pi}{2} \qquad k = 1, 2, 3, \ldots \tag{2.58}$$

$$\theta_{SL} = \cos^{-1}(-\frac{\pm\frac{(2k+1)\pi}{N} - \alpha}{\beta d}) \qquad k = 1, 2, 3, \ldots \tag{2.59}$$

The first side lobe happens at $\psi_{SL} = \pm\frac{3\pi}{N}$ and the amplitude of the first side lobe is achieved by substituting in eq.(2.54),

$$|AF_{1^{st}SL}| = \frac{\sin(\frac{N}{2}(\frac{3\pi}{N}))}{N\sin((\frac{1}{2})\frac{3\pi}{N})} = \frac{\sin(\frac{3\pi}{2})}{N\sin(\frac{3\pi}{2N})} = \frac{1}{N\sin(\frac{3\pi}{2N})} \tag{2.60}$$

which represents the Side Lobe Level (SLL).

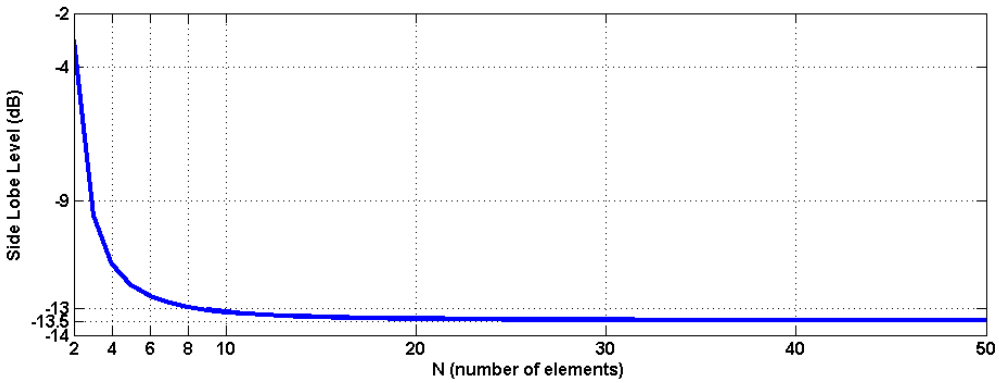

Figure 2.16: Variation of SLL of an uniform linear antenna array with the number of array elements

The Fig.(2.16) denotes the calculation of the SLL (in dB) through the eq.(2.60) with the increase of the number of array elements N. According to the figure, there is a limit to the minimum value of the first side lobe of a uniform array, when the number of elements tends to infinity, which is about -13.5dB relative to the main lobe.

Beamwidth - Regarding the beamwidth, the two main widths that characterizes the main-lobe of an array factor, and consequently an antenna, are the First-Null Beam Width (FNBW), and the Half-Power Beam Width (HPBW).

- **First-Null Beamwidth (FNBW)** -The FNBW is found calculating the difference between the positions of the first null $\theta_{null(n=0)}$ and the maximum $\theta_{max(m=0)}$, multiplied by two [1], ie,

$$\Theta_{FNBW} = 2\left|\theta_{max(m=0)} - \theta_{null(n=0)}\right| \tag{2.61}$$

- **Half-Power Beamwidth (HPBW)** - The HPBW is found calculating the difference between the position of the 3dB point θ_{hp}[1] and the maximum $\theta_{max(m=0)}$, multiplied by two, ie,

$$\frac{N\psi}{2} = \frac{N}{2}\beta d\cos\theta_{hp} + \alpha = \pm 1.391 \Rightarrow \theta_{hp} = \cos^{-1}(\frac{\frac{\pm 2.782}{N} - \alpha}{\beta d}) \tag{2.62}$$

$$\Theta_{HPBW} = 2\left|\theta_{max(m=0)} - \theta_{hp}\right| \tag{2.63}$$

2.3.2 $N \times M$ - Element Planar Array

Using a linear array, the elements are arranged along one axis, that defines the radiation plane which is possible to shape. Its orthogonal plane is only defined by the antenna element used.

A planar array is commonly used when is required a radiation pattern with some directivity in the two orthogonal planes of radiation. In such case, the array elements are arranged in a plane (ie defined by two axes). The most common geometries are the rectangular or square, as exemplified in the Fig.(2.17).

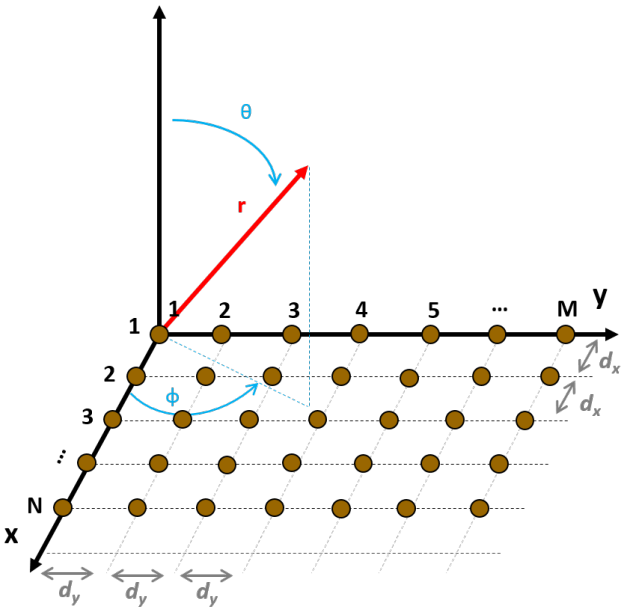

Figure 2.17: $N \times M$-element uniform planar array

Such arrays, typically by increasing the number of elements, provide higher versatility, enabling the beam shaping of the radiation pattern in the two main planes, increasing the gains and directivities, and also apply methods that enable the reduction of SLL.

Another important feature is the ability to steer the radiation pattern toward any local (θ, ϕ) in space, which is particularly important in radar or satellite applications.

A uniform planar array in the xoy-plane, can be analyzed as a uniform linear array of N elements spaced by d_x, along the x-axis, where each of its elements is thereof a uniform linear array of M elements spaced by d_y, along the y-axis.

This is the simple rule to obtain an expression of the total array factor that enable to characterize this type of arrays.

A linear array of N elements, spaced by d_x, placed along the x-axis, and with each element feed with an amplitude a_{xn} and α_x progressive phase shift, can be represented by the following array factor,

$$AF_x = \sum_{n=1}^{N} a_{xn}\, e^{j(n-1)\psi_x} \qquad \psi_x = \beta d_x \sin\theta \cos\phi + \alpha_x \tag{2.64}$$

if each element of array, forms an array of M elements, spaced d_y along the y-axis, each element feed by an amplitude a_{ym} and with a progressive phase shift α_y represented by,

$$AF_y = \sum_{m=1}^{M} a_{ym}\ e^{j(m-1)\psi_y} \qquad \psi_y = \beta d_y \sin\theta \sin\phi + \alpha_y \tag{2.65}$$

then, the array factor of the planar array of $N \times M$ elements is given by,

$$AF = \sum_{n=1}^{N} a_{xn} \left[\sum_{m=1}^{M} a_{ym}\ e^{j(m-1)\psi_y} \right] e^{j(n-1)\psi_x} \qquad AF = AF_x \times AF_y \tag{2.66}$$

If the array planar is uniform, ie the amplitude of each element $a_{nm} = a_{xn} \times a_{ym}$ is equal for all elements, then, from the eq.(2.54), the normalized array factor can be represent by the following expression

$$AF(\theta,\phi)_n = \left\{ \frac{1}{N} \frac{\sin(\frac{N\psi_x}{2})}{\sin(\frac{\psi_x}{2})} \right\} \left\{ \frac{1}{M} \frac{\sin(\frac{M\psi_y}{2})}{\sin(\frac{\psi_y}{2})} \right\} \tag{2.67}$$

2.3.3 Nonuniform Amplitude Excitations

Most of the times using uniform antenna arrays, linear or planar, it is hard to reach some requirements for the array characteristics, in particular the radiation pattern properties (sidelobes, the mainlobe width's, etc.).

There are a number of techniques described in the literature, which being adjusted to each circumstance, and applied to the arrays allow to improve some of these characteristics. These techniques are mainly based on nonuniform amplitude distributions to feed each element of the array, and some of them are presented below.

Binomial Coefficients

Binomial arrays are characterized by the amplitudes of excitation of their elements follow a binomial distribution, ie, its amplitudes correspond to the binomial series expansion coefficients [1, 10, 11] given by,

$$(1+x)^{q-1} = 1 + (q-1)x + \frac{(q-1)(q-2)}{2!}x^2 + \ldots \tag{2.68}$$

in this case q corresponds to the number of elements of an array N. (E.g. $N = 4 \rightarrow q = 4, \Leftrightarrow (1+x)^{4-1} = \underline{1}x^3 + \underline{3}x^2 + \underline{3}x + \underline{1}$)

Calculating this distribution for a number of q values, results in the following triangle of amplitudes, also known as pascal's triangle.

q=1					1					
q=2				1		1				
q=3			1		2		1			
q=4		1		3		3		1		
q=5	1		4		6		4		1	
q=6	1	5		10		10		5		1

These arrays have the great benefit of produce very low SLL, (or even having none, using $d \leq \lambda/2$). Binomial arrays are also characterized by presenting wider beamwidth's than uniform array, and show a significant variation of amplitudes between their elements. This fact can be considered a disadvantage of this distribution since require more complex (and less efficient) array feed networks.

Dolph-Chebyshev Method

Dolph [12] in 1946 proposed a method for the synthesis of array patterns based on their approximation by Chebyshev polynomials. This technique is usually applied to design antenna arrays constrained by the SLL, and for the particular case of SLL=$-\infty$, it reduces to the binomial method [1]. The Chebyshev method is a compromise between uniform arrays and the binomial method, since for a given SLL, this method presents the higher directivity and the narrowest beamwidth [1, 11].

Considering a linear array with an even or odd number of elements, centered on the axis (positioned symmetrically), the array factor given by eq.(2.51), normalized, can be expressed by the following equations [1, 11], ie a sum of cosine terms.

$$AF_{(even:N=2M)} = \sum_{n=1}^{M} a_n \cos((2n-1)u) \tag{2.69}$$

$$AF_{(odd:N=2M+1)} = \sum_{n=1}^{M+1} a_n \cos((2n-1)u) \tag{2.70}$$

$$u = \frac{d\pi}{\lambda}\cos(\theta) \tag{2.71}$$

By theory [1, 10, 11], it is known that a cosine whose argument is an integer multiple of a fundamental frequency, can be decomposed into a sum of several cosines at fundamental frequency, as shown below for various integer values of m (after a mathematical process using the trigonometric identities),

$$\begin{aligned}
&m = 0 \quad \cos(mu) = 1 \\
&m = 1 \quad \cos(mu) = \cos(u) \\
&m = 2 \quad \cos(mu) = \cos(2u) = 2\cos^2(u) - 1 \\
&m = 3 \quad \cos(mu) = \cos(3u) = 4\cos^3(u) - 3\cos(u) \\
&m = 4 \quad \cos(mu) = \cos(4u) = 8\cos^4(u) - 8\cos^2(u) + 1 \\
&\qquad\qquad \vdots
\end{aligned} \tag{2.72}$$

taking $x = \cos(u)$, the expressions in (2.72) becomes a set of polynomials, that correspond to Chebyshev polynomials of m-degree. These polynomials are in accordance with the recursive formula presented to determine the polynomials Chebychev based on the previous two. These

relations are verified to values of x belonging to the interval [-1,1].

$$\begin{aligned} m=0 \quad & \cos(mu) = T_0(x) = 1 \\ m=1 \quad & \cos(mu) = T_1(x) = x \\ m=2 \quad & \cos(mu) = T_2(x) = 2x^2 - 1 \\ m=3 \quad & \cos(mu) = T_3(x) = 4x^3 - 3x \\ m=4 \quad & \cos(mu) = T_4(x) = 8x^4 - 8x^2 + 1 \\ & \vdots \\ & T_m(x) = 2x\, T_{m-1}(x) - T_{m-2}(x) \end{aligned} \tag{2.73}$$

Another way to calculate the Chebyshev polynomials is,

$$T_m(x) = \cos(m \cos^{-1}(x)) \qquad -1 \leq x \leq 1 \tag{2.74}$$

$$T_m(x) = \cosh(m \cosh^{-1}(x)) \qquad x < -1, x > 1 \tag{2.75}$$

Some important characteristics of Chebyshev polynomials [1, 11]:

a) all polynomials, regardless of their order, pass through the point (1,1).

b) all the zeros of the polynomials occur in the interval $-1 \leq x \leq 1$.

c) in the interval $-1 \leq x \leq 1$, the values of polynomials are between -1 and 1, and its maxima and minima are 1 and -1 respectively.

d) for $x > 1$ the function is always increasing.

The idea behind this method involves to achieve an array factor with a similar behavior of the Chebyshev polynomials, imposing the occurrence of the side lobes in the region $-1 < x < 1$ (which presents a unitary maximum amplitude) and its main lobe in zone $x > 1$, in a position x_0 such that enable a ratio between the amplitude of the main lobe and sidelobes as required.

Since the array factor can be represented as a sum of cosines with a format identical to the Chebyshev polynomials, the coefficients (excitation amplitude) of the array factor will be determined corresponding its terms to the terms of the Chebyshev polynomials, of order $m = N - 1$, being N the number of elements of the array.

Design Procedure:

1. select the expression of the array factor, depending on the number of elements N, equation (2.71)
2. extend the array factor, and replace each term $\cos(mu)$ by the respective expansion in terms of $\cos(u)$, through (2.72)
3. using the required side lobe ratio (SLR) (in dB), calculate the voltage ratio R_0, and using equation (2.75) obtain factor x_0

$$R_0 = 10^{\frac{SLR(dB)}{20}} \tag{2.76}$$

$$R_0 = T_{N-1}(x_0) \quad \Rightarrow \quad x_0 = \cosh\left(\frac{\cosh^{-1}(R_0)}{N-1}\right) \tag{2.77}$$

4. replace the term $\cos(u)$ by x/x_0 in the expression of the array factor.

5. equate the expression of the array factor (previous step), to the Chebyshev polynomial equation $T_{N-1}(x)$, and determine the coefficients a_n.

Taylor One-Parameter Distribution

Taylor used the pattern of a uniformly excited aperture of type $\sin(\pi u)/\pi u$, whose side lobes fall asymptotically according to $1/u$, being the amplitude of the first side lobes the main problematic.

Taylor refers that the height of each side lobe is influenced by the nulls pattern position, which are placed in integer values of u, with $u = (d/\lambda)\sin\theta$. To reduce the principal side lobes, Taylor proposed to shift its close-in zeros [1, 13, 14, 15] to,

$$u = \sqrt{n^2 + B^2} \tag{2.78}$$

where B is a real and positive parameter that controls a number of characteristics, such as the SLL, beamwidth, and the efficiency. This parameter can be determined by solving the following equation for a given value of SLR (the inverse of SLL),

$$SLR(dB) = 20\log(\frac{\sinh(\pi B)}{\pi B}) + 13.26dB \tag{2.79}$$

the pattern using the taylor distribution is then,

$$SF(u) = \begin{cases} \frac{\sinh(\sqrt{B^2-u^2})}{\pi\sqrt{B^2-u^2}} & u \leq B \\ \\ \frac{\sin(\pi\sqrt{u^2-B^2})}{\pi\sqrt{u^2-B^2}} & u \geq B \end{cases} \tag{2.80}$$

The source distribution is given by,

$$I_n(z) = J_0\left[j\pi B\sqrt{1-\left(\frac{2z}{l}\right)^2}\right] \qquad -\frac{l}{2} \leq z \leq \frac{l}{2} \tag{2.81}$$

where J_0 is the Bessel function of first kind and zero order, and l is the length of the continuous source.

Applying to an array of N discrete elements with a spacing between elements d,

- odd number of elements: $N = 2M + 1$,

$$z_m = md \qquad m = 0, \pm 1, \ldots, \pm M \tag{2.82}$$

- even number of elements: $N = 2M$,

$$\begin{cases} z_m = d\frac{2m-1}{2} & 1 \leq m \leq M \\ \\ z_m = d\frac{2m+1}{2} & -M \leq m \leq -1 \end{cases} \tag{2.83}$$

2.3.4 Circular Polarization using Antenna Arrays

Usually, the generation of circular polarization in an antenna array is performed simply by using circularly polarized elements. When are used microstrip elements, the techniques were described above, with the problem of the methods that use single feed patches, present narrow circular polarization bandwidths.

In the literature is reported a technique that creates circular polarization in antenna arrays, known as technique of sequentially rotation [16]. This method consists of physically rotate the feeding point of the elements on a sub-array structure, followed by the corresponding phase shift in the feeding of each element. This technique creates circular polarization, with a significantly wider bandwidth ($\geq$ 10%), and the elements of the array can be linearly or circularly polarized [16, 17].

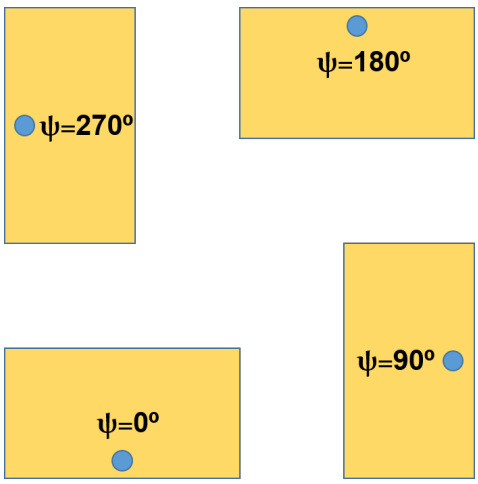

Figure 2.18: Sequential rotated technique: 2×2 sub-array with 0º, 90º, 180º, 270º arrangement

The rotation can be performed by distributing the various elements according to the angles $0^o, 90^o, 0^o, 90^o$, or in the most common way, with the $0^o, 90^o, 180^o, 270^o$ rotations, as shown in the Fig.(2.18). The second arrangement provides an advantage over the first, since undesired radiation due to higher modes is canceled [16, 17].

The great advantage of using this technique is the huge increase in circular polarization bandwidth ($\geq$ 10%) and reduction of the mutual coupling between elements due to the orthogonal position of the neighboring elements.

Chapter 3

Antennas for Dedicated Short Range Communications

The growth of wireless communications in recent decades has been evident in several areas of application, one example is the industry of transportation, combining the constant development of vehicle technologies and intelligent transport systems (ITS), enabling a number of new features and applications, contributing to minimize important concerns such as accidents, traffic jams or pollution.

The Dedicated Short-Range Communications (DSRC) [18, 19] is the wireless technology used to implement a vehicular network with a low latency communication, essential for the use by safety applications. In a DSRC system there are mainly two types of equipments, as shown in the Fig.(3.1), the On-Board Units (OBU) placed into the vehicles, and the Road Side Units (RSU) located at the fixed infrastructures in the roads, enabling to establish Vehicle-to-Vehicle (V2V) and Vehicle-to-Infrastructure (V2I) communications, being regulated by a group of standards set forth below, and used by different applications and services.

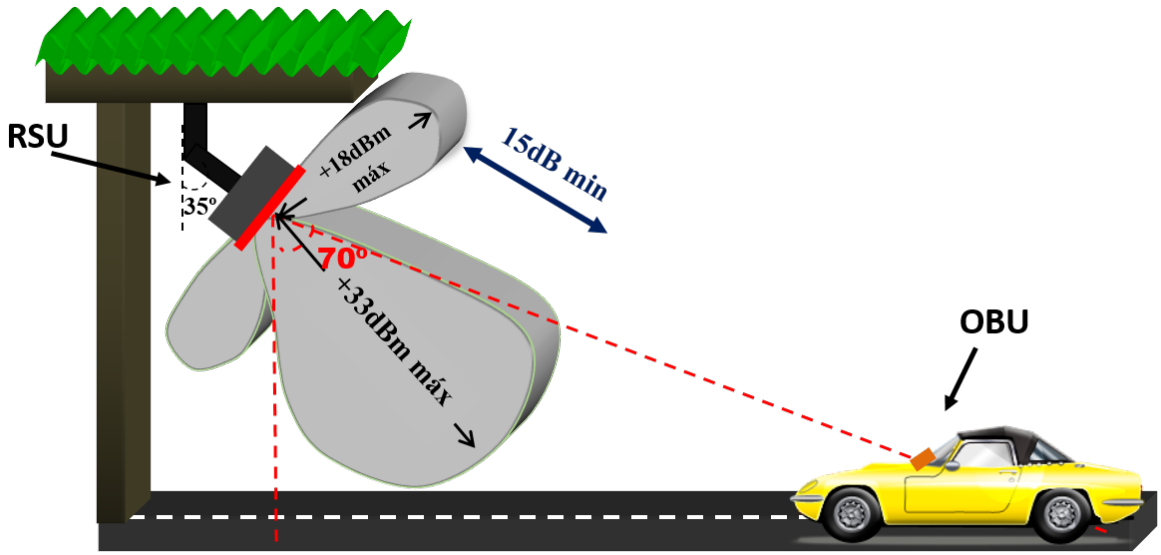

Figure 3.1: DSRC System

3.1 DSRC Standards and Applications

The DSRC in Europe, operates in two frequency bands, as shown in Fig.(3.2), in the region of 5.8GHz using a ISM (Industrial, Scientific and Medical) band, particularly for tolling applications, and at 5.9GHz for ITS applications, being regulated by a set of standards.

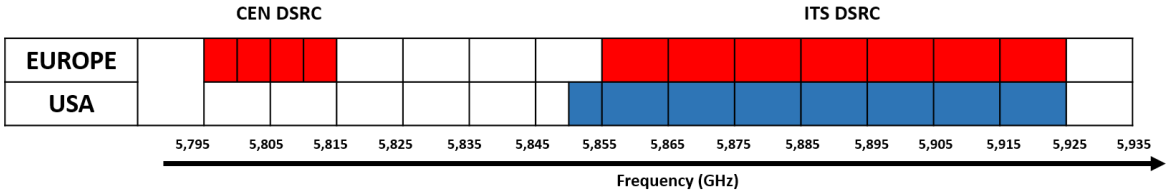

Figure 3.2: DSRC frequency bands

ITS DSRC operates in Europe, in a 70MHz band (75 MHz in the USA due to a guard band of 5 MHz at the beginning), from 5.855 GHz to 5.825 GHz, as shown in Fig.(3.2). It consists of 7×10 MHz channels with a maximum EIRP of 33 dBm (depending on the channel). The IEEE802.11P [20], adapted from the IEEE802.11a, is the standard that specifies the ITS DSRC. The European standards ETSI 202-663 [21] and ETSI 302-571 [22] gathers the characteristics profile for the physical and medium access control layer of ITS operating in the 5 GHz frequency band.

The CEN DSRC band is primarily used for electronic payments, and its framework in Road Transport and Traffic Telematics (RTTT) environment is defined by standards: EN12253, EN12795, EN12834 and EN13372, for each layer of the DSRC architecture, physical, data link, application and management respectively. The EN12253 [23] standard specifies the physical layer of the DSRC system, presenting the requirements for the medium of communication between RSU and OBU, including a number of important parameters.

The most significant constraints for the RSU antenna design are summarized below.

- **Frequency** - The standard establishes a minimum of 20 MHz bandwidth, covering the 4×5MHz communication channels, as shown in Fig.(3.2), with the carriers centered at:
  - CH1 - 5.7975 GHz
  - CH2 - 5.8025 GHz
  - CH3 - 5.8075 GHz
  - CH4 - 5.8125 GHz
- **Radiation Properties** - These radiation characteristics are illustrated in Fig.(3.1). The standard limits the EIRP to +33dBm up to an angle of 70° with the vertical, whereas outside this region, the power may not exceed +18 dBm. This restriction involves for the RSU antenna:
  - $SLL \leq -15$ dB
  - $HPBW_{vertical\ plane} \leq 70^{o}$
  - $HPBW_{horizontal\ plane}$ - depends on the application
- **Polarization** - The polarization of the electromagnetic waves should be LHCP, with a rejection of the RHCP component of:

  - $\geq 15\,\text{dB}$ - in boresight
  - $\geq 10\,\text{dB}$ - in the zone where the gain drops 3dB (half power)

The V2V communication opens news perspectives for on-road safety. Cars may serve as mobile sensors, collecting and sharing a range of sensed information related to the car, the driving conditions, the road, the traffic, and the environment. This data can be uploaded through the infrastructures to be queried by other cars or by some monitoring data center. V2I communications allow internet access from cars, which can maintain the car occupants entertained and informed, and can potentially generate services and applications especially for in-car use.

The DSRC applications, V2V or V2I, can be divided into two main groups: Safety and Non-Safety.

Examples of Safety applications:

- Vehicle collision avoidance
- Extended Electronic brake lights
- Approaching Emergency Vehicle warning
- Emergency alerts
- Several Hazard Warnings on the road
- Highway-rail intersection warning

Examples of Non-Safety applications:

- Electronic payments:
  - tolls
  - car parks
  - gas stations
- Access control
- Navigation and Traffic management
- Internet access
- Signing of vehicles

Electronic payments consist of one of most used V2I applications, with a great development, first for road tolling, and today already are deployed also in car parks, or gas stations, due to the comfort and convenience that it allows to the users. The vehicles do not need to stop, avoiding the establishment of long queues to make payments, saving time and fuel, and contributing to improvements from the environmental point of view.

This work was focused on the application of Electronic toll collection (ETC) on highways. In the coming sections, multiple antennas are proposed for the different equipments of a DSRC system, OBU and RSU, aiming to apply in an ETC system in highways, although its application, mostly, can be extended to other DSRC applications.

3.2 The OBU antenna

The On Board Unit is the mobile device of a DSRC system, located inside the vehicle or in its structure. These devices are typically located at a 1.5 m height relative to the road level, with an angle which ensures the better communication with the RSU (typically affixed to the windshield).

The RSU sends a beacon signal (ASK modulated) and waits for an OBU response, which is commonly in the sleep-mode, to save energy. When a vehicle (with an OBU) enters the communication zone, the OBU wakes-up and starts to communicate. Then, by applying the backscattering method, the OBU uses this carrier to modulate a sub-carrier, and then sends it back to the RSU.

The OBU antenna should ensure the compact and lightweight characteristics, and fully compliant with European DSRC standards. The antenna should therefore have the necessary bandwidth according to its application in CEN, ITS DSRC, or both. The radiation pattern should be omnidirectional for ITS applications, or unidirectional with a main lob width of 70^{o} in the vertical plane, for tolling applications. The polarization should be LHCP with a cross polarization rejection greater than 10 dB in boresight direction and greater than 6 dB within the zone when the gain drops 3 dB.

Several antennas have been proposed over the years for vehicular applications, particularly for use inside the OBU module.

In [24, 25, 26] are provided some dual-band antennas using different configurations, to work with GPS and DSRC bands. Regarding to the DSRC, there are solutions at 5.8 GHz (CEN) and ITS band (5.9 GHz). In terms of bandwidths, these antennas cover the frequencies of interest, whereas the radiation pattern is broadside and asymmetric, although with some back radiation. [27] proposes a microstrip dual band antenna for vehicular applications in Japan. The antenna consists of two square patches, a dielectric substrate and an air layer. The upper patch is shorted to the lower patch. The antenna operates at 5.8 GHz, with circular polarization.

In [28] is described the design of a microstrip antenna for DSRC applications with reconfigurable circular polarization (between right-handed and left-handed) using PIN diodes. The antenna is a circular patch, fed by a coplanar-waveguide diagonal slot, and its radiation pattern is semi-spherical, as the element is a microstrip patch. In [29, 30, 31] are shown three antennas, circularly polarized and designed for 5.8 GHz to DSRC applications. These antennas consist of square patches using FR-4 substrate, fed by coupling at a single point and in two orthogonal points, and finally using an air layer to increase the bandwidths (larger than 1 GHz) and manufacturing tolerances.

In general, most of antennas have been developed for DSRC applications which communicate in a single direction, such as tolling systems, since its OBU are mainly constituted by microstrip antennas, with hemispherical radiation patterns.

For the new ITS applications, it is desirable that the communication be established regardless of the vehicle position, i.e, that the vehicles are able to communicate with each other or with nearby infrastructures regardless if they are in front, side or even behind them. It is therefore important that the antennas that constitute the new OBUs may have an omnidirectional radiation patterns in the road plane (horizontal).

The dipoles and monopoles are the group of antennas that allow to achieve these radiation features in an easy way [1].

3.2.1 Printed Monopole

The use of monopole rather than dipole is just because monopole allows to achieve a more compact antenna. Moreover, the printed monopole antenna combines the main characteristics of planar printed antennas and the monopole antennas in terms of the omnidirectional radiation pattern in horizontal plane, the compactness and the easiness to produce at low cost, characteristics of the printed antennas.

The planar monopole antenna can be considered as a variation of microstrip antennas in which the ground plane is located at infinity (assuming a large value of h substrate thickness) [32]. Many configurations of printed monopole antennas have been proposed and discussed to be used with a wide or ultra-wide impedance bandwidth [33].

In this scope, the following scientific contributions were achieved, **[C1]**, **[C2]**, **[C3]** with antenna solutions for OBU module of a DSRC system, which culminate with an innovative approach for a printed monopole structure with LHCP radiated omnidirectionally on the road plan. These antennas are provided below.

Linearly Polarized Printed Monopole

A printed linear monopole antenna is presented as the first approximation to the radiation requirements for an OBU, compatible with the ITS DSRC applications, including the essential omnidirectional radiation.

This work is part of a paper **[C1]** accepted by the scientific community, and that was presented at an international conference.

In its traditional form, a monopole (as a dipole) produces linear polarization. This antenna ensures the functionality of a DSRC system, communicating in an omnidirectional way, however, due to the linear polarization, it is assumed losses of 3 dB in the communication, since the RSU transmits circularly polarized waves.

In [34, 35] are presented two rectangular monopole antennas with some changes in its physical structure in order to obtain ultra-wide bandwidths. However, their complexity is avoidable, considering that simpler solutions have wide bandwidths enough to DSRC communications applications. In [36] a printed monopole antenna is shown with a physical structure more elaborated, but although it shows an omnidirectional radiation pattern in the horizontal plane, its dimensions are relatively large for the intended application in this work.

This monopole, shown in the Fig.(3.3a), has a rectangular shape, printed on the upper side of the dielectric substrate, while the bottom side is partially filled with conductive material, operating as a ground plane, finally a microstrip line is designed to feed the monopole. In this configuration was also performed a smooth transition between the transmission line and the monopole to create a wideband performance. Its main characteristics are simplicity and small size, which are crucial features for this application.

The monopole was designed using the dielectric substrate Arlon CuClad217, which has as main properties a relative dielectric constant of $\epsilon_r = 2.17$, a thickness $h = 0.787\,\text{mm}$ and a loss tangent $\tan\delta = 0.0009$. Its dimensions are shown in Table (3.1).

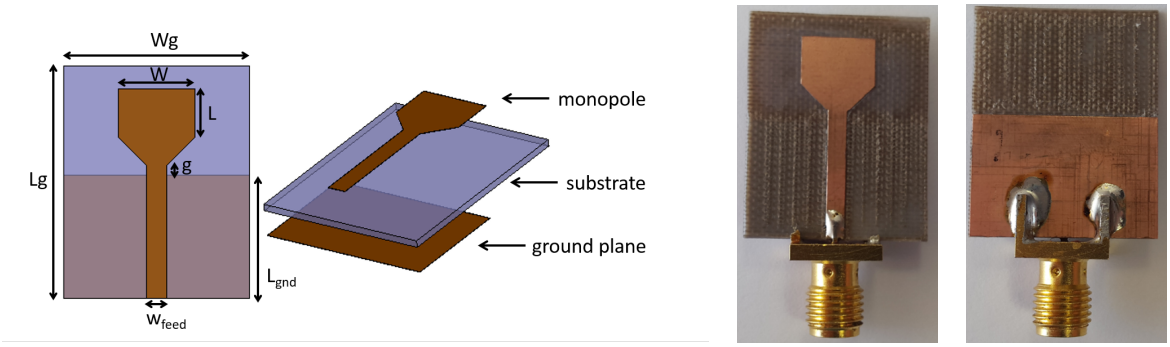

(a) Linear Polarized Printed Monopole (b) Top View (c) Bottom View

Figure 3.3: Designed structure of printed monopole antenna and manufactured photography

Table 3.1: Dimensions of printed monopole linearly polarized

Parameter	W_g	L_g	L_{gnd}	w	l	g	w_{feed}
Dimension (mm)	20	25	13.3	8.2	5.37	1	2.2

The antenna was designed and simulated using HFSS electromagnetic simulator [37], and then manufactured and characterized according to its main parameters. The prototype is shown in Figs.(3.3b) and (3.3c).

The results are presented in the Figs.(3.4) and (3.5). Since the manufacturing process using this substrate is limited and with poor quality (although the substrate is good, it is too soft for the CNC milling machine), the measured results are not perfect, however it is possible to see similar behaviors.

Fig.(3.4) shows the simulated and measured S_{11} of the antenna. Assuming as a good impedance matching an S_{11}<-10 dB, the printed monopole designed shows a simulated 4 GHz bandwidth [4.8 - 8.8]GHz covering all DSRC frequency bands. In the DSRC 5.8/5.9 bands it has a measured S_{11} <-20 dB.

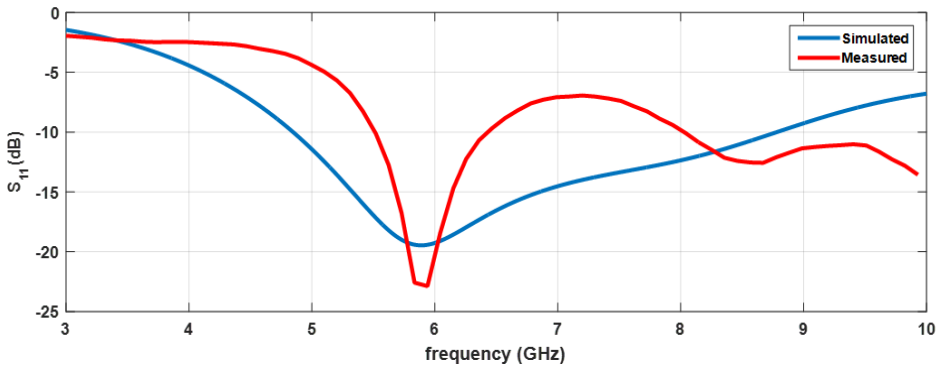

Figure 3.4: S_{11} simulated and measured of the designed monopole

In the Fig.(3.5) is presented the 2D simulated and measured radiation pattern of the designed monopole at 5.9 GHz, in the two main orthogonal planes, $\theta = 0^o$ and $\theta = 90^o$ (using

the monopole in the vertical position). It should be considered that the anechoic chamber used has a shadow zone, so, it was only possible to measure the vertical plane between -110° and 110° angles.

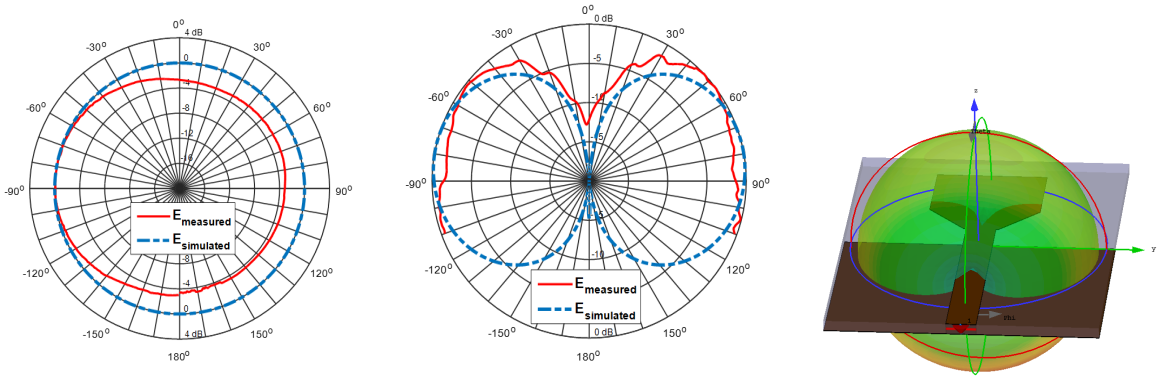

(a) Horizontal Plane - $\theta = 90°$ (b) Vertical Plane - $\theta = 0°$ (c) 3D Radiation pattern

Figure 3.5: Simulated and measured radiation pattern of the designed monopole

It is possible to observe that the antenna radiates in omnidirectional way in the horizontal plane ($\theta = 90°$), Fig.(3.5a), whereas in the vertical plane ($\theta = 0°$) also follows the typical radiation characteristic of this type of antenna, commonly referred as *donut cut or '8'*.

The measured gain of monopole was 3.4 dB and the 3D radiation pattern is shown in Fig.(3.5c), illustrating the radiation shape (*donut*), characteristic of this type of antennas.

Circularly Polarized Printed Monopole

A printed circularly polarized monopole antenna was designed as a second approach to overcome the signal loss of 3dB in the communication between OBU and RSU, due to linear polarization. This monopole was designed according to a configuration that allows circular polarization generation using an asymmetric feeding and with a slit in the ground plane.

This work is also part of the paper **[C1]** accepted by the scientific community, and was presented at an international conference.

As already mentioned, the OBU should have an antenna with an omnidirectional radiation on the road plane, with LHCP. To obtain circular polarization in a printed monopole antenna, [38] uses an asymmetrical feeding with a slit cut in a ground plane, in order to excite two orthogonal fields with phase difference of 90 degrees and equal amplitude. In [39] a printed y-shaped monopole antenna with circular polarization is proposed. This antenna also presents identical problems as [38], without an omnidirectional LHCP.

The developed antenna is a circularly polarized square printed monopole as is shown in Fig.(3.6). The radiator element is feed asymmetrically with a cut corner, and a slit in ground plane, all to generate the circular polarization.

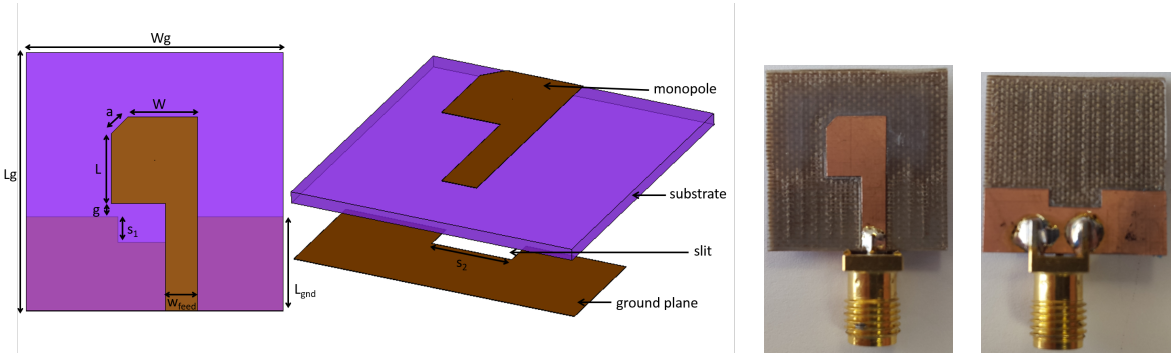

(a) Circularly polarized printed monopole (b) Top View (c) Bottom View

Figure 3.6: Designed structure of printed monopole antenna and manufactured photography

The substrate used is Arlon CuClad 217, which has a relative dielectric constant of $\epsilon_r = 2.17$, a thickness $h = 0.787\,\text{mm}$ and a loss tangent $\tan\delta = 0.0009$. To help to design the solution, the electromagnetic simulator HFSS [37] was used.

The dimensions of the designed monopole are presented in the Table (3.2), showing a reduced global size, which is an important feature to have a compact OBU module.

Table 3.2: Dimensions of printed monopole circularly polarized

Parameter	W_g	L_g	L_{gnd}	w	l	g	w_{feed}	a	$s1$	$s2$
Dimension (mm)	20	20	7.3	6.7	6.7	1	2.4	1.8	2	5.7

The monopole was manufactured, as shown in Figs.(3.6b) and (3.6c), and was characterized according to its main parameters. The results are presented in the Figs.(3.7) - (3.9).

As in the previous prototype, some problems happened in the manufacturing process due to the physical characteristics of the substrate. Possibly due to the manufacturing quality of this antenna and the accuracy of its dimensions, it is possible to observe some deviations in terms of simulated and measured results.

Fig.(3.7) shows the simulated and measured S_{11} of the monopole. Assuming the $S_{11} < -10\,\text{dB}$ as the criterion for a good impedance matching, according to the figure is possible to notice a measured 1.8 GHz band in with the antenna is well matched.

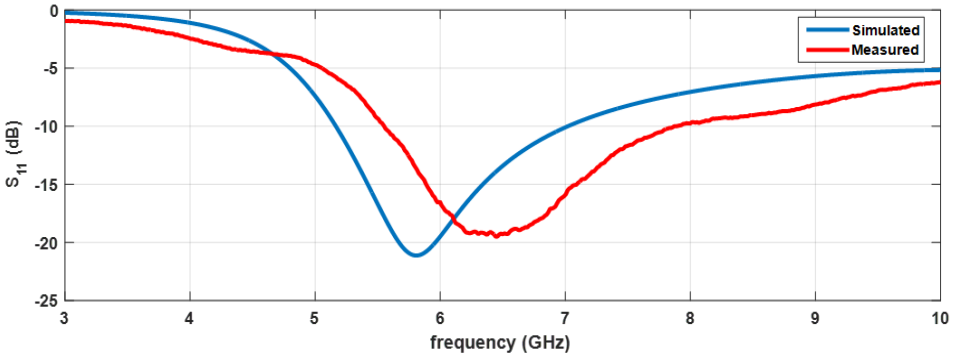

Figure 3.7: S_{11} simulated and measured of the designed monopole

According to the circular polarization bandwidth, using as a criterion for a good circular polarization the well accepted criterion of AR<3 dB, the Fig.(3.8) shows that the monopole has a 900 MHz simulated band within a good circular polarization.

In terms of measured results, the antenna has an axial ratio higher than 3 dB (about 5/6 dB) which results in a polarization almost circular, but still elliptic, (but far from being linear) and is possibly due to manufacturing problems.

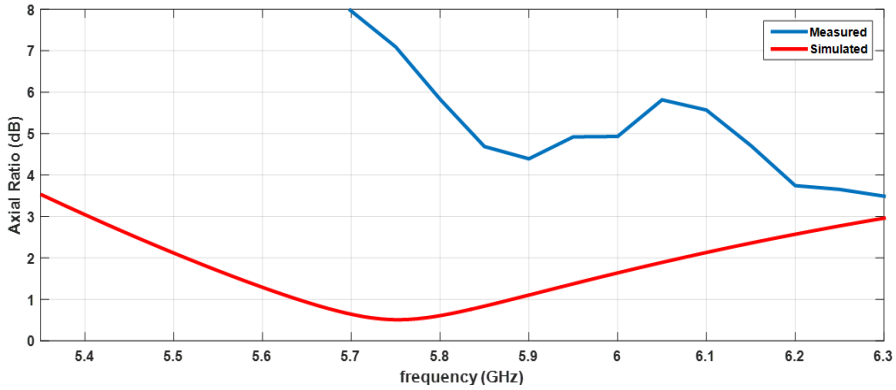

Figure 3.8: Simulated and measured axial ratio of the designed monopole

In Fig.(3.9) is shown some radiation pattern results, in terms of E_{LHCP} and E_{RHCP} components. According to the Fig.(3.9a), it is possible to notice that the LHCP only overcomes the right hand, in half of the radiation pattern, with a good rejection between the two components. In the opposite side, the principal polarization is the RHCP, with good rejection of the orthogonal component.

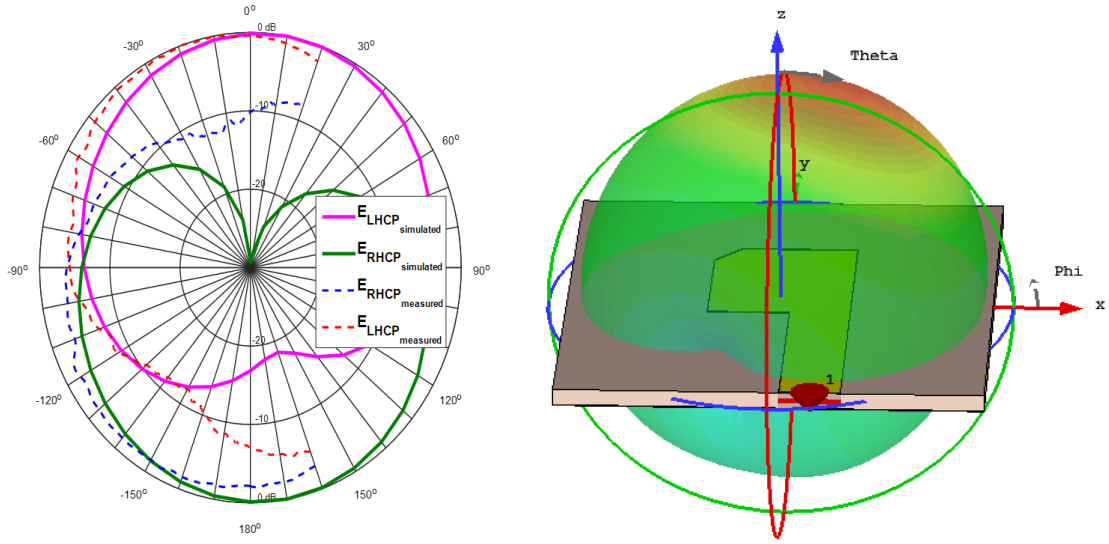

(a) Horizontal Plane - $\theta = 90°$ (b) 3D Radiation pattern

Figure 3.9: Simulated and measured radiation pattern of the designed monopole

In terms of measured results, the behavior of the two curves is similar to the simulated results, although (as the axial ratio is poor) there isn't a sufficiently good rejection between the two components. The 3D antenna radiation pattern is shown in Fig.(3.9b) and the simulated gain is 2.5 dB.

Although the monopole presents a small size and a nearly omnidirectional radiation pattern, with wide impedance matching and axial ratio bandwidths, this solution cannot be used in the OBU, due to the domain of right circular polarization in a part of radiation pattern which would involve a non-communication in one direction.

3.2.2 Printed Monopole with Omnidirectional Circular Polarization

A new approach to overcome the difficulty to get an omnidirectional circular polarized radiation pattern (with the same sense) is presented, and an antenna structure was proposed and simulated, showing an omnidirectional LHCP radiation pattern together with compact dimensions and a wide bandwidth over 2 GHz, covering the DSRC frequency bands.

The work done allowed to publish two scientific contributions, accepted, presented and discussed in two reputable international conferences **[C2]** and **[C3]**.

According to the previous results, it is possible to generate circular polarization in a printed monopole antenna. However, it was also verified that the LHCP wasn't accomplished in an omnidirectional way of the radiation pattern, property that is essential for vehicles being able to communicate independently of its position, and consequently, the considered antennas do not correspond to the ITS DSRC demands.

The main objective was then, to design an antenna that presents simultaneously an omnidirectional and LHCP radiation pattern, rejecting the right hand of polarization. The considered approach in the design of this antenna started from the previous circularly polarized printed monopole. The main idea was to replace the region of undesired polarization by a radiation with the opposite (and desired) polarization.

It could be performed using a second equal monopole, symmetrically placed on the back of the first monopole, in such way that, the LHCP could be reached in two spatial semi-spheres (wherein each monopole has LHCP). The problem has become the radiation between the two monopoles (undesired), with the RHCP waves, since the monopoles radiate in an omnidirectional way. To overcome this undesired radiation, a structure with absorbing characteristics has been used, because it allows to suppress the unwanted RHCP radiation, without affecting the other properties of the arrangement composed by the two monopoles.

The use of absorbent materials is frequent in microwave applications, to reduce or suppress the impact of interference radiation. The electromagnetic absorbent materials are those that attenuate the intensity of the field which affect them, by different types of losses.

In such materials the complex relative permeability $\mu_r = \mu'_r - j\mu''_r$ and complex relative permittivity $\epsilon_r = \epsilon'_r - j\epsilon''_r$ are fundamental physical parameters to estimate its attenuation and reflection characteristics. The absorption process happens due to the high magnetic property of the material, that concentrates the electromagnetic waves in the material. One of the well-known absorbent materials, which also incorporate several elements which compose anechoic chambers is the Ferrite. The Ferrites have both high value of μ_r and ϵ_r.

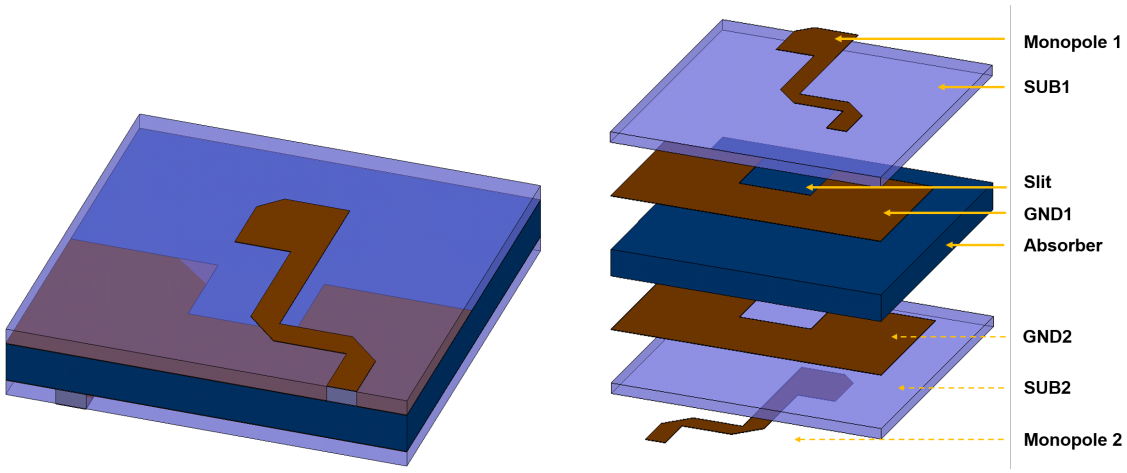

(a) Printed monopole (b) Layer structure view

Figure 3.10: Designed printed monopole antenna with omnidirectional LHCP

The proposed antenna is shown in Fig.(3.10). It is a structure composed by two circularly polarized monopole antenna elements, with a slit in the ground plane, identical to the shown in Fig.(3.6) and also using a substrate absorber layer between them as illustrated in the Fig.(3.10b).

The substrate used for both antennas was Arlon CuClad 217, which presents a relative dielectric permittivity of $\epsilon_r = 2.17$, a thickness $h = 0.787\,\text{mm}$ and a loss tangent $\tan\delta = 0.0009$.

In this design, due to impossibility to access to ferrite plates, properly characterized, or even to characterize one, and with acceptable dimensions, it was used the existing ferrite material, pre-defined in the HFSS electromagnetic simulator, whose characteristics are: a conductivity $\sigma = 0.01$ S/m, relative permeability $\mu_r = 1000$, relative permittivity $\epsilon_r = 12$. Using this material, which is an approximation, the intended concept can be analyzed, as well as the viability to further explore it. An absorber plate with these characteristics was created with a thickness of $h_f = 2\,\text{mm}$, and added to the two monopole structure shown in Fig.(3.10).

The monopoles were designed using the electromagnetic simulator Ansoft HFSS HFSS for the 5.9 GHz DSRC band. The global dimensions of the antenna are 20mm×20mm× ≈ 3.5mm, which allow it to integrate in any receiver, keeping the reduced size of the device. It was simulated and the main results are presented below.

Fig.(3.11) shows the simulated S_{11} of the designed antenna, each curve corresponds to the S_{11} at each input port, since the antenna is composed by two monopole elements. Using a commonly accepted criterion of a good impedance matching of $S_{11} < -10\,\text{dB}$, it is possible to note a broad operation bandwidth, around 3 GHz, covering the DSRC bands.

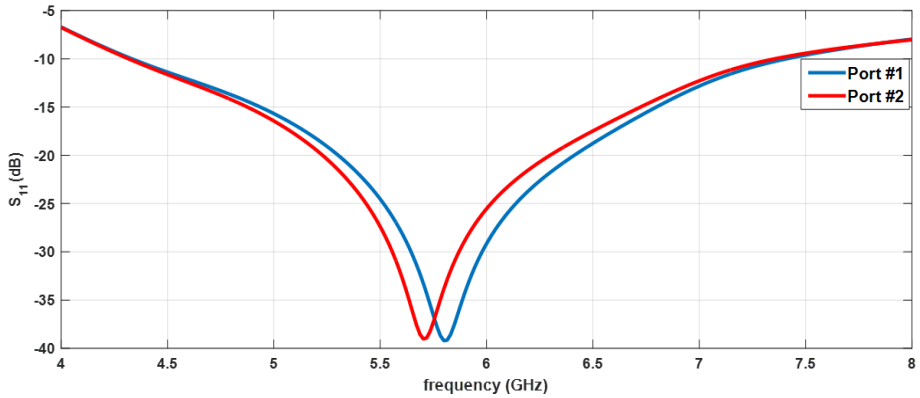

Figure 3.11: Simulated S_{11} and S_{22} of the antenna

The Fig.(3.12) presents the simulated axial ratio of the proposed antenna. An usual criterion for a good circular polarization is the axial ratio below than 3 dB. According to the Fig.(3.12), it is possible to notice a frequency band of 2.3 GHz covering the DSRC bands, in which the antenna preserves a good circular polarization.

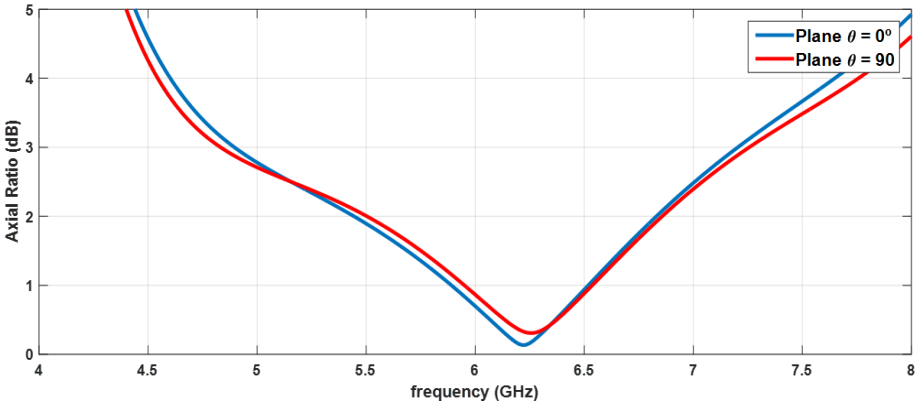

Figure 3.12: Simulated axial ratio of the antenna

Fig.(3.13) shows the two main planes of radiation pattern of the monopole structure which are $\theta = 0^o$ and $\theta = 90^o$. The monopoles were fed simultaneously and in phase, and was assumed the arrangement in the vertical. In each sub-figure, there are presented the two components of electric field in terms of circular polarization, E_{LHCP} and E_{RHCP}. As is expected since the antenna basis is a printed monopole, the designed antenna preserves an omnidirectional radiation pattern shape, with a maximum simulated gain of 2.4 dB.

Regarding Fig.(3.13) is perceptible that the LHCP dominates completely the radiation pattern of the antenna, keeping a good level of cross polarization rejection. In the more critical regions in terms of rejection between LHCP and RHCP, there is at least a 10 dB difference, which complies with DSRC standards.

This characteristic is very important because by using this antenna on the vehicle roof, it will be possible to communicate in any direction on the road plane with other vehicles and infrastructures, without the 3 dB losses in the V2I communications.

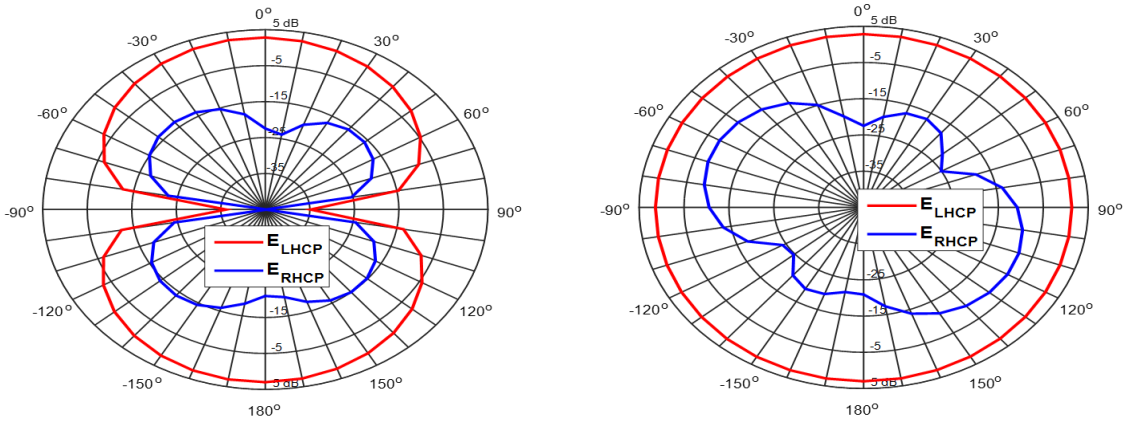

(a) Vertical Plane - $\theta = 0°$ (b) Horizontal Plane - $\theta = 90°$

Figure 3.13: Simulated radiation pattern of the proposed antenna

Due to the impossibility of getting a set of appropriate ferrite to test in practice this designed solution for the antenna will be implemented as soon as is possible to access to a properly characterized ferrite to test.

3.3 The RSU antenna

The RSU is the equipment placed in the infrastructures located at the edge or overhead the road, allowing through it to establish V2I communications, or serve as a bridge for V2V communications, with vehicles that are moving on its coverage range. An RSU consists of one transmission and one reception module, and therefore, has a transmitting (TX) antenna responsible for sending the signals to the OBUs, and a receiving (RX) antenna responsible to receive the information back from the OBU.

In [40, 41] are described phased array antennas at 5.8 GHz used for ETC. [40] consists of two antenna arrays, one with a steerable narrow beam (4×8) to receive and the other (2×8) with a static radiation pattern to transmit in a free-flow multi-lane environment. This antenna involves a lot of complexity, since the main lobe scans the covered area to locate a vehicle. In [41] the phased array is composed by two arrays, one (3×8) for transmitting and the other (4×8) for receiving, designed with a multilayer structure. Being phased arrays, they are necessarily expensive, voluminous and complex due to the use of controllable phase shifters.

A double-looped monopole array antenna for the RSU of a DSRC system using four monopole elements is described in [42]. This array does not have circular polarization and requires a large ground plane. In [43] is shown a microstrip fed Quasi-Yagi antenna array for DSRC, with four printed elements. Although it shows a good S_{11}, the antenna does not have LHCP and, it lacks information about the radiation pattern.

A high gain antenna array, with multiple superstrate layers for RSU is presented in [44]. This antenna has 230MHz of S_{11} bandwidth, but exhibits some problems in axial ratio, besides it does not show the radiation pattern. For the 5.8 GHz DSRC system, [45] presents an

antenna using metamaterials to increase the gain of microstrip patch antenna from 6.5 dBi to 15.3 dBi. The antenna is an array of four elements, with a final beamwidth of 30°. There is no information of the array polarization and it is highly voluminous.

A novel circularly polarized antenna is described in [46] for the RSU equipment. The elements have a H-shape with a T-slot, and the antenna has a 4×4 arrangement with a multilayer structure. The antenna presents around 24° of beamwidth, reduced SLL, a gain of 15.9 dBi, about 109 MHz of bandwidth and good circular polarization. A microstrip array antenna for ETC is presented in [47]. The antenna has a 4×4 structure with sequential rotated elements using a microwave absorbent material made of Korean paper with Chinese ink, to reduce the side lobes (about 8 dB to 10 dB). The final results, present 20.26 dBi of gain, with less than 20 dB of SLL.

Almost all of these antennas shown above have in common the complexity in the structure and in its design.

In this band of frequencies used by DSRC, and for this application, the microstrip antennas are suitable and have been increasingly used due to its great benefits. However, using this type of antennas, its center frequency may undergo a shift due to small deviations in the dimensions of the elements or in dielectric constant of the dielectric substrate. A wide bandwidth of the antenna is important because it increases the tolerance to those deviations, which is needed to achieve high yields in mass production. Moreover, an antenna that operates over both DSRC bands would be advantageous because the same antenna could be used in various applications.

In the next sub-sections a group of antennas for the RSU module of a DSRC system have been designed and are presented. Their planar structures, using a single layer, the wide bandwidth and low-cost of manufacturing are common characteristics.

3.3.1 Planar 2×4 Antenna Array for RSU-TX

The proposed antenna regarding to the preceding cited references shows a number of characteristics in accordance with the DSRC standards and with a reduced size, which is important because the whole RSU system can be more compact. Also, it is a simpler antenna, in the way that it has a single layer (besides the ground plane) allowing an easy manufacturing with reduced costs. Finally, this antenna shows a wide bandwidth exceeding 300 MHz, either in polarization and in return loss.

This work was acknowledged by two scientific contributions, one presented in an international conference **[C4]**, and another in a journal **[J1]**.

Microstrip Array Element

The microstrip antenna element used in the array was designed using a transmission line technique, reported in the section (2.2). This technique enables the estimation of the antenna parameters according to the frequency and dielectric substrate characteristics. The element has a square shape and its characterization through simulated and measured results is presented in the published paper **[C4]**.

Array Structure

Using a single microstrip antenna, due to its ample radiation pattern is impossible to comply with the European DSRC directives referred in section (3.1), so the use of an antenna array was necessary.

According to the array theory, eq.(2.63), the minimum number of elements that allows to achieve a HPBW in the vertical plane less or equal to 70° (DSRC standards) using a uniform linear array is $N_y = 2$ elements. Moreover, to cover the road lane ($\Delta_L \approx 3\,\text{m}$ width), the RSU antenna should ensure an HPBW about 30°. Similarly, were used $N_x = 4$ elements in the horizontal plane to reach that beamwidth.

Therefore, the final configuration of the antenna array is planar, in a $N_x \times N_y = 2 \times 4$ structure. Taking as starting point the array theory equations, reinforced by additional simulations, the distance between elements in the lines (vertical plane) $d_y = 0.65\lambda$ and $d_x = 0.8\lambda$ in the columns (horizontal plane) were obtained.

Polarization

A requirement for the RSU antenna is that its polarization should be LHCP. A simple way to circularly polarize an antenna array, is using circularly polarized elements in that array. In a microstrip antenna, there are several techniques to generate circular polarization, some of them are presented in the section 2.2. Chamfer some corners of a square microstrip element, as shown in Fig.(2.13b), is one of the most common technique.

Taking the 2×4 planar structure, it can be viewed as a group of two 2×2 sub-arrays, side by side. The Fig.(3.14a) shows an example of LHCP placement in a 2×2 sub-array, with circularly polarized square microstrip elements. This technique has as main disadvantages the reduced bandwidth, lower than 1% [16].

To increase the polarization bandwidth, in addition to the technique applied to the array elements, it was implemented the sequential rotation technique, described in the section 2.3.4. This technique uses a progressive rotation of the array elements in a 2×2 sub-array configuration, using offsets 0°, 90°, 180° and 270°, both in the feed position of each element, and in their phase of feeding.

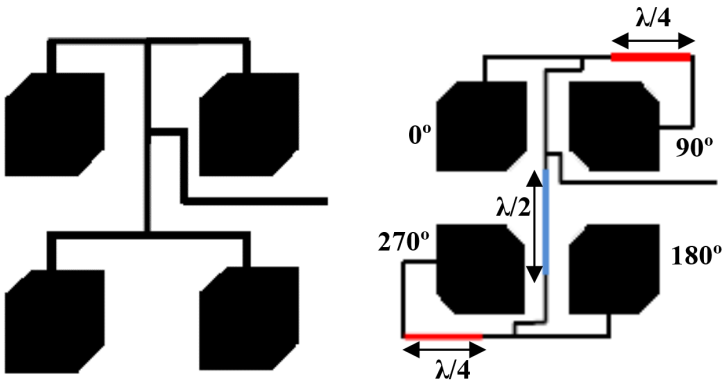

(a) Conventional feeding (b) Sequential rotated feeding

Figure 3.14: Circularly polarized 2×2 antenna array

This configuration is illustrated in Fig.(3.14b). Using an array of microstrip elements, the phase delays in the feeding of the elements are created in the design of the array feed network (AFN), made using microstrip transmission lines, and additional $\lambda/4$ and $\lambda/2$ line sections. Further using this technique, it is also possible to improve sidelobe level regarding the maximum value that can be achieved using simple uniform antenna arrays, important

property since according to the DSRC standards it is necessary to obtain a SLL greater or equal to 15 dB in both planes.

The antenna array was designed using the electromagnetic simulator HFSS [37], based on the described characteristics, and its dimensions were adjusted in order to optimize its impedance matching and radiation properties. The used dielectric substrate was the Arlon Cuclad 217 which has as main characteristics the relative dielectric constant $\epsilon_r = 2.17$, the loss tangent $\tan\delta = 0.0009$, and $h = 0.787\,\text{mm}$ of thickness.

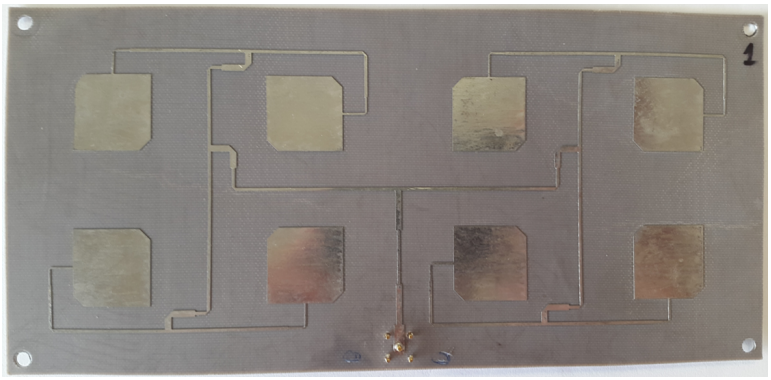

Figure 3.15: Photography of the designed microstrip antenna

The final array structure is shown in the Fig.(3.15), presenting the photography of the performed prototype. The global dimensions are $80 \times 170\,\text{mm}^2$, with all the elements being fed with equal amplitude and with phase differences according to sequential rotation technique applied. The AFN was designed using microstrip transmission lines and quarter wavelength transformers to adapt the impedance of the lines to the input impedance of each array element. The dimensions of each element are $w = l = 16.7\,\text{mm}$.

Results

The antenna was measured and characterized in terms of its main parameters: impedance matching, polarization, and radiation pattern, and the measured results were compared with those obtained by simulation and are shown in the Figs.(3.16)-(3.18).

Fig.(3.16) shows the comparison between the simulated and measured S_{11} of the array. It is possible to note a good agreement between simulated and measured results. Assuming as a good impedance matching the widely accepted criterion of $S_{11} < -10\,\text{dB}$, it is possible to observe that in terms of measurement results, the array is well matched in a band of 540 MHz [5.62GHz - 6.16GHz], covering all DSRC frequency bands.

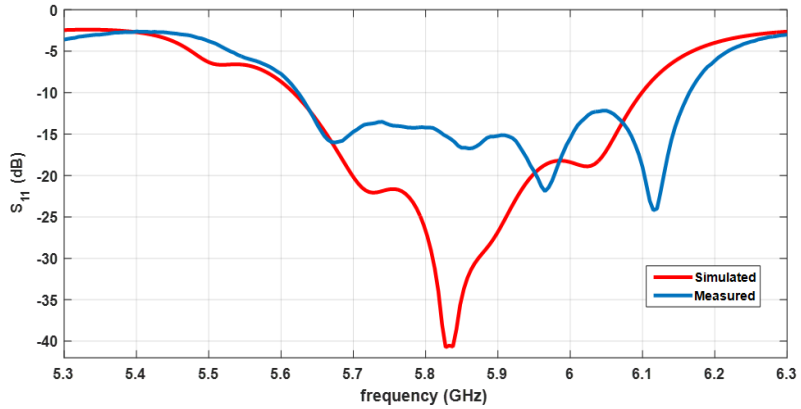

Figure 3.16: Simulated and measured S_{11} of the antenna array

The axial ratio is a commonly used parameter in antennas because it allows to characterize the quality of circular polarization. Fig.(3.17) shows the simulated and measured axial ratio of the array. The first impression that can be taken from the figure, is the slight deviation between the two curves. Assuming as a good circularly polarized antenna, an antenna whose AR $<$3 dB (common used criterion), in terms of measured results the antenna array presents a good circular polarization in a 300 MHz band, [5.75-6.05]GHz, covering all DSRC bands.

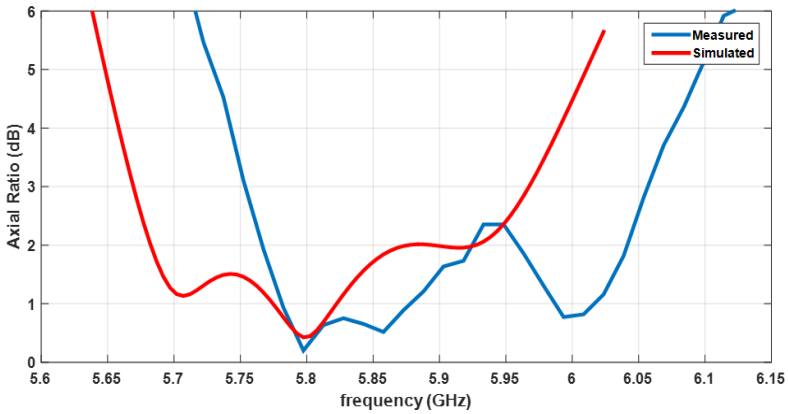

Figure 3.17: Simulated and measured Axial Ratio of the antenna array

The Fig.(3.18) shows a comparison between the simulated and measured normalized radiation pattern of the antenna, in both principal planes: horizontal plane (or road plane - $\phi = 0^o$) and vertical plane ($\phi = 90^o$). The radiation pattern in each plane shows the left and right components of the electric field, that allows also an easier analysis in terms of circular polarization.

The main features that can be taken from the Fig.(3.18) are the HPBW, the SLL, and the cross polarization rejection, i.e the difference between the left (desired) and the right component (undesired). These values are summarized in Table (3.3).

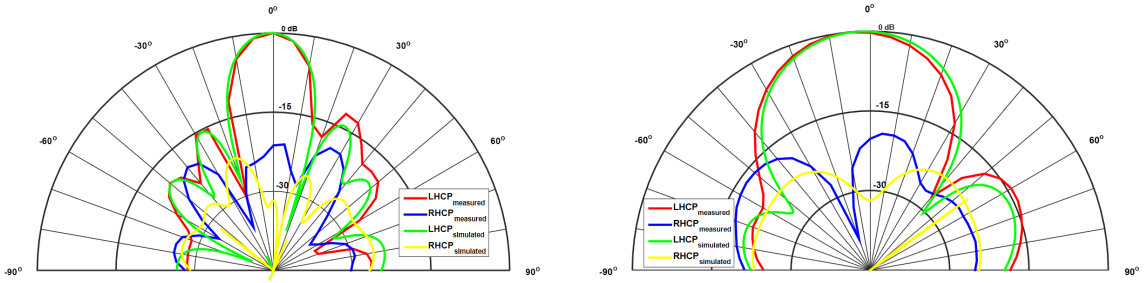

(a) Horizontal Plane - $\phi = 0^o$ (b) Vertical Plane - $\phi = 90^o$

Figure 3.18: Radiation Pattern - simulated vs measured

Table 3.3: Radiation Pattern at 5.8 GHz: simulated and measured characteristics

$Plane(\phi)$	0^o	90^o
$HPBW_{simulated}$	18^o	45^o
$HPBW_{measured}$	18^o	44^o
$\Delta_{15dB-simulated}$	32^o	76^o
$\Delta_{15dB-measured}$	30^o	75^o
$SLL_{simulated}(dB)$	-14.5	-15.9
$SLL_{measured}(dB)$	-12.5	-14.2
$Rejection_{\theta=0^o-simulated}(dB)$	32	31
$Rejection_{\theta=0^o-measured}(dB)$	21.3	20

Through Fig.(3.18) and Table (3.3), it is possible to notice that, in the vertical plane, the array has a beamwidth in the zone 15 dB below the maximum (Δ_{15dB}) of 76^o, and a HPBW of 45^o. In the horizontal plane, the designed array has a Δ_{15dB} of 30^o and a HPBW of 18^o. The sidelobes simulated are always below than -15dB, however, in terms measured results, the SLL fluctuates between -12 dB and -14.5 dB. The rejection in boresight ($\theta = 0^o$) is always over than 20 dB, which confirms the good quality of circular polarization. The antenna has a gain of 15 dBi.

The array was tested in a RSU of a tolling system. Practical issues in measurements at the tolls revealed that a radiation pattern with wider horizontal coverage allows more reliable and uniform communication, even for motorcycles. However, resorting to antenna arrays with an overly wide main lobe should be avoided to mitigate interference from adjacent lanes. Bearing in mind the reported practical issues, the antenna HPBW was estimated to be approximately 20^o and the Δ_{15dB} about 45^o, to confine the main lobe over the road lane. In this sense, an antenna was designed to fulfill these practical issues, and that best fits to DSRC standards.

3.3.2 Planar 12-Element Antenna Array for RSU-TX

Considering the practical issues identified and the DSRC standards, a new antenna array was designed outperforming the state of the art arrays described, with a radiation pattern suitable for tolling communications. This new antenna incorporates many advantages of the microstrip antennas. Besides, its array configuration was meticulously designed to achieve the required radiation pattern fulfilling the reported practical issues. Moreover, it has a wide matching and circular polarization bandwidth over 1GHz and covering broadly all the DSRC frequency bands.

This research work that led to the described antenna, enabled two scientific publications, published in a recognized journal **[J2]**, and in an international conference **[C5]**.

Using uniform antenna arrays, it is not possible to achieve the desired radiation pattern beamwidths, at half power ($HPBW/\Delta_{3dB} \approx 20^{o}$) and at 15 dB below the maximum ($\Delta_{15dB} \approx 45^{o}$) to comply with the referred requirements. Additionally, the side lobe levels ($SLL \leq -15dB$) cannot be reduced enough to conform with the standards.

It is therefore fundamental to move to the nonuniform arrays, as well as studying alternative techniques to apply to the antenna array in order to find the beam shaping in accordance with the objectives.

Array Design

To design the antenna array, according to the array theory formulas also set out in the section 2.3, to achieve the desired HPBW has been chosen $N = 4$, $d = 0.75\lambda$ as an initial point. The antenna array to be developed should not be a uniform excitation array, since it cannot reach the SLL under the theoretical limit (-13.46 dB) and simultaneously fulfill the Δ_{3dB} and Δ_{15dB} beamwidths.

So, the designed antenna array arrangement starts from the 4×4 planar structure (16 elements), the minimum number of elements required to accomplish the desired beamwidth and also to provide enough room to apply nonuniform techniques to reach the desired SLL.

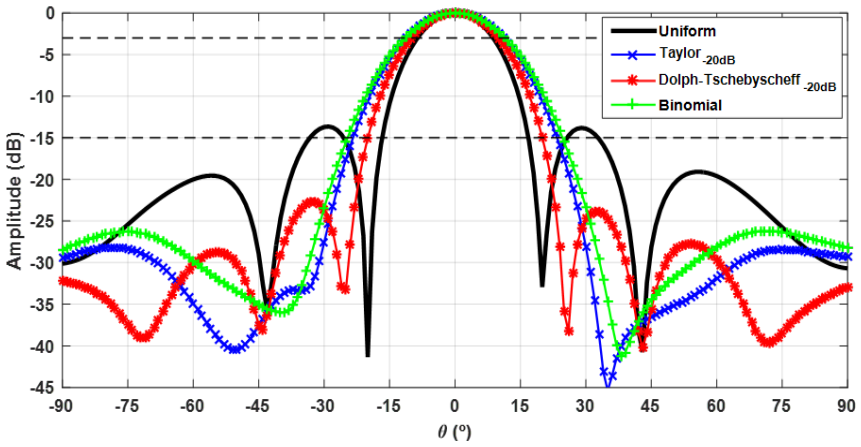

Figure 3.19: Comparison of the normalized radiation patterns, using four different excitation techniques

In the Fig.(3.19), the black filled curve represents a cut of the simulated normalized radiation pattern of a uniform 4×4 array (all the elements fed with equal amplitude and phase). There are also displayed dashed lines indicating the -3 dB and -15 dB zones.

It can be observed that the Δ_{3dB} can be achieved, as expected, however the Δ_{15dB} is too narrow, and the side lobes are too high.

A group of nonuniform feeding techniques was then selected in order to explore the possibility to enlarge the radiation pattern at 15 dB (Δ_{15dB}) and reduce the SLL. Assuming a linear array of 4 elements, the techniques Taylor Line-Source, Dolph-Chebyshev, and Binomial were applied to estimate its coefficients. This group of four coefficients was after converted into the planar configuration used, and are shown in the Table (3.4). The binomial coefficients for N=4 are identical to a particular case of Taylor technique for N=4 and SLL=21 dB.

Table 3.4: Estimated coefficients from excitation techniques for a 4×4 antenna array

(a) Chebyshev Matrix

1	1.75	1.75	1
1.75	3	3	1.75
1.75	3	3	1.75
1	1.75	1.75	1

(b) Taylor Matrix

1	2.6	2.6	1
2.6	6.8	6.8	2.6
2.6	6.8	6.8	2.6
1	2.6	2.6	1

(c) Binomial Matrix

1	3	3	1
3	9	9	3
3	9	9	3
1	3	3	1

In Fig.(3.19), despite the curve of the normalized radiation pattern of a 4×4 uniform antenna array, it is also provided the normalized radiation patterns using each of the above mentioned excitation techniques, applying to the array the weights presented in the Tables (3.4). The amplitude of each element of the array corresponds to the coefficient in its position of the matrix.

The first characteristic to be noted is that the width Δ_{3dB}/HPBW is similar to the four curves, although the corresponding to the uniform array is the narrower. However, regarding to the Δ_{15dB} width and SLL, some changes are noticeable. Analyzing the Fig.(3.19), and bearing in mind the desired goals, the distribution that best fits them corresponds to binomial, since it presents the wider Δ_{15dB} and keeps reduced SLL. This scheme allows to achieve the necessary constraints in terms of beamwidths and SLL, since it is possible to simultaneously reach the 20^o of HPBW and 45^o of Δ_{15dB}, and also a SLL lower than -20 dB.

Furthermore, being the distribution with the highest ratio between the highest and lowest amplitude of elements, especially between the center and the corner elements, it will enable to simplify the array structure, as will be shown below.

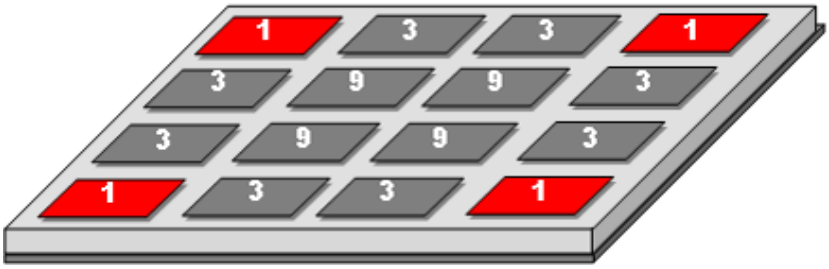

Figure 3.20: Binomial coefficients for a 4×4 antenna array

Then, the antenna array will exhibit a 4×4 planar structure, with a nonuniform excitation of its elements whose amplitude corresponds to the coefficients provided from binomial series expansion, as shown in the Fig.(3.20), and given by:

$$f(x, m) = (1 + x)^{m-1} \tag{3.1}$$

where m is the number of elements of the array, in each direction, and x an arbitrary variable. $(e.g. \quad for : m = 4, \quad f = \underline{1}x^3 + \underline{3}x^2 + \underline{3}x + \underline{1})$

In the designing the antenna array, a new approach was investigated and implemented.

After selecting the binomial technique, the significant amplitude difference between the center elements of the array and the ones located in the corners, as it is possible to observe in Fig.(3.20), caught my attention. This ratio between the amplitudes of the central and the outer elements, further increases when the number of array elements N increases.

This has led to the investigation of the impact of removing these elements, focusing on a 4×4 array structure using binomial excitation.

Considering the planar array factor (AF) given by the equation (see Section 2.3):

$$\begin{aligned} AF &= \sum_{n=1}^{N} \sum_{m=1}^{M} a_{m,n} e^{j(m-1)\psi_x} e^{j(n-1)\psi_y} \\ \psi_x &= \frac{2\pi}{\lambda} d_x \sin\theta \cos\phi + \beta_x \\ \psi_y &= \frac{2\pi}{\lambda} d_y \sin\theta \cos\phi + \beta_y \end{aligned} \tag{3.2}$$

where, λ is the wavelength, M and N are the numbers of elements along x and y directions, respectively, d_x and d_y are the distances between elements, and β_x and β_y are the progressive phase shifts between elements. Finally, $a_{m,n}$ is the amplitude of the (m, n) element of the array.

By substituting into the equation the parameters already established,

$$\begin{cases} \phi = 0^{\circ} \\ N = M = 4 \\ d_x = d_y = 0.75\lambda \\ \beta_x = \beta_y = 0^{\circ} \end{cases} \tag{3.3}$$

and expanding the summation, the AF of the 4×4 planar array with binomial excitation becomes,

$$\begin{cases} AF = \underbrace{2 + 2e^{j3\psi_x}}_{corner\ elements} + \underbrace{6 + 24e^{j\psi_x} + 24e^{j2\psi_x} + 6e^{j3\psi_x}}_{others} \\ \\ \phi = 0^{\circ}, \beta_y = 0^{\circ} \Rightarrow \psi_y = 0 \end{cases} \tag{3.4}$$

which can be separated by the contributions of the corner elements from those of the remaining elements.

The AF of the complete 4×4 planar array using binomial excitation (16 elements - AF_{16}), and of the same array but removing its 4 corner elements (12 elements - AF_{12}) is given by,

$$\begin{cases} AF_{16} = 2 + 2e^{j3\psi_x} + 6 + 24e^{j\psi_x} + 24e^{j2\psi_x} + 6e^{j3\psi_x} \\ \\ AF_{12} = 6 + 24e^{j\psi_x} + 24e^{j2\psi_x} + 6e^{j3\psi_x} \end{cases} \tag{3.5}$$

The Fig.(3.21) shows the curves of the planar AF with the outlined characteristics (3.3), and fed by the binomial technique, Fig.(3.20), with and without the corner elements (AF_{16} and AF_{12}). These curves are normalized to the max of AF_{16}, and represent the plane $\phi = 0^o$.

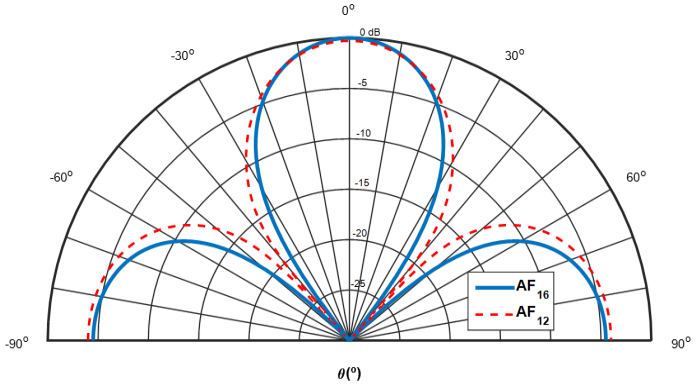

Figure 3.21: Comparison between the calculated AF_{16} and AF_{12} for the plane $\phi = 0^o$ (normalized)

Clearly, it is possible to note two relevant properties: 1) The behavior of both curves is similar, although the AF_{12} presents a main lobe width, particularly the Δ_{15dB}, wider than AF_{16}. 2) In terms of side lobes, AF_{12} has a small deterioration, however it is not very significant.

The Table (3.5) presents a comparison between the AF_{16} and AF_{12}, for two significant locations (θ, ϕ) of the radiation pattern, such as the maximum, and the first sidelobe position. These angles are $\theta = 0^o$ and $\theta = 70^o$, as can be seen in Fig.(3.22).

Table 3.5: Comparison between the 4×4 antenna array with binomial excitation with and without the 4 corner elements

θ	ϕ	ψ_x	ψ_y	$\lvert AF_{16}\rvert_{dB}$	$\lvert AF_{12}\rvert_{dB}$
0^o	0^o	0	0	18.06	17.78
70^o	0^o	4.42	0	11.4	12.44
0^o	45^o	0	0	18.06	17.78
70^o	45^o	3.13	3.13	-119	-30
0^o	90^o	0	0	18.06	17.78
70^o	90^o	0	4.42	11.4	12.44

According to the Table (3.5), the removal of the 4 elements resulted in reducing the antenna gain ($\theta = 0^o$) by 0.28 dB, whereas for the side lobes ($\theta = 70^o$), the biggest difference appears in the plane $\phi = 0^o$ and $\phi = 90^o$ with an increase of 1.04 dB.

To reinforce the theoretical results obtained in the process thus far described, a planar 4×4 array was simulated, using microstrip elements, each element fed with the corresponding amplitude of the binomial distribution, being subsequently withdrawn the 4 corner elements and compared their respective radiation patterns, which are illustrated in Fig.(3.22) for different planes.

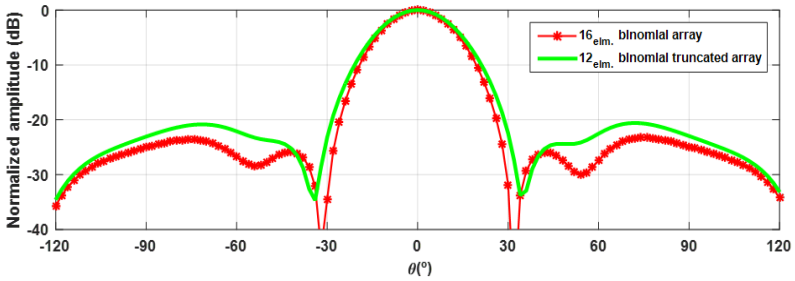

(a) Plane $\phi = 0^{\circ}$

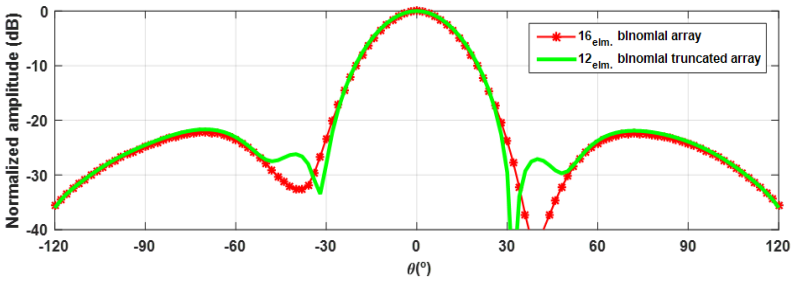

(b) Plane $\phi = 45^{\circ}$

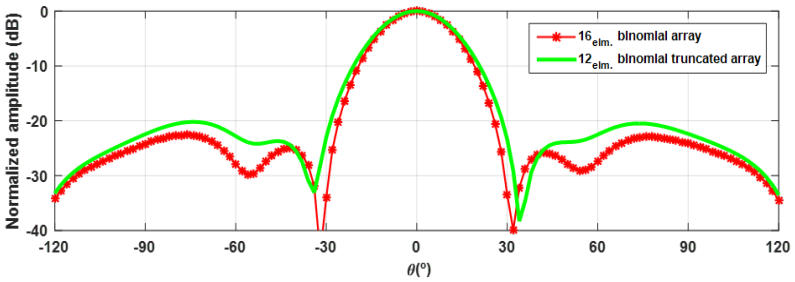

(c) Plane $\phi = 90^{\circ}$

Figure 3.22: Comparison between the normalized simulated radiation patterns, with and without removing the corner elements

According to the Fig.(3.22), the results are broadly consistent with the estimations. The main difference that can be easily visualized is in the region of the side lobes, however, as already predicted, is not very significant. Another detail is also the increase of the main lobe beamwidth when the 4 corners elements are removed.

In conclusion, from the obtained results it is possible to conclude that the impact of removing the four corners elements in an antenna array with a 4×4 planar structure and fed a binomial distribution is not significant.

This approach has been implemented in the antenna design for the RSU module, as the reduced impact resulting of the removal of the four corners elements is largely compensated by decisive aspects that simplify the design of the antenna.

First, removing those elements, eliminates one level of the feed distribution used, the lowest 1, simplifying the entire design of the AFN, as can be seen below. Then, without these elements, it allows to use the space left by them for placing the AFN, allowing a significant reduction in the interference of the AFN to the antenna elements, and keeping the main characteristics of low SLL and radiation pattern beamwidths within the required specifications. Finally, it allows to maintain the array with a single dielectric layer, simplifying both the array structure complexity and manufacturing process.

Microstrip Array Element

The antenna array element used is microstrip type and was designed using a transmission line technique provided in section (2.2). Its corners were chamfered to generate LHCP, as shown in Fig.(3.23).

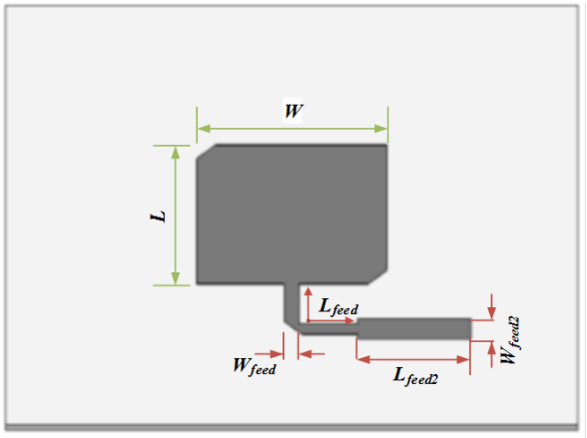

Figure 3.23: Microstrip Patch Element

The dielectric substrate used was Arlon CuClad 217 that has as main characteristics the relative dielectric constant $\epsilon_r = 2.17$, thickness $h = 0.787\,\text{mm}$ and loss tangent $\tan\delta = 0.0009$.

The antenna is a square microstrip patch using a double quarter wavelength transformer to match the input impedance of the element to the $100\,\Omega$ characteristic impedance microstrip lines of the AFN.

The antenna element was simulated and optimized using the Computer Simulation Technology's Microwave Studio [48], and its dimensions are presented in the Table (3.6).

Table 3.6: Dimensions of Microstrip Antenna Element

Parameter	W	L	L_{feed}	W_{feed2}	L_{feed2}	W_{feed2}
Dimension (mm)	16.6	16.6	9.63	1.3	9.4	2.44

Array Feed Network

The feed network plays an important role in the overall performance of the antenna, by implementing the above-discussed nonuniform excitation technique, to obtain the radiation pattern of the antenna with the desired constraints, and contributing to the generation of the desired LHCP.

To enable that the final antenna array preserves important features like simplicity, low profile and ease of manufacture, it was ensured that the AFN using microstrip lines was designed in the same layer as that of the antenna elements.

To describe the AFN, the power divider that will create the power differences given by the excitation technique adopted, and that will feed each of the array elements will be explained. Then, the application of the sequential rotation technique to reinforce the generation of circular polarization is addressed, and finally the entire AFN is analyzed.

Unequal power divider design To create the AFN that implements the nonuniform excitation based on binomial coefficients of Fig.(3.20), Wilkinson unbalanced power dividers were used [49, 50].

The Wilkinson power divider is a three port matched circuit, which splits the input signal into two output ports. These output ports are (ideally) isolated, which means that any mismatching in one output port won't affect the other output port. The option for this type of power divider regarding to the common and simple T-junction was due to the good isolation between ports which protects that unwanted reflections from some elements may affect other elements.

If the corner elements of the 4×4 planar array of Fig.(3.20) are removed, three patches remain in each quadrant, being the peripheral patches fed with the same power and threefold in the central one. This means that, looking at each quadrant independently, their input power is divided into 3/5 (-2.21 dB) + 1/5 (-6.99 dB) + 1/5 (-6.99 dB), for the three patches.

Since each Wilkinson power divider has only two output ports, it is necessary to use a cascade of two Wilkinsons. So, each quadrant of the antenna array will be fed with two cascaded Wilkinson power dividers, as shown in Fig.(3.24a).

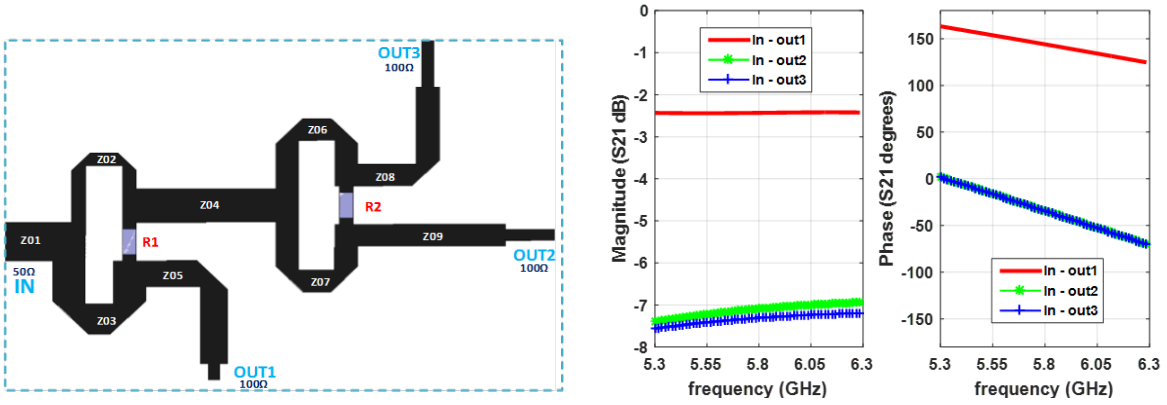

(a) Power divider structure (OUT1/OUT2=3) and (OUT3/OUT2=1)

(b) Simulation results

Figure 3.24: Designed unequal power divider

The first splitter is asymmetrical and its largest power output port (thicker arm) will feed the center element. The second splitter is symmetrical and feeds the two outside elements. The power ratio of any of these two last outputs (out#2 and out#3), relative to the strongest output (out#1), should be 1/3 (-4.77 dB).

This unequal power divider was designed in accordance with formulas presented in [50]. Each output port was matched to 100Ω, that corresponds to the impedance of transmission lines that feed the designed antenna elements (with 100 Ω input impedance). The characteristic impedance of each arm of the designed power divider is shown in Table (3.7).

Table 3.7: Power Divider - Impedance Characteristics (Ω)

Z01	Z02	Z03	Z04	Z05	Z06	Z07	Z08	Z09	R1	R2
50	87	58	55	64	71	71	71	71	102	100

The power divider was simulated and the results are shown in Fig.(3.24b). The results demonstrate that the 2 and 3 outputs are approximately 4.7 dB lower than output 1, as is required. The phase delay between output 1 and outputs 2 and 3 is 180 degrees, since the path to the output 1 does not pass the second divider. This phase difference must be accounted for and compensated in the design of the feeding network.

Circular Polarization Considering that the antenna array is circularly polarized, the phases play an important role in the design of the AFN. For the generation of circular polarization, established by the DSRC standards, by now it has been created by circularly polarizing each single element of the array, chamfering the corners of the microstrip patch, as shown in Fig.(3.23).

To improve generation of LHCP, the technique of sequential rotation referred in the Section 2.3.4 was used. This technique is very advantageous, because it allows for significant increase in the polarization bandwidth (>10%), by using circularly or even linearly polarized array elements. Moreover, this technique substantially reduces the mutual coupling between successive elements of the array, because the neighboring elements become orthogonal.

In the AFN design, the sequential rotation concept was implemented by physical rotation of the array elements, using the phase delays 0^o, 90^o, 180^o and 270^o, as shown in Fig.(3.25), but also with a corresponding phase delay in feeding each array element. The phase delays were made using sections of microstrip transmission lines, with appropriate length. To accommodate the entire length of microstrip lines in the remaining space between array elements, to avoid couplings and other disturbances in the radiation of the array, in the design of AFN meanders lines were created.

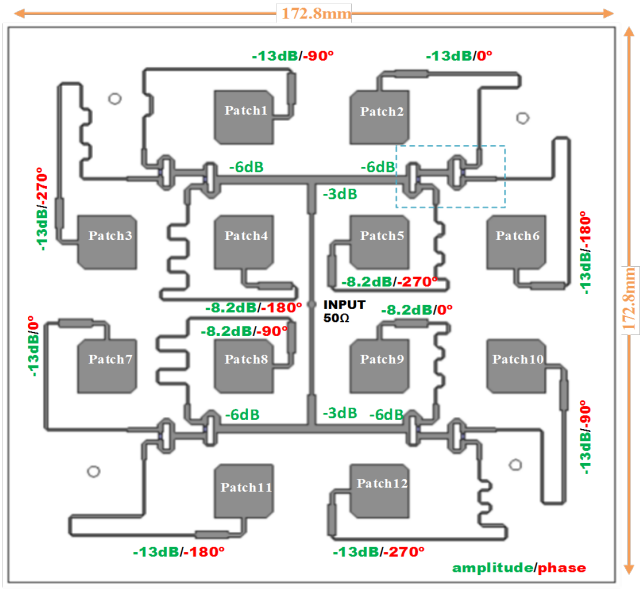

Figure 3.25: Array Structure - Array feed network

Array feed network description The AFN designed, from the input to each of the 12 antenna elements is shown in Fig.(3.25). The input was divided to feed each of the four power dividers. Then, each divider output was connected to the respective antenna element with using 100 Ω microstrip lines with suitable length to produce the appropriate phase delay.

This figure also shows the theoretical amplitude distribution, and the desired phase for LHCP, created by the AFN. It is possible to note that the four center patches are fed with -8.2 dB power (-6 dB(power divider input)+ -2.21 dB(OUT1 power relating to IN)), whereas the eight outer are with -13 dB(-6 dB (power divider input)+ -6.99 dB(OUT2/OUT3 power relating to IN)), fulfilling the desired amplitude ratio of 1/3 (-4.77 dB).

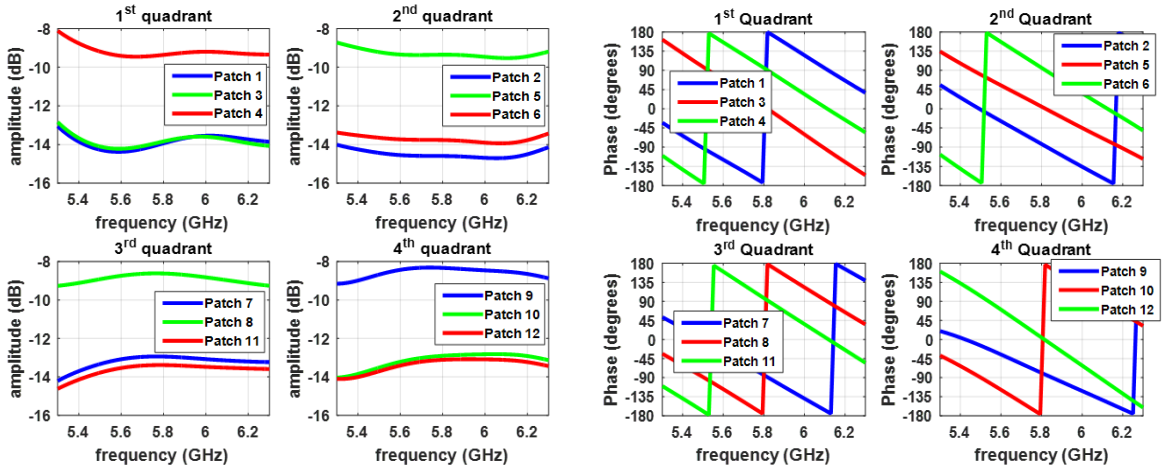

(a) Amplitude (b) Phase

Figure 3.26: Simulated AFN distribution

The AFN was simulated and the Fig.(3.26) compiles the feed distribution it implements, in terms of amplitude and phase. To simplify the analysis, both figures were divided into quadrants, corresponding to each set of three patches of the array.

It is possible to observe from Fig.(3.26a), at 5.8 GHz, that all the four central patches (P4, P5, P8 and P9) are fed with a power close to the theoretically expected (-8.2 dB, see Fig.(3.25)), only with a offset of 1 dB in both first and second quadrants. Regarding the external elements (P1, P2, P3, P6, P7, P10, P11 and P12), they are fed with a power approximately 4.77 dB below with respect to their central element in its quadrant.

Analyzing the Fig.(3.26b) at 5.8 GHz, it is possible to verify that the various patch elements are fed with the required phase differences, indicated in Fig.(3.25). Each group of patches in identical position within the quadrant (ex. P2, P7 and P9 or P1, P8 and P10, or P3, P5 and P12 or P4, P6 and P11) are fed in phase. Successively, each group presents itself an 90^{o} offset relative to the next group. Overall, it is possible to find that the sequential rotation technique applied to generate LHCP is verified.

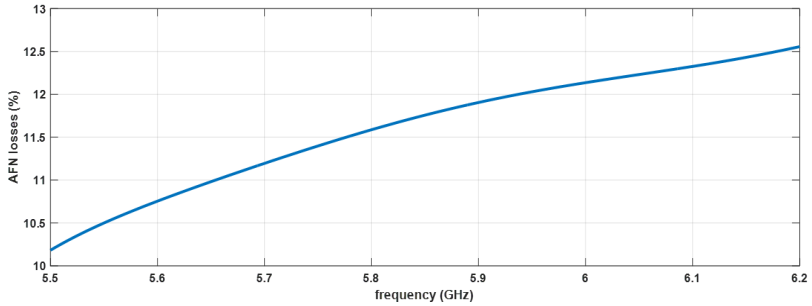

Figure 3.27: Simulated total losses of the AFN

Fig.(3.27) shows the simulated power losses of the AFN, as a function of the frequency. An important aspect that is noticeable, and already expected, is that the losses of transmission lines increase with frequency, being at 5.8 GHz about 11.5% of the input power, a tolerable value given the complexity the AFN, designed close to the array elements and using several meanders lines.

Concluding the array design, it is possible to affirm that the innovative technique investigated and applied by removing the corner elements comprises a set of advantages. Firstly, the number of the elements to be fed is, of course, reduced. Secondly, the power splitters are also simplified, not only in terms of the number of ports, but also in terms of the power ratios needed and/or the number of cascaded splitters. Thirdly, enough board area is freed to accommodate the splitters farther enough from the elements. For last, the free board space is also useful to route the microstrip lines, many of them with meanders. Hence, the full antenna can be manufactured in a very simple, two layer printed circuit board (the other layer is a full ground plane).

The array was designed using the above mentioned dielectric substrate, was simulated and optimized using the electromagnetic simulator CST[48].

Results

The antenna array was manufactured and the prototype is shown in Fig.(3.28). It was measured and characterized for its main aspects: reflection coefficient, polarization and radiation pattern, and the results were compared to the simulated ones, and are presented in the next Figures.

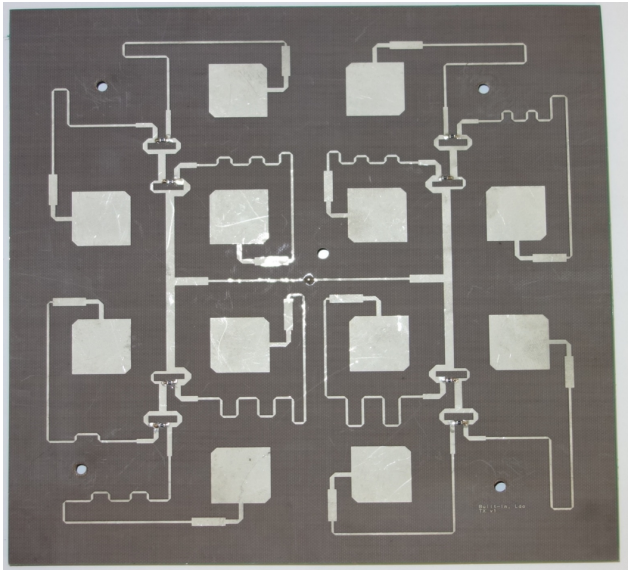

Figure 3.28: Manufactured nonuniform antenna array for the RSU

A comparison between the simulated and the measured S_{11} of the antenna is illustrated in the Fig.(3.29). It is possible to visualize a similar behavior in the two curves, with only a small deviation in frequency. Assuming $S_{11} < -10\,\text{dB}$ as the well-accepted criterion for a good impedance matching, it was possible to find that the antenna array is well matched in a 2 GHz [4.9-6.9]GHz band.

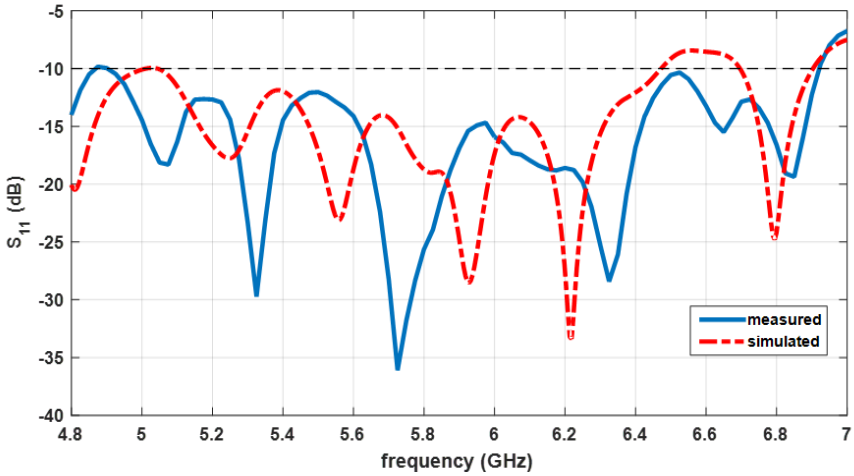

Figure 3.29: Simulated and measured S_{11} of the array

Another important aspect to characterize the antenna, and also established by the DSRC standards, is the circular polarization. In this sense, the E_{LHCP} and E_{RHCP} components of the electric field were measured over the frequency, for the boresight direction.

Fig.(3.30a) presents the normalized measured LHCP and RHCP components of the electric field of the antenna. It is clearly noticeable a huge difference between the two components, with a clear supremacy of the E_{LHCP} component, over the measured band of frequencies. This property confirms that the direction of the circular polarization is, as intended, left.

Considering 15 dB of cross-polarization rejection as a criterion for good circular polarization, the designed antenna presents an ample range of frequencies, from 5.37 GHz to 6.5 GHz, wherein the antenna rejects well enough the cross polarization.

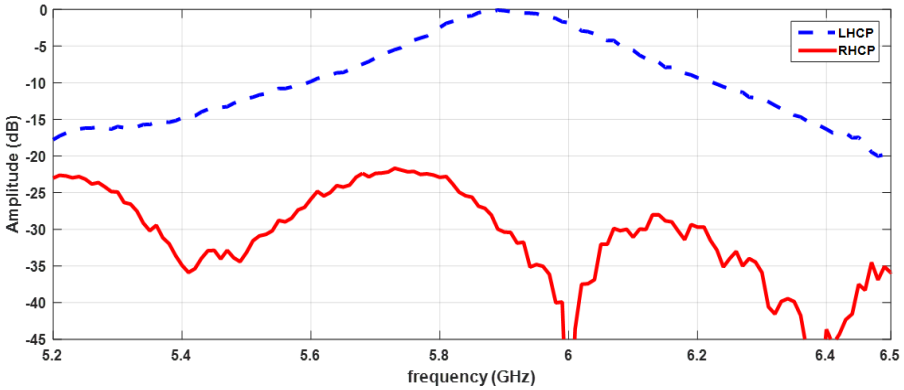

(a) Normalized measured LHCP vs RHCP over the frequency

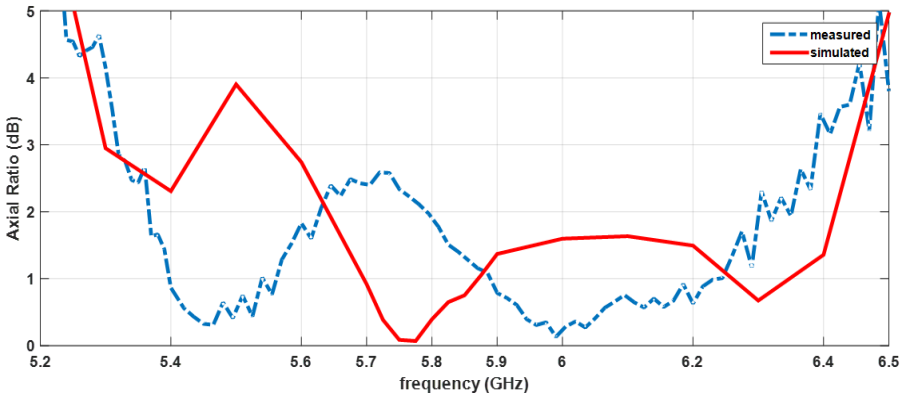

(b) Comparison between simulated and measured Axial Ratio

Figure 3.30: Circular polarization results

Another parameter that is commonly used to characterize the quality of circular polarization (which can be computed through the LCHP and RHCP components) is the axial ratio. The simulated and measured axial ratio of the designed antenna array is presented in Fig.(3.30b), in which is possible to find a good agreement between the simulated and measured values. Assuming an axial ratio lower than 3 dB, as the commonly used criterion for a good circular polarization, it can be seen that the antenna array has a frequency band of 1.13 GHz [5.37-6.5GHz] in which it presents a good value of the measured axial ratio.

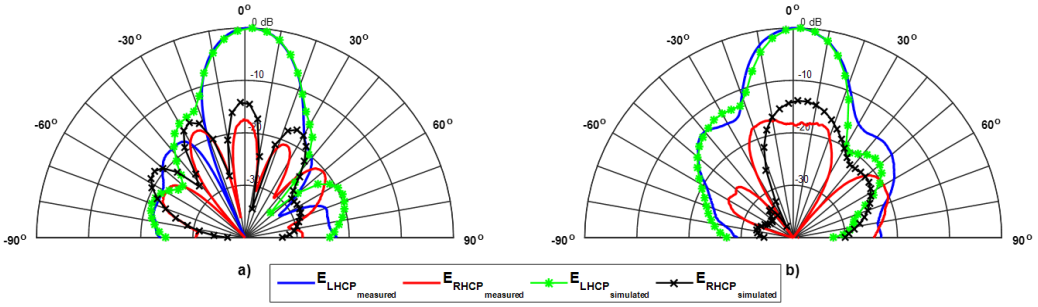

(a) at 5.7GHz

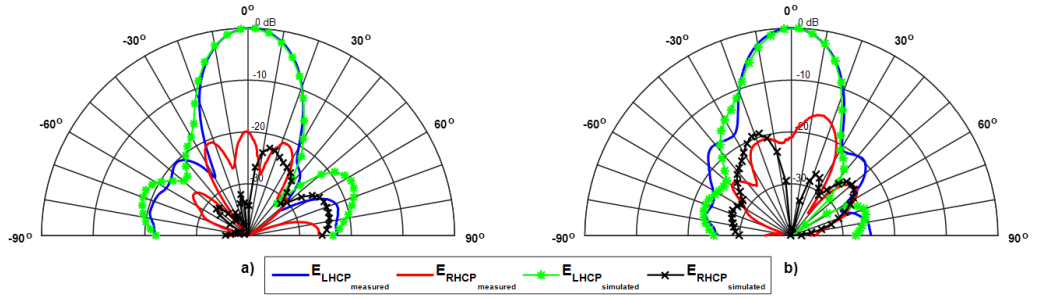

(b) at 5.8GHz

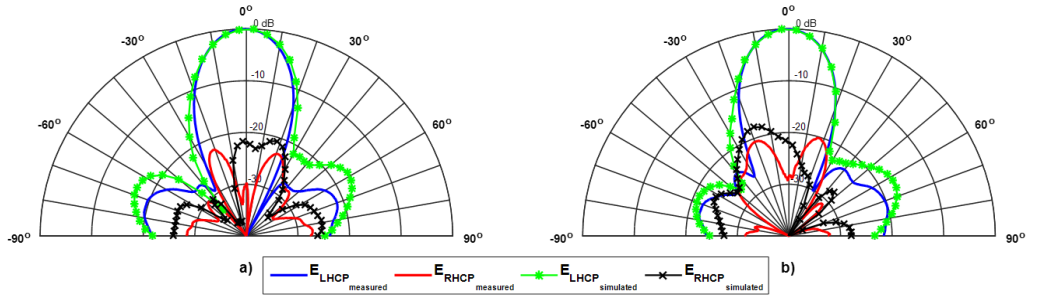

(c) at 5.9GHz

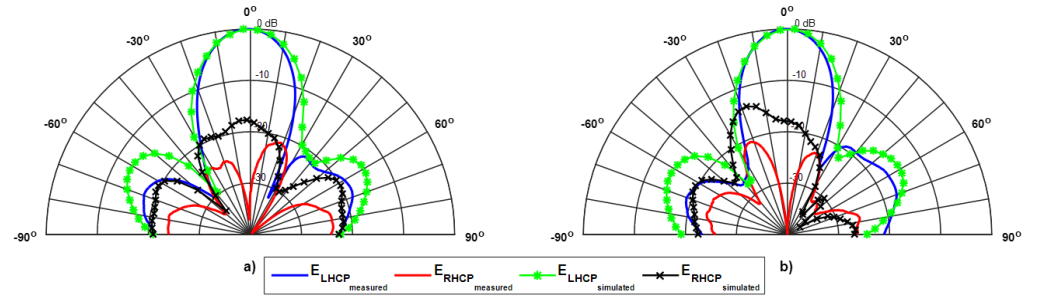

(d) at 6.0GHz

Figure 3.31: Simulated and measured normalized radiation patterns : a) plane $\phi = 0^o$ b) plane $\phi = 90^o$

After the characterization of the developed antenna in terms of input impedance and of polarization, it is necessary to describe the antenna concerning to its radiation characteristics, also constrained by the DSRC standards.

The Fig.(3.31) shows the simulated and measured normalized radiation patterns of the array, in the two components of electric field (E_{LHCP} and E_{RHCP}), in the two main radiation planes $\phi = 0^o$ and $\phi = 90^o$, and at different frequencies belonging the bands of interest: 5.7 GHz, 5.8 GHz, 5.9 GHz and 6 GHz.

The first aspect that can be observed is the reasonable agreement between the measured and simulated results, mainly in the E_{LHCP} component, which is the dominant. Regarding the cross-polarization (E_{RHCP} component) differences between simulated and measured results, these are acceptable given their low power when compared to the maximum level.

The main parameters that can be taken from radiation patterns, beamwidths (Δ_{3dB} and Δ_{15dB}), SLL and rejection between E_{LHCP} and E_{RHCP} components, are summarized in the Table (3.8), for simpler analysis.

Table 3.8: Radiation Pattern characteristics

Frequency (GHz)	5.7		5.8		5.9		6	
$Plane(\phi)$	0^o	90^o	0^o	90^o	0^o	90^o	0^o	90^o
$\Delta_{3dB}/HPBW_{simulated}$	21^o	21^o	23^o	22^o	22^o	21^o	21^o	22^o
$\Delta_{3dB}/HPBW_{measured}$	21^o	23^o	23^o	23^o	21^o	21^o	23^o	21^o
$\Delta_{15dB}[simulated]$	60^o	71^o	50^o	55^o	50^o	48^o	51^o	50^o
$\Delta_{15dB}[measured]$	46^o	77^o	47^o	48^o	45^o	43^o	45^o	42^o
$SLL_{simulated}(dB)$	-19	-13	-18	-22	-17	-17	-14	-15
$SLL_{measured}(dB)$	-18	-15	-20	-17	-20	-21	-18	-17
$Rejection_{boresight}[measured](dB)$	18	19	20	21	30	29	34	39
$Rejection_{-3dB}[measured](dB)$	22	15	22	14	27	20	20	25

Through the Table (3.8) it can be seen that, regarding the main radiation parameters, there is a great concordance between simulated and measured results. Focusing on the frequencies of most interest to the application, 5.8 GHz and 5.9 GHz, all parameters are within the limitations set by the standards, some of them with a good margin of protection. In terms of SLL, it is possible to observe measured values of -20 dB in the plane $\phi = 0^o$ and -17 dB in the plane $\phi = 90^o$, while at 5.9 GHz these values are -20 dB and -21 dB respectively. (Note that by the standards these values shall be at least -15 dB)

Regarding to the beamwidths, at 5.8 GHz the array shows a measured HPBW of 23^o in both planes, and these values drop to 21^o, also in the two planes, at 5.9 GHz. In terms of Δ_{15dB} width, at 5.8 GHz the measured value is 47^o in the plane $\phi = 0^o$ and 48^o in the plane $\phi = 90^o$. At 5.9 GHz, the Δ_{15dB} measured is 45^o in the plane $\phi = 0^o$ and 43^o for the $\phi = 90^o$ plane.

In terms of circular polarization, the standards states that the antenna should have a rejection of cross-component, both in the boresight and at half power directions. It is possible to see that for boresight the rejection is always greater than 18 dB (when the standard specifies a minimum of 15 dB), and in the zone where the gain drops 3 dB is always greater than 14 dB (when the standard refers to a minimum of 10 dB).

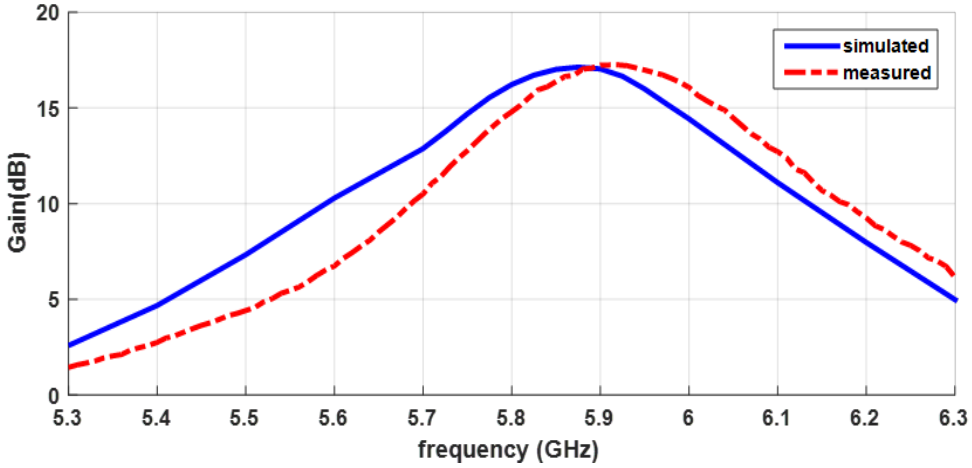

Figure 3.32: Simulated and measured antenna gain vs frequency

Fig.(3.32) shows the simulated and measured gain of the antenna with frequency. It is possible to conclude that the behavior is similar, with a slight deviation of about 50 MHz of the measured results for the simulated. According to the figure, the antenna measured gain has a maximum of 17 dBi at 5.9 GHz, and 14.7 dBi at 5.8 GHz.

The radiation efficiency of the antenna as function of frequency is shown in Fig.(3.33). It is clearly observed a maximum of efficiency in the band of interest, more than 80%. For 5.8 GHz radiation efficiency reaches the value of 83% while the 5.9 GHz is 88.5%.

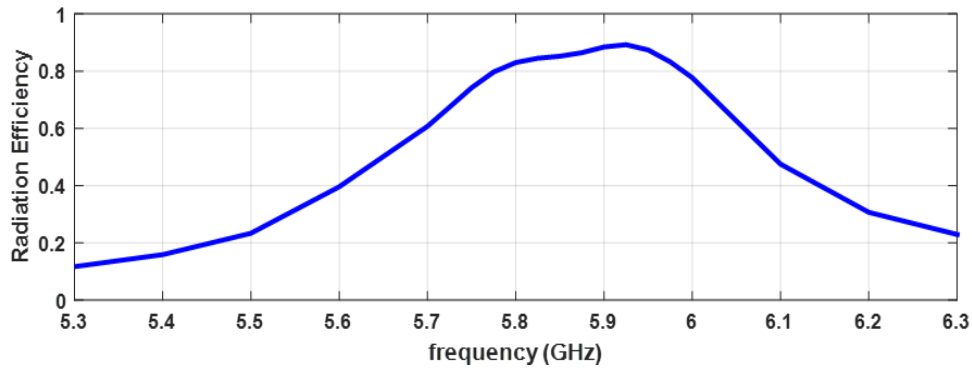

Figure 3.33: Simulated radiation efficiency of the antenna

The array designed with the investigated approach of removing the four corner elements in a 4×4 antenna array using binomial excitation, reveals a good agreement between the simulated and measured results. Its structure, using one single layer with elements and AFN, the broad band of circular polarization of 1 GHz, covering the complete range of DSRC bands, and the particular radiation pattern, makes this antenna overcome the already presented solutions, including those shown as state of the art.

3.3.3 RSU Antenna for Tolling - RX

Multiple antennas have been proposed, always with particular attention to the transmitting part of the RSU, and the receiving antenna isn't commonly discussed. Often, in the RSU system it is used for the RX part a similar version to the TX antenna, since the constraints to the receiving part are not so strict. However, as the cost and size are important restrictions in design of a RSU as compact as possible from parameters set by DSRC standards, an antenna was developed precisely for the RX part of the RSU, smaller than the previously designed for the transmitter, since the RX does not demand for so narrow beamwidths.

The development of this antenna has enabled a scientific publication **[C6]** in an international conference, with the presentation and discussion of its structure and results.

The receiving antenna must follow the directives of aforementioned DSRC standards, although in this situation the sidelobes do not exhibit particular importance, despite ideally they are desired the smallest as possible. The RX antenna must radiate LHCP waves with a rejection of the cross-polarization at boresight higher than 15 dB and at half power greater than 10 dB. Regarding to the radiation pattern, taking into account some feedback of practical operation on the road that has been provided to us, it must be confined to the road lane, although slightly wider than the TX antenna, with a HPBW/Δ_{3dB} about 35°, and at zone 15 dB lower the maximum, Δ_{15dB} of 70°.

Array Design

For the radiation pattern, using either single elements or uniform arrays, it is not possible to reach the desired shape, in terms of beamwidth, Δ_{3dB} and Δ_{15dB} simultaneously, whereby, nonuniform antenna arrays must be used.

In order to fulfill the necessary goals in the antenna design, a new structure was explored and adopted, which is illustrated in Fig.(3.34).

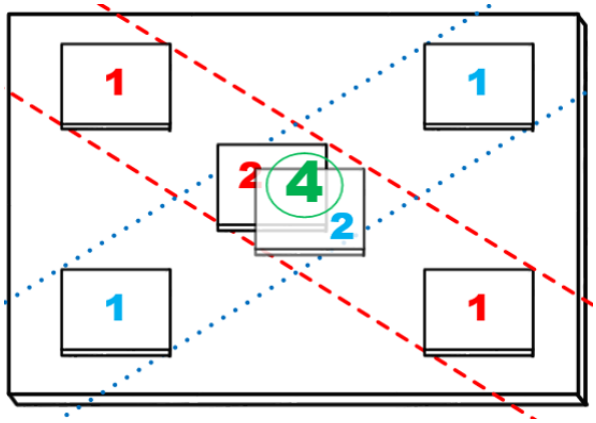

Figure 3.34: Array structure with binomial based excitation

This structure consists of a nonuniform antenna array with four elements in a planar configuration 2 × 2, and with a fifth element at the center, as shown in Fig.(3.34). Each peripheral element is fed with the same amount of power, while the power of the center element is fourfold.

This arrangement can be analyzed as an approximation to a binomial configuration of 3rd order, (see section (2.3.3)), looking at the array as two linear arrays of N=3 elements, using a binomial power distribution in its feeding, and with its central element being shared by both linear arrays, as illustrated in Fig.(3.34). The distance between elements used in the 2×2 structure was $d = \lambda$, which implies that each sub-array of 3 elements has a distance between elements $d' = \frac{\sqrt{2}}{2}\lambda$. The elements of the array used were the square microstrip patches of $W = L = 16.75\,\text{mm}$, due to the good benefits that this type of antennas provides to the application.

To perform the desired LHCP, the corners of each element were truncated, combined with the implementation of the sequential rotation technique applied to the four external elements.

The antenna AFN was designed in the plane of array elements and consists of a power splitter of T-junction type, with 3 output ports, one of them (the central) with half of the impedance compared to the remaining two. Each higher impedance output is then divided by another T-power splitter, with two equal outputs, that will feed each one of the four outer patches of the array.

Overall, the designed AFN performs the desired power distribution reported in Fig.(3.34), and the lengths of each branch of AFN were carefully adjusted to achieve the desired phase delays of 0^o, 90^o, 180^o, 270^o to apply the technique of sequential rotation.

The antenna with the proposed structure was designed, simulated and manufactured using the substrate Arlon CuClad 217 ($\epsilon_r = 2.17$, $h = 0.787\,\text{mm}$, $\tan\delta = 0.0009$), and the prototype is shown in Fig.(3.35).

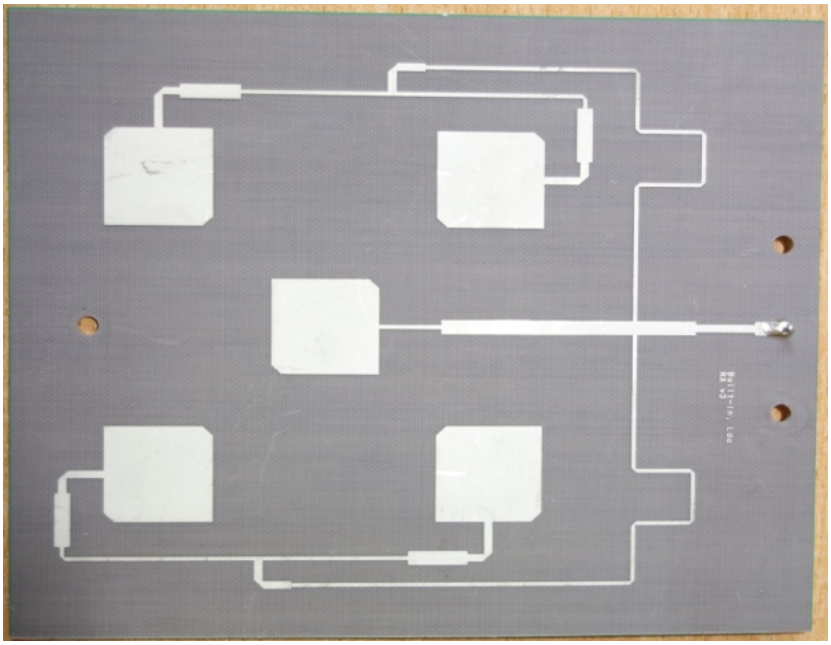

Figure 3.35: Manufactured prototype antenna array

Results

The manufactured prototype presented in the Fig.(3.35) was measured for impedance adaptation, polarization and radiation pattern, and its results were compared with those obtained by simulation.

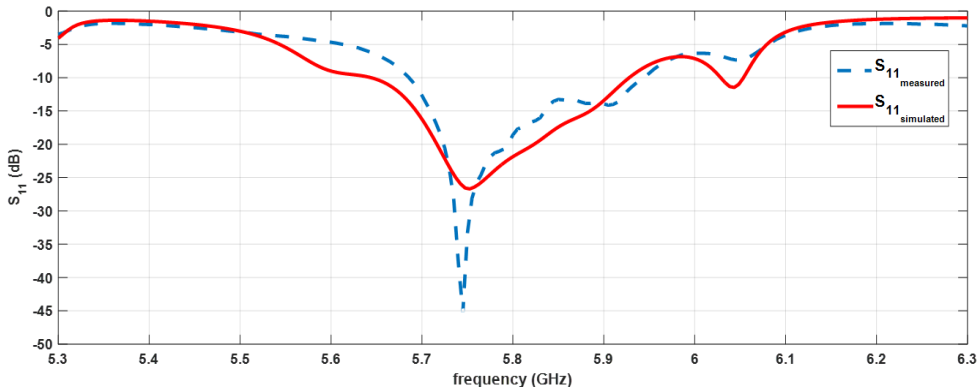

Figure 3.36: Simulated and measured S_{11}

Fig.(3.36) shows the simulated and measured S_{11} of the antenna array. A good agreement between simulation and the measurements can be observed. Considering the S_{11}<-10 dB as the well-accepted criterion for a good impedance matching, the antenna has an operation bandwidth of 260 MHz.

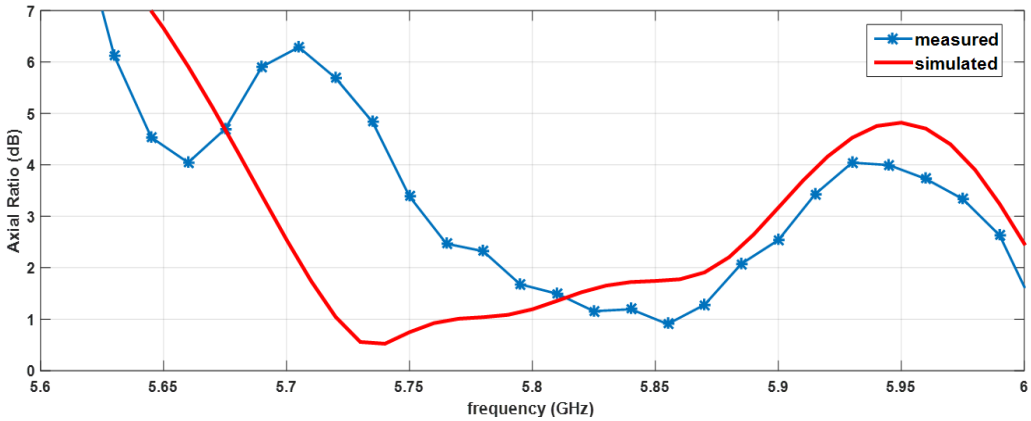

Figure 3.37: Simulated and measured axial ratio

The simulated and measured curves of the axial ratio of the antenna are presented in the Fig.(3.37). A similar behavior of both curves may be observed, however, the measured bandwidth is narrower than the simulated. Assuming an axial ratio below than 3 dB as an acceptable value to characterize a good circular polarization, a 150 MHz bandwidth was obtained.

The simulated and measured radiation pattern of the array in terms of E_{LHCP} and E_{RHCP} components, for both main radiation planes, $\phi = 0^o$ and $\phi = 90^o$, are presented in the Fig.(3.38).

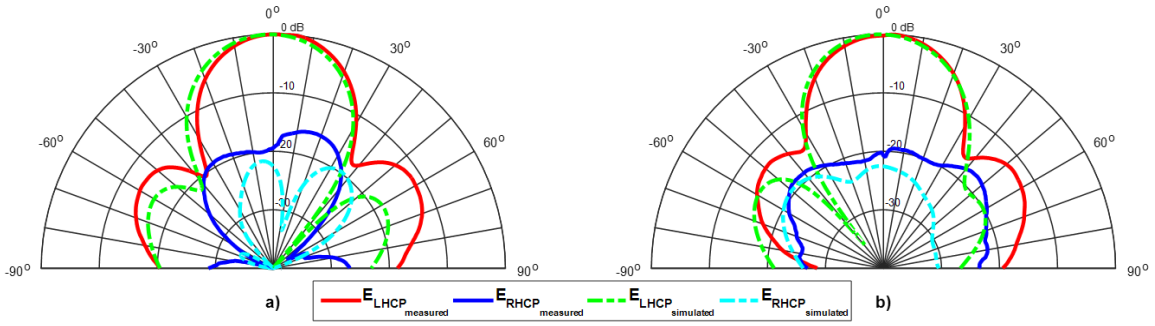

Figure 3.38: Simulated and measured normalized radiation patterns : a) plane $\phi = 0^o$ b) plane $\phi = 90^o$

It is possible to recognize that the left component (E_{LHCP}) is dominant around the radiation pattern, proving that the antenna is circularly polarized in the left direction. Furthermore, a good agreement in terms of simulated and measured along the antenna main lobe can be observed. The measured gain was of 13.8 dBi. The main relevant results that can be withdrawn from the radiation diagram are summarized in the Table (3.9).

Table 3.9: Radiation Pattern: simulated and measured characteristics

Frequency (GHz)	5.8GHz	
$Plane(\phi)$	0^o	90^o
$HPBW/\Delta_{3dB}[simulated]$	32^o	32^o
$HPBW/\Delta_{3dB}[measured]$	32^o	32^o
$\Delta_{15dB}[simulated]$	67^o	68^o
$\Delta_{15dB}[measured]$	64^o	66^o
$SLL_{simulated}(dB)$	-16.3	-15
$SLL_{measured}(dB)$	-11.6	-12.1
$Rejection_{boresight}(dB)[measured]$	19.4	21
$Rejection_{3dB}(dB)[measured]$	16.4	18.3

According to the Table (3.9), in terms of beamwidths, a good agreement between simulated and measured results can be noticeable, in both planes, with a HPBW of 32^o, and at 15 dB lower the maximum, Δ_{15dB} is about 64^o. In terms of cross-polarization rejection, the antenna shows a measured value at boresight, of 19.4 dB in the plane $\phi = 0^o$ and 21 dB in the plane $\phi = 90^o$. At half power, these values are 16.4 dB and 18.3 dB, respectively.

The parameter where there is a higher disagreement between simulation and measures, although it is not a critical parameter neither had devoted much attention in the design, is the SLL. Based on the previous experiences, it is believed that this phenomenon may be due to the little isolation between output ports, a characteristic of the T-splitters. Any mismatch in one element will hence affect other elements and affect the overall performance.

3.3.4 Tolling in Access roads in highways

A different way for location of the tolling infrastructures, recently thought, consists in placing them in the highway access roads, allowing a number of benefits over the common gateways infrastructures, divided into several lanes, and using complex systems. In this section an innovative array whose characteristics suit the needs for tolling application in access roads of highways is presented, including their innovative radiation pattern, with a uniform gain across the road width, with negligible side lobes and operating in a significant bandwidth. Furthermore, the entire array was designed using microstrip structures with its advantages, in terms of light weight, simplicity and low cost.

The development of this antenna array has led to three scientific contributions, in a national conference **[C7]**, in which the approach and a first simplified structure was presented, in an international conference **[C8]**, in which was presented an intermediate step, still using a linear array, and in a journal **[J3]**, already with the final array and all the results provided here.

In Europe, the electronic toll collection applied to highways is usually made based on input and output road logs, when the vehicle enters and exits from the highway, or using several gateways along the highway being charged the passage of the vehicle through these locals. These infrastructures cover several lanes, and allows a quick access and fluency of traffic. However, they involve at least one system covering each lane, and also requires a great care to overcome potential interferences between the various RSU's, or with the vehicles passing in adjacent lanes.

A recent approach suggests that these gateways infrastructures (with RSU's) could be placed in the input and output access roads of the highways, which are typically single lane, as shown in the Fig.(3.39). This concept allows the use of only one RSU system, avoiding interference problems between lanes, and a simpler system, as in these lanes, commonly with curved shape, the speeds are much lower than in the highways.

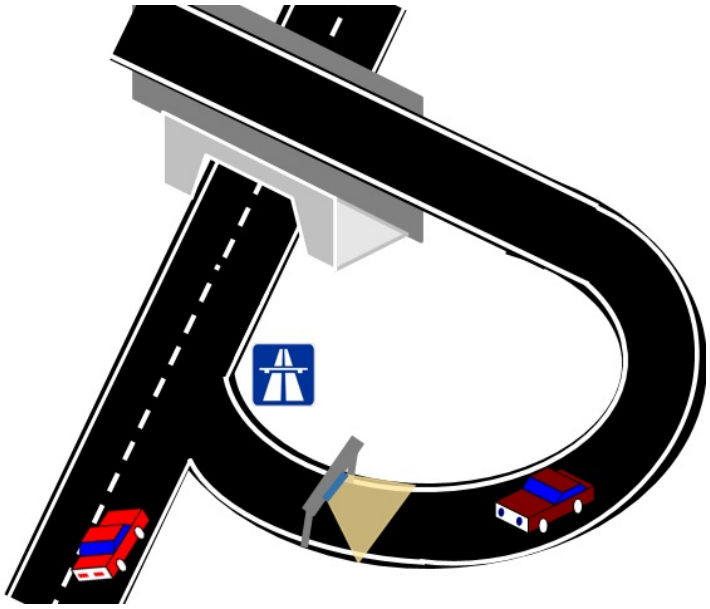

Figure 3.39: Highway tolling system in access lane

In the development of the array, the requirements imposed by the DSRC standards described above, both in terms of polarization or radiation, are also applied. However, since the access roads tend to be wider than the highways lanes, the specific application imposes a radiation pattern on the road plane (horizontal) larger than the usual applications, and with a uniform gain across the width, to avoid communication failures at borders or passing without detection.

As shown before, all the antennas that have been proposed for the RSU module of a DSRC systems are focused on the common toll gates, showing radiation patterns with a narrow HPBW in the horizontal plane, in addition to highly complex structures. A new antenna, suitable for this new approach is presented and described in the following subsections.

Array Element

In the design of this antenna, the microstrip antennas were used due to its benefits of simplicity and versatility, achieving low profile antennas, with simple and inexpensive manufacture. Moreover, they enable the design of AFN using microstrip transmission lines in the plane of the array elements, allowing simple structures.

The array element used in this design consists of a circular microstrip patch, shown in Fig.(3.40). In such a patch shape, the resonance frequency varies with the radius r.

Additionally, two side slits ($\Delta_y \times \Delta_r$) were created, to produce LHCP in the element. Finally, to match the antenna input impedance to the impedance of AFN transmission lines used, a double quarter wavelength transformer was inserted (with lengths l_{t1} and l_{t2}). The dimensions of the microstrip element designed to 5.8 GHz are presented in the Table (3.10).

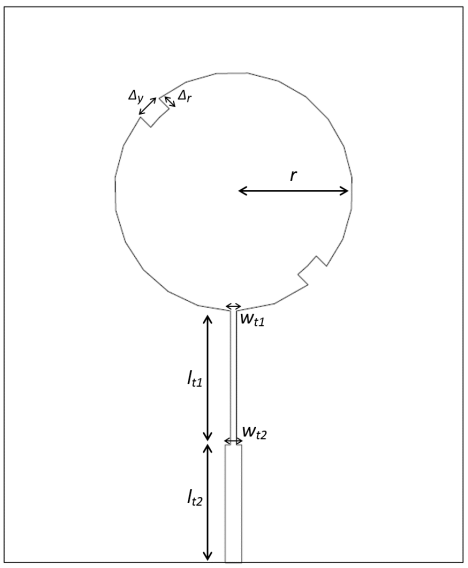

Figure 3.40: Circular microstrip patch element

Table 3.10: Dimensions of the circular Microstrip Patch element

Parameter	r	Δ_y	Δ_r	l_{t1}	w_{t1}	l_{t2}	w_{t2}
Dimension (mm)	9.1	2	1.1	10.2	0.45	9	1.25

Array Structure

The access lanes of highways are usually larger than the highways lanes, due to the curved route done, mainly by the long vehicles. The RSU antenna must have a wider radiation pattern in the horizontal plane, with a HPBW estimated roughly about 60^o.

Using uniform antenna arrays, it is not possible to achieve an HPBW of 60^o with a uniform gain across the entire main lobe, and ensuring low sidelobes, so, nonuniform excitation techniques must be used.

To achieve a radiation pattern with these characteristics, it was investigated the effect and subsequently applied, the Fourier Transform Method (FTM) [1]. This technique allows to find a feed distribution for a set of array elements, in a way to achieve a particular radiation pattern.

For an odd number of elements ($N = 2M + 1$), each element feed coefficient can be calculated by the following equation:

$$a_m = \frac{1}{T}\int_{-T/2}^{T/2} AF(\psi)\, e^{-jm\psi}\, d\psi = \frac{1}{2\pi}\int_{-\pi}^{\pi} AF(\psi)\, e^{-jm\psi}\, d\psi \quad -M \leq m \leq M \tag{3.6}$$

with,

$$\psi = kd\cos\theta + \beta \tag{3.7}$$

The $AF(\psi)$ represents the desired array factor for the array. The Fig.(3.41) shows the desired array factor for this application, which ideally consists of an amplitude maximum over a $\Delta\theta$ width (lane width) and then zero outside of this area. To provide some guard margin, since the HPBW is smaller than the width between nulls, was chosen for calculations $\Delta\theta$=70^o, $\approx 0.39\pi(rads)$ (greater than the 60^o, roughly the desired value for the HPBW).

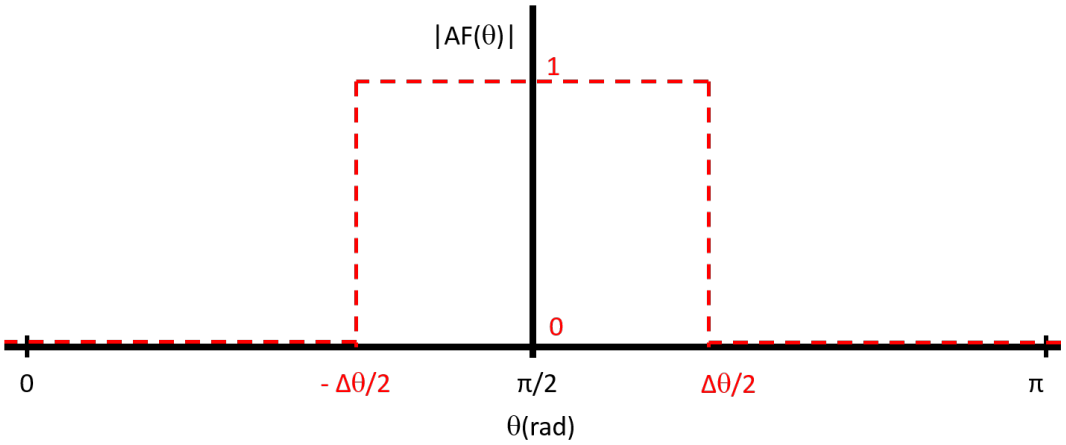

Figure 3.41: Desired Array Factor

Therefore the coefficients may be calculated as,

$$a_m = \frac{1}{2\pi}\int_{-\Delta\theta/2}^{\Delta\theta/2} 1\, e^{-jm\psi}\, d\psi \quad -M \leq m \leq M \tag{3.8}$$

which, solving the integral using $d = \lambda/2$ as the distance between elements and $\beta = 0$,

$$a_m = \frac{1}{2\pi}\left[-\frac{1}{jm}\, e^{-jm\psi}\right]_{-\Delta\theta/2}^{\Delta\theta/2} \tag{3.9}$$

results in the following expression, as function of m, the position of the element on the array:

$$a_m = \frac{1}{m\pi}\sin(0.57\pi m) = 0.57\frac{\sin(0.57\pi m)}{0.57\pi m} \tag{3.10}$$

The Fig.(3.42) shows the theoretical estimation of the array factor, using $d = \lambda/2$ as the distance between elements, with the weights estimated through the FTM method applied to each element, and by varying the number of elements N ($N = 9, 11, 21$).

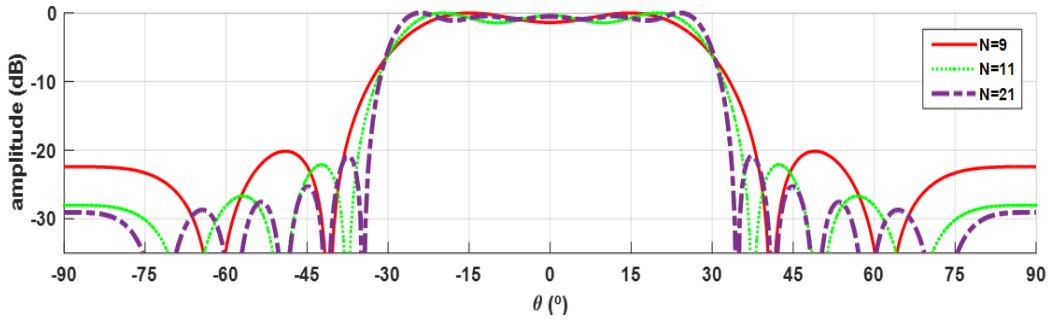

Figure 3.42: Variation of theoretical array response with N, using the FTM coefficients.

Analyzing the Fig.(3.42), it is possible to understand the effect of increasing the number of elements in the array N, fed according to this technique. A higher definition of the array factor with a reduction of SLL can be obtained by increasing N, tending to the shape of Fig.(3.41), when N goes to infinity. However, it dramatically increases the complexity of the array and of the necessary AFN.

The $N = 9$ elements was the number of array elements chosen, since it is the best compromise between the desired radiation characteristics, the good performance, and the design complexity of the array (including the needed AFN).

The coefficients to create the AFN to feed each element of the array, for N=9, are presented in Fig.(3.43).

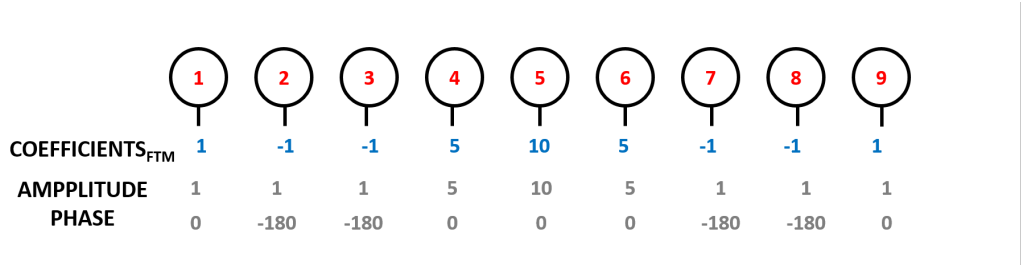

Figure 3.43: Coefficients from FTM for N=9

Using the presented linear array of 9 elements placed along the horizontal plane (1×9) with $d_1 = 0.5\lambda$, the desired radiation shape in the horizontal plane can be obtained, however, the radiation pattern in the vertical plane has a wide HPBW (just being constrained by the radiation pattern of the microstrip element), not fulfilling with the DSRC standards, which establishes a maximum of 70° in this plane.

To meet that condition, an additional line elements was inserted, positioned at $d_2 = 0.6\lambda$, and with equal feed distribution, so that the final antenna array consists of a planar structure of 2×9 elements.

Based on the technique proposed here, the array feed network was designed.

Array Feed Network

The AFN has a great importance in the array design, by implementing the power distribution according the estimated coefficients, and shown in Fig.(3.43). The AFN was designed to provide characteristics of simplicity, low profile and ease of manufacture, on a single dielectric layer structure, placed in the plane of the radiating elements.

Fig.(3.44) shows the structure of designed array, with the AFN created using microstrip lines (of 100 Ω characteristic impedance), T-junction power dividers (PDs), and quarter wavelength impedance transformers.

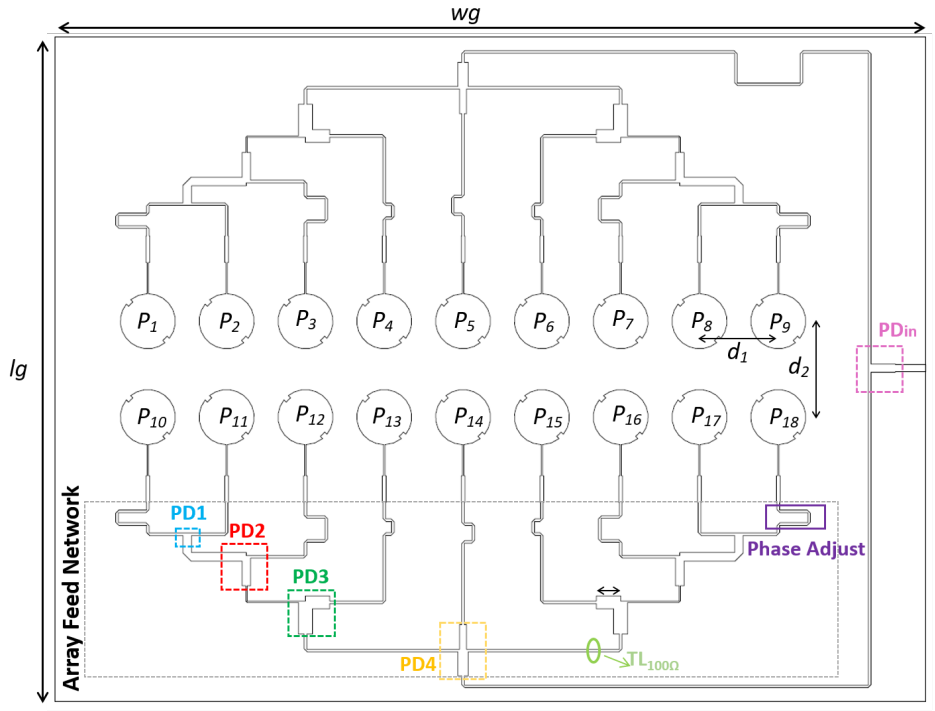

Figure 3.44: Antenna array structure

The AFN has a symmetrical arrangement, with two branches, feeding each line of 9 elements. Each branch is connected to one output of the array input power divider ($PDin$ divider), and the physical rotation between the two lines of 9 elements is compensated by a 180° phase delay between the two branches, created through an additional length of line.

The feed distribution, was accomplished using unequal power dividers ($PD1$, $PD2$, $PD3$ and $PD4$), with the appropriated ratios.

Additionally, the lengths of the 100 Ω microstrip lines that connect the output of the power dividers to each circular microstrip patch, P1... P18, were individually adjusted, to feed of all the microstrip elements with the desired phases.

The antenna was designed using the Rogers RO4725JXR substrate whose main characteristics are the relative dielectric constant $\epsilon_r = 2.55$, a thickness $h = 0.78$ mm and a loss tangent $\tan\delta = 0.0026$. The array was simulated using the electromagnetic simulator: Computer Simulation Technology's Microwave Studio [48].

Fig.(3.45) shows the simulation results of the AFN, providing the amplitude and phases of the signals that get to each microstrip patch of one of the branches (in the other branch are identical). These values, at 5.8 GHz are summarized in Table (3.11). It is possible to realize that both results, amplitude and phases, are consistent with the theoretical relationships desired.

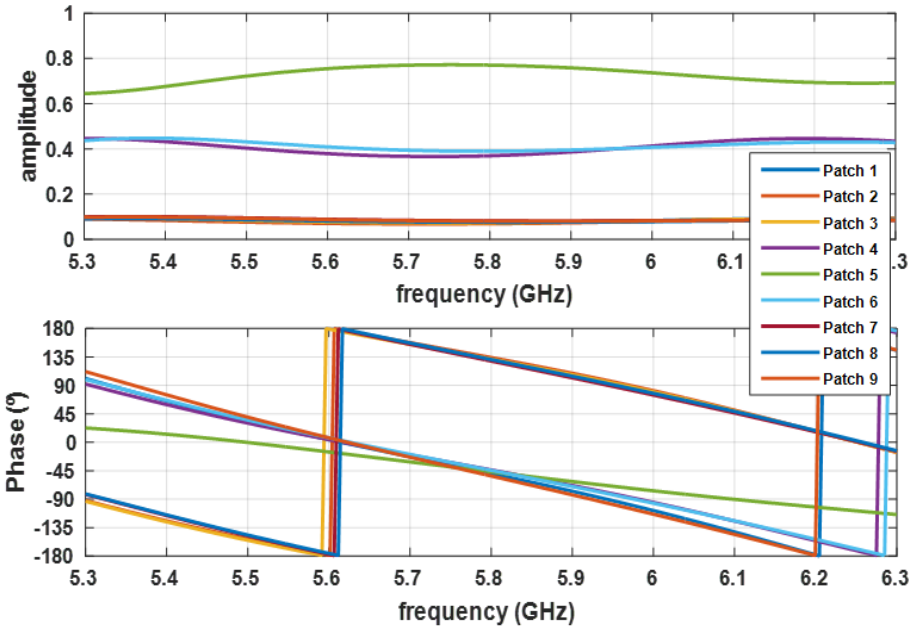

Figure 3.45: Amplitude and phase distribution of the AFN

Table 3.11: AFN - simulated amplitude and phase (5.8 GHz)

Patch	1	2	3	4	5	6	7	8	9
Amplitude	0.073	0.07	0.073	0.37	0.77	0.39	0.08	0.076	0.08
Phase(°)	-50	134	131	-45	-47	-45	128	130	-54

Results

The designed array was manufactured and measured in an anechoic chamber in terms of its main parameters. The results were compared with those simulated, and are presented

below. The prototype is shown in Fig.(3.46), presenting global dimensions of $Wg \times Lg = 286 \times 218\,\text{mm}^2$.

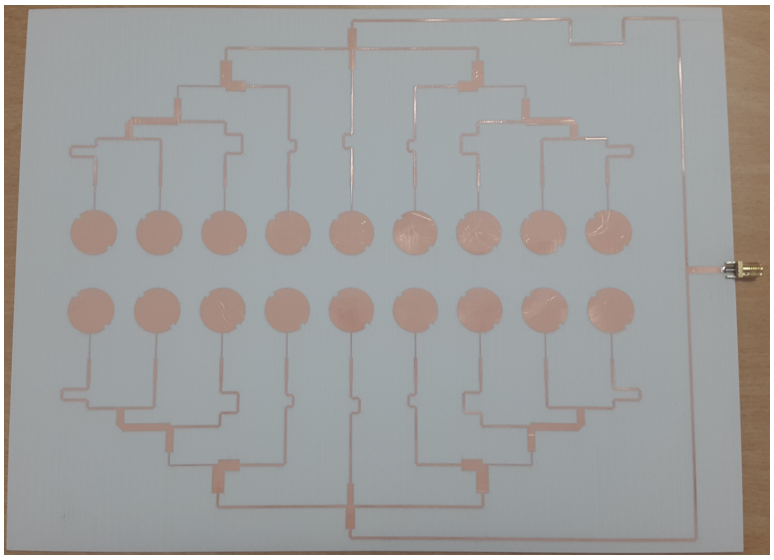

Figure 3.46: Photography of antenna array

The simulated and measured S_{11} of the antenna is presented in the Fig.(3.47). It is possible to notice that there is a good agreement between simulated and measured results, with the two curves exhibiting a similar behavior, despite a slight deviation in terms of frequency, which does not affect the antenna performance. Assuming as a common criterion for an impedance matching, an $S_{11} < -10\,\text{dB}$, the antenna has a bandwidth of 358 MHz.

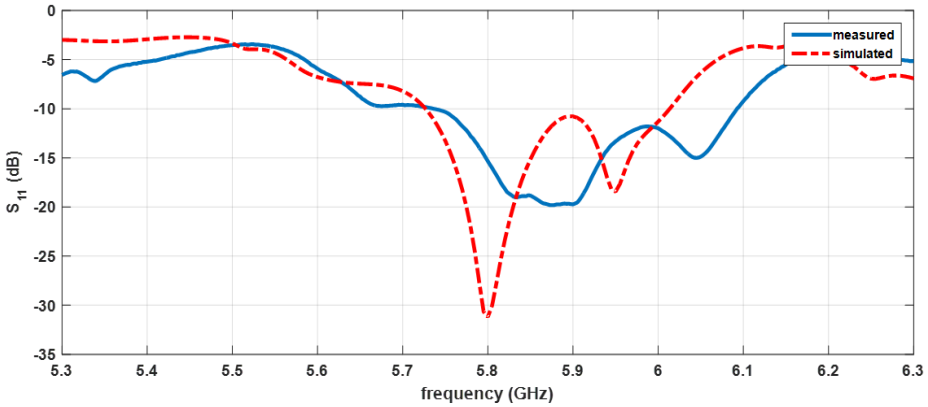

Figure 3.47: Simulated and measured S_{11} of the antenna

In order to characterize the polarization of the array, Fig.(3.48) illustrates the simulated and measured AR of the designed antenna. It is possible to observe an acceptable agreement between the two results, with only a small deviation. Considering the well-accepted criterion for circular polarization, $AR < 3\,\text{dB}$, it can be seen that the antenna array has a 100 MHz band in which presents a good measured AR.

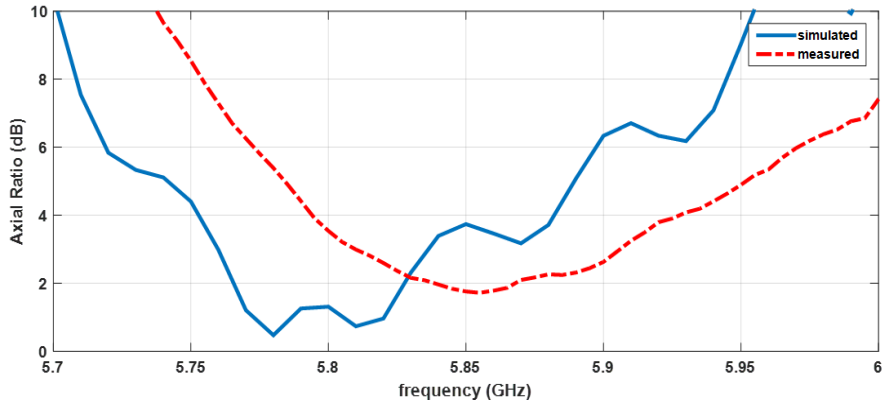

Figure 3.48: Simulated and measured axial ratio of the antenna

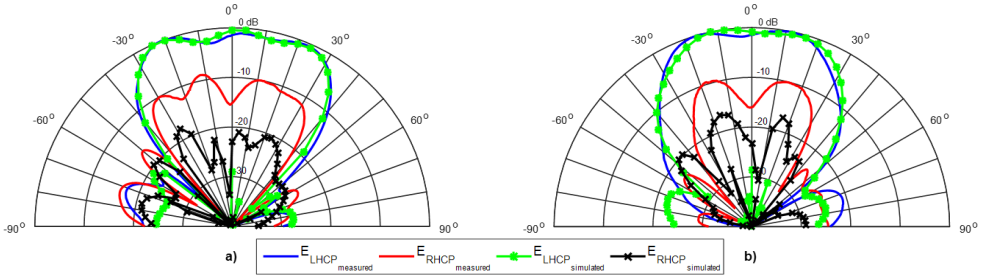

(a) at 5.8 GHz

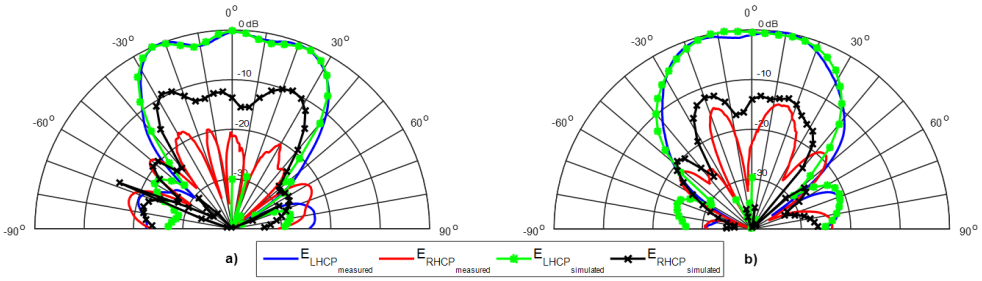

(b) at 5.85 GHz

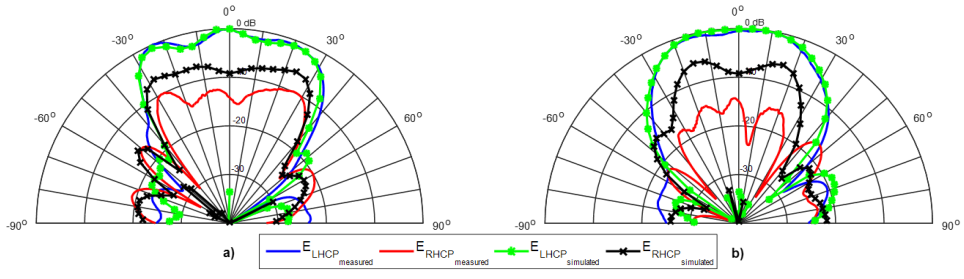

(c) at 5.9 GHz

Figure 3.49: Normalized radiation pattern - a) plane $\phi = 0^o$ b) plane $\phi = 90^o$

Fig.(3.49) presents the normalized simulated and measured radiation pattern of the designed antenna array, in the two main radiation planes, $\phi = 0^o$ and $\phi = 90^o$, at 5.8 GHz, 5.85 GHz and 5.9 GHz frequencies. In each figure are shown the left (E_{LHCP}) and right (E_{RHCP}) components of the electric field. For a straightforward analysis, the main radiation parameters are summarized in the Table (3.12).

The first aspect that can be seen is the good agreement between the simulated and measured results, particularly in the dominant component E_{LHCP}. The rejection between the measured E_{LHCP} and E_{RHCP} components have a small variation, but are consistent with the frequency shift in the AR curve.

The sidelobes are negligible, close to -20 dB, while the HPBW in the horizontal plane is about 60^o, with a magnitude that tends to be uniform along the width, as desired, while in the vertical plane is near to 50^o ($<70^o$), complying to the DSRC standard. The array presents a radiation efficiency close to 85% at 5.8 GHz and a measured gain of 11.3 dBi.

Table 3.12: Radiation Pattern characteristics

Frequency (GHz)	5.8		5.85		5.9	
$Plane(\phi)$	0^o	90^o	0^o	90^o	0^o	90^o
$\Delta_{3dB}/HPBW_{simulated}$	62^o	51^o	62^o	51^o	61^o	50^o
$\Delta_{3dB}/HPBW_{measured}$	62^o	51^o	61^o	49^o	60^o	48^o
$SLL_{simulated}(dB)$	-21	-22	-22	-21	-19	-18.6
$SLL_{measured}(dB)$	-19	-21	-20.5	-21	-23	-21

3.4 Concluding Remarks

In this chapter the topic of vehicular communications was addressed, focusing on a DSRC system for tolling applications. In this sense, a set of antennas/antenna arrays were proposed for all the elements composing the system, OBU and RSU. These antennas constitute advances in the state of the art, exhibiting planar and single layer antennas, with different degrees of complexity in the design, compactness, functional, with agreement with the DSRC standards and with reduced manufacturing cost.

Regarding the OBU module, three monopoles were developed with the purpose of achieving an omnidirectional radiation that ensures a better communication V2V/V2I. A printed monopole antenna containing linear polarization in a wide bandwidth and an omnidirectional radiation pattern was presented as a first approach, however, due to the linear polarization (RSU has LHCP), there is 3 dB loss in communication, that must be accounted. A second approach, trying to overcome this issue has been designed, with a monopole attempting to generate circular polarization. A second approach, trying to overcome this issue was designed, with a monopole attempting to generate circular polarization. This was achieved, and with an omnidirectional radiation pattern, however, it was verified that in each side there was a different polarization sense i.e., LHCP in one side and RHCP to the other, which completely prevents communication to one side. Finally, a structure has been studied by simulation, using this mentioned monopole, and using an absorbent layer, that allows to foresee the possibility to obtain an omnidirectional radiation diagram with LHCP. However, still some work needs to be done to characterize a ferrite plate and building a prototype.

Concerning the RSU, a set of nonuniform antenna arrays were developed, two for the trans-

mission part and one for the receiving part. Also, another array for a new approach for tolling communications was presented. A 2×4 antenna array was proposed, with characteristics that are approaching to the DSRC standards, whose the wide bandwidth covering all the DSRC bands, the small size and the simplicity were important achievements.

Emphasizing the good cooperation with a motorway company, and the feedback they provided based on practical measures on the road, a new antenna array was investigated and developed, covering all the recommendations and the DSRC standards. A planar array of 12 elements with a complex structure, but designed in a single substrate layer, with reduced sidelobes, a broad bandwidth of polarization, over 1 GHz and covering the DSRC bands, and the radiation pattern consistent with the objectives were the main findings. For the receiving part of the RSU, an array of five elements was developed in concordance with the specific requirements, with reduced size and complexity compared to the developed array for TX. A new nonuniform antenna array was also developed for a new approach presented for tolling applications, exhibiting a planar structure of 18 elements whose main feature, in addition to complying with all DSRC requirements (although a slight deviation in measurements compared to simulations), is the wide radiation pattern (approximately 60^{o} of HPBW) with a almost uniform amplitude in the main lobe.

Chapter 4

Antenna Arrays for Wi-Fi applications in Sports Arenas

Wireless communications had a great progress over the last decades and nowadays they are present everywhere, increasingly used for different applications. New challenges have emerged to deploy Wi-Fi networks in densely populated places, such as sports stadiums, extending their capacity and coverage. Their application in the business of sports events as a means to improve the experience and involvement of the fans during games is becoming essential, offering to the public a set of facilities.

In this chapter this topic is addressed with the design of an antenna array for an access point of a Wi-Fi network with characteristics that meet the requirements for the 2.4/5.2 GHz wireless communications applied to sports stadiums.

4.1 Wi-Fi in Sports Arenas

Wireless communications are under constant progress, and in recent years the use of Wi-Fi has been exponential, as a consequence of the increasing number of electronic devices, smartphones especially.

Nowadays people expect to have access to a Wi-Fi network any time, in any place, whether in our homes or in public places. In most of small public places such as cafes and bars, these networks are already commonly implemented. However the big challenge nowadays is to develop Wi-Fi networks in densely populated places with high needs for access, such as sports stadiums.

In the future, clubs and sports organizations consider to create a technological revolution in their stadiums, expanding the multimedia experiences they provide for their fans and attract them to the events, fighting against the complacency that makes them stay at home, watching events on TV and enjoying all the comfort that it provides.

There are stadiums composed of 60, 70 or even 80 thousand seats, filled by fans, almost all using mobile devices. Sending messages, accessing websites, sports applications, statistics, replays and social networks, sharing photos and videos, are a set of experiences that fans expect to enjoy. In addition, further strategies can be taken to improve the connection between the club and their fans, and the way they live that moment, for example using hashtags in the published photos, and thus making them appear on the screens of the stadium, allowing them to also buy club merchandise, or even tickets for future games.

Currently, the main existing Wi-Fi networks in sports venues are not designed for such high density of users, limiting the capacity of the network. Therefore, a more robust network, capable of withstanding the access needs, and of providing a good quality service in order to satisfy all users is required.

To accomplish such objectives of increasing the capacity, it is necessary to divide the stadium in a huge number of sectors, each covered by an access point (AP), close to each other. This approach requires a careful study of the arrangement of these APs, covering small adjacent sectors and limiting the number of users that connects to each AP/sector, as shown in Fig.(4.1). Also, a great care should be taken to minimize interference between sectors.

Depending on the area to cover and the desired capacity, it is established the necessary number of sectors/APs. With the larger the number of APs installed, the greater will be the interference between them.

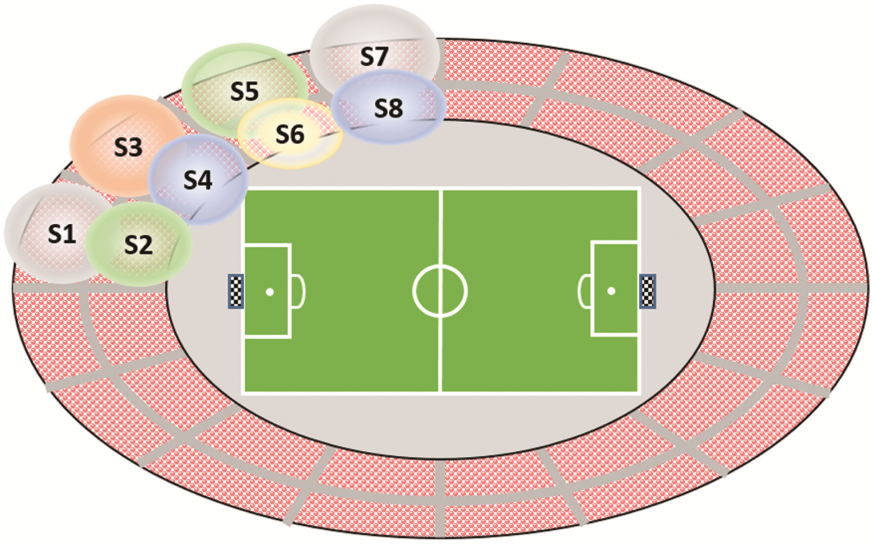

Figure 4.1: Football Stadium using sectorized Wi-Fi links

Typically, the APs operate at dual-band, in both 2.4 GHz and 5.2 GHz Wi-Fi frequency bands, supported by most of the devices, enabling to double the capacity. A crucial component for the AP is therefore its directional antenna and its respective location.

About the AP antenna, it must have a narrow beam and must operate in dual band respectively at 2.4 GHz and 5.2 GHz, containing dual linear polarizations. The set of requirements for the antenna is shown in Table (4.1).

In addition, and given the huge number of sectors necessary to cover a stadium, the requirements of simplicity, low profile, and reduced manufacturing cost are also important for its antennas.

Table 4.1: AP-antenna requirements

Band	BW (MHz)	Polarization	HPBW	Gain (dBi)	Side Lobe Level (dB)
Wi-Fi 2.4GHz	80 [2400 – 2480]	Linear	25^{o}	> 12	≥ 18
Wi-Fi 5.2GHz	200 [5150 – 5350]				

A number of antenna arrays developed for Wi-Fi communications in the 2.4GHz band are reported in the literature [51, 52, 53, 54].

A high-gain multilayer antenna, that consists of a 2×2 array for application in WLAN access point is presented in [51]. This antenna was fabricated using FR-4 substrate with an air gap to the ground plane, and has about 30^o of HPBW. However, in addition to not providing measured results, it is possible to observe that the SLL are not lower as intended. In [52] is shown a 2.4 GHz planar dipole array that can achieve four high directive radiation patterns using the switches placed between the elements and the feed network. This antenna has 240 MHz bandwidth despite its wide beamwidth, low gain and complex structure are some drawbacks.

For Wi-Fi access points, [53] presents a Bow-Tie dipole antenna array. This antenna has more than 1.2 GHz bandwidth, but the radiation pattern does not agree with our requirements, in addition to having a complex and bulky structure. A low profile antenna array for 802.11b/g (2.4-2.485 GHz) is shown in [54]. The antenna has a 3×3 structure and uses probe-fed elements in a metallic cavity with a dielectric radome. Although the antenna presents 30^o of HPBW, the bandwidth is limited, the SLL is out of requirements, and the array shows a complex structure.

For the 5.2 GHz Wi-Fi band, in [55, 56] are presented two antenna arrays. In [55] is presented the design of wideband microstrip Yagi-Uda antenna suitable for various applications such as radar and wireless networks. This antenna covers the frequency band of 5.04-5.85 GHz with minimum value of 13 dB for return loss, however the radiation pattern doesn't agree with the requirements. The design of a 2×2 microstrip array antenna suitable for wireless applications is presented in[56]. The larger bandwidth about 1.85 GHz (4.69-6.54 GHz) is achieved, but the antenna has about 60^o of HPBW, which is too large for this application.

In [57] is presented a wideband printed dipole array for WLAN applications. In this antenna a broadband characteristic greater than 12% centered at 3.5 GHz is achieved. Important advantages are the simplicity in structure, low cost, and ease to manufacture and produce. The measured radiation pattern at 3.5 GHz shows about 19^o of beamwidth and side lobe levels 16 dB below the main beam. The cross-polarization level is -25 dB and the directivity is 18.5 dBi. However, the frequency band doesn't match the requirements.

In [58, 59, 60, 61] is presented a group of antennas for WLAN, operating both at 2.4 GHz and 5.2 GHz bands.

The paper [58] suggests a multi-band antenna with 32 elements for WLAN/WiMAX applications, but the radiation pattern of the antenna at 2.4 GHz shows a high SLL. A planar dual band antenna array operating at 2.4-2.5 GHz and 5.1-5.5 GHz is presented in [59]. The antenna consists of four branches suspended above a ground plane, presenting a HPBW of 25^o, however this solution shows some complexity in the structure and high SLL.

In [60] is presented a planar wideband linear antenna array that covers multiple wireless standards. This array consists of four microstrip-line fed open-ended quarter-wavelength slot elements, and has 83% of relative impedance bandwidth, from 2.55 GHz to 6.1 GHz. Although the antenna is designed for wireless applications, the radiation pattern cannot fulfill our requirements.

In [61] the antenna consists of two different antenna elements, which are combined in one structure: a radial line slot array antenna operating at the 2.4 GHz and a microstrip patch antenna operating at the 5.2 GHz frequency band. Both antennas are aimed to feature circular polarization in horizontal plane. However, the radiation pattern is not as narrow as required and do not have linear polarization.

The design of two antenna arrays, for the 2.4 GHz and 5.2 GHz Wi-Fi frequency bands, with radiation characteristics that meet the requirements for wireless communications applied to sports stadiums is presented. The planar structure, with the radiating elements and the nonuniform AFN printed on the same plane on a single dielectric layer, is also designed using low cost materials, and with considerable tolerance to deviations in manufacturing and in the material properties, which are important and differentiators aspects.

The design and development of these arrays enabled two scientific contributions accepted by the scientific community, a paper presented and discussed at an international conference **[C9]**, and a paper published in a journal **[J4]**.

4.2 Antenna Design

To ensure the desired requirements, to guarantee the low cost, simplicity, and ease of manufacture, and to contribute to reliability of mass production the design of the antennas comprises a number of options to take.

Microstrip antennas were used, given their great benefits aforementioned in the chapter 2, such as the simplicity, versatility, low profile, light weight, and ease of integration with integrated microwave circuits.

To reach the radiation requirements referred in Table (4.1), particularly in terms of HPBW, Gain and SLL, since the radiation pattern of a single microstrip element has a wide beamwidth, an antenna array must be used. The number of elements chosen for the array structure was $N = 4$, since it is the minimum number of elements that allows to obtain the desired HPBW, and also that provides some degree of freedom to use nonuniform techniques to reduce the SLL to acceptable values. To obtain a symmetric radiation pattern, in the two main orthogonal planes, a planar 4×4 array structure was applied. The distance between antenna elements was selected to find the intended HPBW, and based on the array theory, eq.(2.63), and some electromagnetic simulations was fixed $d = 0.7\lambda$.

It is known that using the traditional uniform excitation in the array, the side lobes of the radiation pattern cannot be under the theoretical limit of about -13.5 dB, as shown in Fig.(2.16), which is far from the required. Nonuniform excitation methods must be used to reduce the SLL.

The technique used to reduce the side lobes was the Dolph-Chebyshev method, referred in the section (2.3.3). This method, compared to Binomial or Taylor, guarantees the narrowest HPBW. Moreover, this technique is usually applied to design antenna arrays with SLL constraints. The coefficients estimated from Dolph-Chebyshev technique to obtain a radiation pattern with SLL of -20 dB, using a 4×4 antenna array, are presented in the Fig.(4.2).

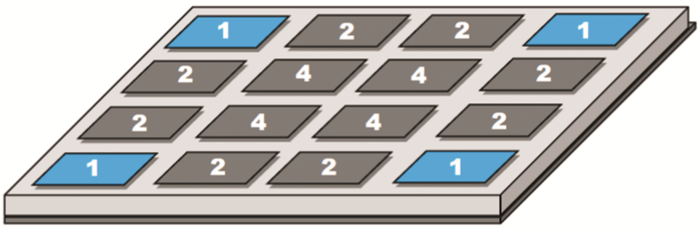

Figure 4.2: Dolph-Chebyshev amplitude distribution for the 4×4 antenna array

To comply with the needs for low cost, the use of FR-4 substrate is crucial. This material is composed by fiberglass cloth embedded in epoxy resin, and is very popular because it has good strength and is inexpensive. However, as its main properties, particularly the dielectric constant and loss tangent are quite dependent of the frequency, temperature, and also the direction of propagation, it is crucial to attenuate this dependence.

A simple way to minimize the impact of the variations in FR-4 substrate properties is to use a two dielectric layer structure, using air as the second dielectric material. Since the dielectric constant of air is $\epsilon_{r_{air}} = 1$, according to the equations in [62], some fluctuations around the value of FR-4 dielectric constant ($\epsilon_{r_{FR-4}} = 4.4$) will have a diminished influence in the equivalent dielectric constant of the structure composed by the two layers (similar behavior happens in the calculation of the parallel of two resistors with a high discrepancy values, which result is mainly influenced by the lower resistance). This structure allows therefore to desensitize the main characteristics of the array to the variations in the dielectric properties of the used substrate material, and is an important advantage that will allow also a greater reliability for mass production. Furthermore, this process permits to increase the bandwidth of the antenna array, which is important to support any deviation in the antenna manufacturing process.

To feed each microstrip patch using the power distribution shown in the Fig.(4.2), it is essential to design an appropriate feed network for the array. The AFN is designed applying transmission lines and Wilkinson power dividers, using microstrip structures printed on the substrate. To meet the requirements of simplicity and ease of manufacture, this AFN must be built on the same plane of the array elements. However, the available space for routing the AFN in the 4×4 array structure tends to be limited.

The adopted solution consists of using the technique described in the section (3.3.2), and presented in **[J2]**, which consists in removing the four elements of the corners of the 4×4 structure, since their minor impact is widely compensated for by the increased area available to create the AFN in the plane of antennas, making also the AFN simpler with the absence of the 4 elements discarded.

4.2.1 Array for 2.4GHz Wi-Fi Band

The thickness of the air layer was fixed $h_{air} = 5\,\text{mm}$, since it is the best compromise (for the frequency of interest) between size and manufacturability of transmission lines and patches, as well as the bandwidth and loss of the structure. Considering the two-layer structure, as aforementioned, with one air layer $\epsilon_{r_{air}} = 1$, and assuming the dielectric substrate FR-4 has the following characteristics $h = 1.6\,\text{mm}$, $\tan\delta = 0.02$ and $\epsilon_r = 4.4$, then, the equivalent dielectric constant of the two layers calculated through [62] is $\epsilon_{r_{eq}} = 1.72$.

The structure of the designed array is presented in the Fig.(4.3). It consists of a planar 4×4 arrangement of rectangular microstrip patches without its 4 corner elements, designed according to the transmission line model to the central frequency $f_c = 2.44\,\text{GHz}$ and tuned by simulation. The dimensions of the patch ($w \times l$) are 52×42 mm^2.

In the Fig.(4.3) it is also possible to observe that the 6 elements at the bottom of the array are rotated 180º relative to the six elements of the upper part, in order to simplify the design and construction of the AFN. However, this rotation is properly compensated with a corresponding phase delay in feeding of those elements.

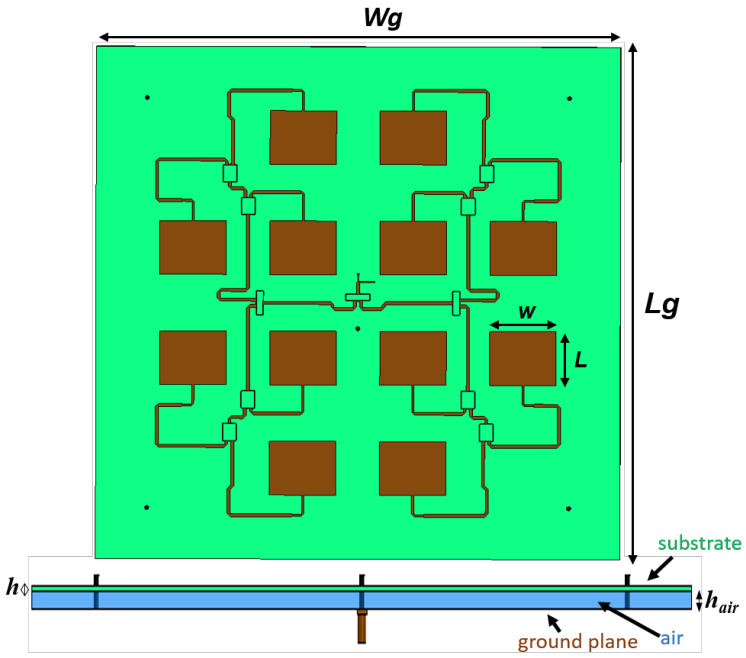

Figure 4.3: Antenna array structure

Also, the Fig.(4.3) shows the designed AFN that creates the desired feed distribution of Fig.(4.2), which can be decomposed into four quadrants. Each quadrant consists of a cascade of two symmetric Wilkinson power dividers and 150 Ω characteristic impedance microstrip transmission lines, that connects each Wilkinson output to each patch through a quarter wavelength transformer, transforming the output impedance of the dividers $Z_{out-dividers} = 150\,\Omega \rightarrow Z_{in}$ to the patch input impedance. Each Wilkinson power divider includes soldered a resistance of 300 Ω. The transmission line lengths were carefully adjusted to ensure that all elements are fed with the same phase.

Finally, the AFN starts with an open stub matching network that transforms the 50 Ω input impedance to 150 Ω and also compensates the reactance introduced by the wire that connects the coaxial feed and the AFN, through the two layers. The FR-4 structure is fixed to the plane metallic ground plane using five metal screws and the spacing is ensured using five Nylon spacers of 5 mm height. The overall dimensions of the antenna are $L_g = 40$ cm, $W_g = 41$ cm and $h_{air} = 5$ mm. The array was simulated and optimized using the electromagnetic simulator CST MWS- Computer Simulation Technology's Microwave Studio [48].

The first analysis that is important to evaluate by simulation is the impact of variations in either the dielectric constant of the used substrate (FR-4) and in the height of the air layer, essential to ensure that the antenna keeps the good characteristics even subject to occasional failures, as result of mass production.

To observe the impact of the deviations in the dielectric constant of the FR-4 material in the impedance adaptation of the designed array, the antenna was simulated for different values of the ϵ_{FR4} around the initial value of 4.4, and the results are presented in the Fig.(4.4).

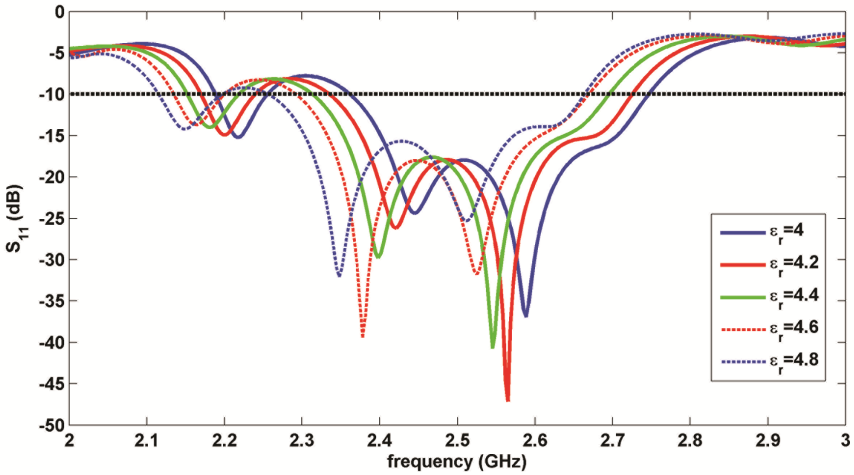

Figure 4.4: Simulated S_{11} for different values of dielectric constant

Although the variations made in the dielectric constant reached the 10%, the antenna remained with good S_{11} results (assuming the common criterion of $S_{11} < -10\,\text{dB}$), and showing an wide bandwidth characteristic.

Another important aspect is the effect of variations in the thickness of the air layer in the fabrication process. Some simulations were made changing the h_{air} around 5 mm, and the results are shown in the Fig.(4.5).

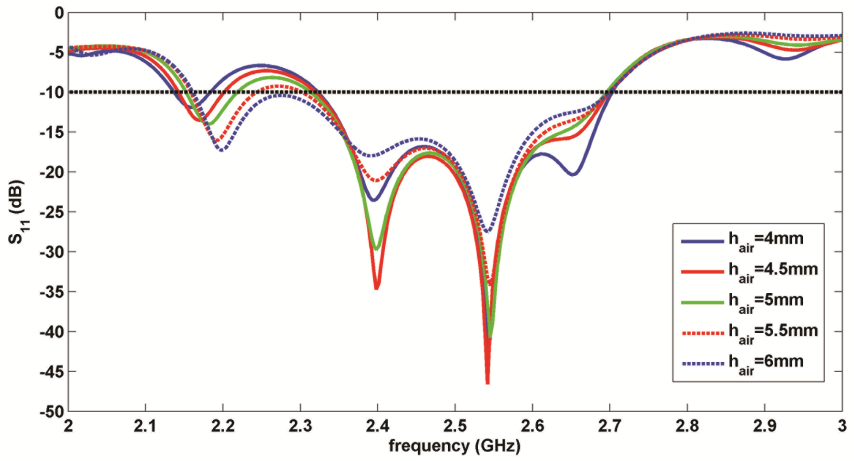

Figure 4.5: Simulated S_{11} for different values of air layer thickness

According to the Fig.(4.5), it is possible to conclude that small variations in the thickness of the air layer have a reduced impact in the antenna adaptation and in its bandwidth.

The designed antenna array was manufactured and the prototype is shown in Fig.(4.6). It was measured and characterized for its main aspects: reflection coefficient, polarization, and radiation pattern, and their comparison with the simulated results of the antenna is presented in the Figs.(4.7-4.8).

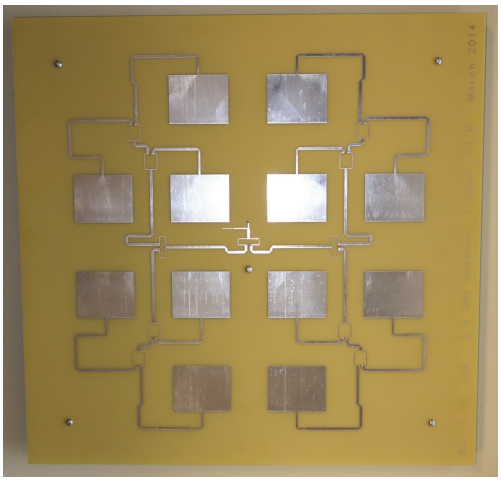

Figure 4.6: Photography of antenna array

The Fig.(4.7) shows the comparison between the simulated and measured S_{11} of the antenna in a band encompassing the band of frequencies of interest. Despite a very slight deviation in the frequency, it is possible to realize that there is a good agreement between the simulated and measured results, with a similar behavior of both curves. Assuming as a criterion for a good impedance matching an $S_{11} < -10\,\text{dB}$, the antenna has an impedance bandwidth of 300 MHz.

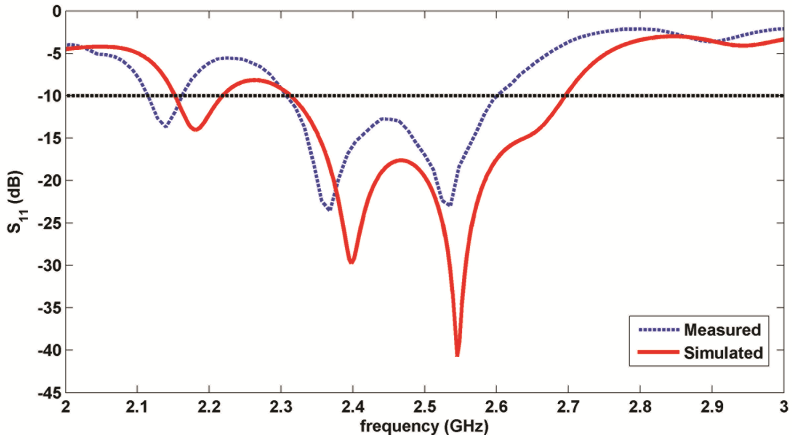

Figure 4.7: Simulated and measured S_{11} of the antenna

The simulated and measured normalized radiation patterns of the developed antenna array are presented in the Fig.(4.8), for the center and for the edges of the interest frequency band: 2.4 GHz, 2.44 GHz and 2.48 GHz.

In each sub-Figure are shown the two components of the electric field, simulated and measured, in the two main orthogonal planes, in which it is possible to observe a good agreement between measured and simulated curves.

The main radiation characteristics that can be withdrawn from the Fig.(4.8) are summarized in the Table (4.2). In terms of HPBW, the antenna has about 26°, which agrees with the initial expectations. Also, the measured side lobes follow the simulated results, and are

always lower than 18 dB, imposed by the requirements. The measured gain of the antenna is 16.21 dBi.

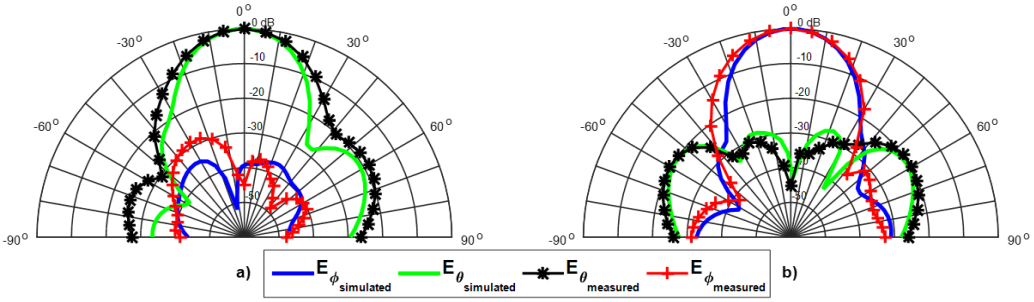

(a) at 2.40 GHz

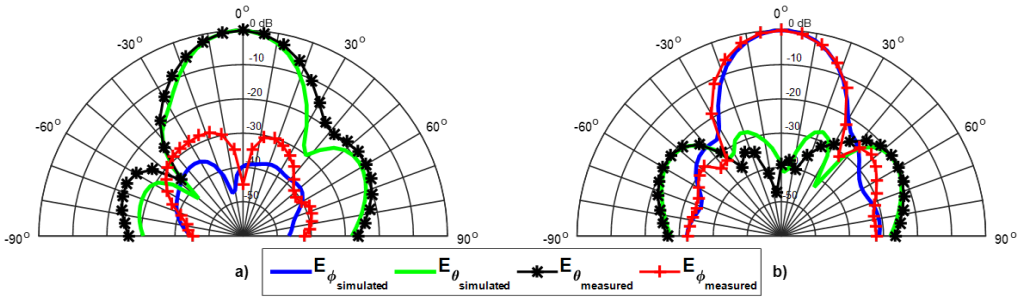

(b) at 2.44 GHz

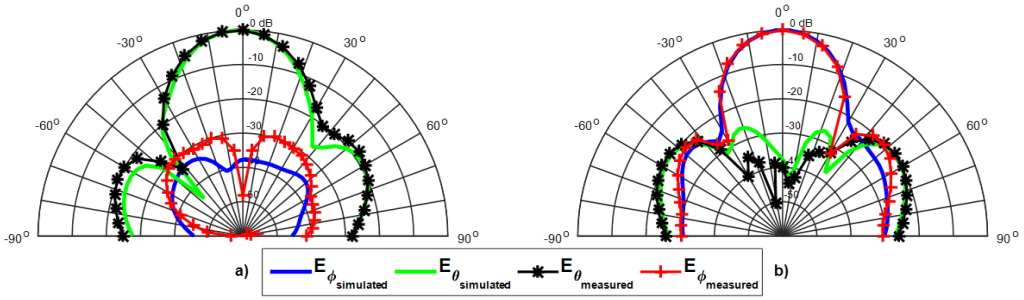

(c) at 2.48 GHz

Figure 4.8: Normalized radiation pattern: a) plane $\phi = 0^o$ b) plane $\phi = 90^o$

Table 4.2: Radiation Pattern characteristics

Frequency (GHz)	2.4		2.44		2.48	
$Plane(\phi)$	0^o	90^o	0^o	90^o	0^o	90^o
$HPBW_{simulated}$	24^o	24^o	24^o	23^o	23.5^o	22.5^o
$HPBW_{measured}$	27.5^o	27^o	26^o	25^o	25^o	23.5^o
$SLL_{simulated}(dB)$	-20.8	-20.3	-19.8	-20.4	-19.1	-19.5
$SLL_{measured}(dB)$	-18.3	-19.5	-18.2	-19.8	-18	-19

4.2.2 Array for 5.2GHz Wi-Fi Band

The geometric configuration and structure of the designed antenna to operate at 5.2 GHz, preserve identical rules as used in the design of the array for 2.4GHz. It consists of an array N=12 microstrip elements, using two dielectric layers, being one of air and the other is the FR-4 substrate already described.

The height of the air layer was settled $h_{air} = 2\,\text{mm}$, by ensuring a compromise between the dimensions of the transmission lines and patches at the frequency of interest, as well as the loss of structure. The equivalent dielectric constant of the structure composed by the two material layers ($\epsilon_{r_{\text{FR4}}} = 4.4$, $h_{\text{FR4}} = 1.6\,\text{mm}$, $\epsilon_{r_{air}} = 1$, $h_{air} = 2\,\text{mm}$) calculated is $\epsilon_{r_{eq}} = 2.21$.

The microstrip patches were designed and optimized for this frequency band, exhibiting a square shape whose dimensions are $w = l = 17.4\,\text{mm}$.

In terms of the AFN, it is similar to the previous antenna (for 2.4 GHz), each quadrant (made up by a group of three patches) is fed by a cascade of two Wilkinson power dividers with equal splitting, and each output of Wilkinson divider connects to the corresponding patch element through a quarter wave-length transformer and 150 Ω microstrip transmission lines. Each quadrant is fed with equal amplitude and the phases were carefully adjusted ensuring that all elements are fed in phase and properly compensated (in terms of the feeding phase) the physical rotation in the array structure between the top elements to the bottom. At the end, a matching circuit transforms the 50 Ω input impedance to the impedance of the lines (approximately 58 Ω (115 Ω//115 Ω)), properly compensating the inductive part created by the wire connecting the connector to the AFN, passing through the two dielectric layers.

The FR-4 substrate structure is fixed to the metallic ground plane by five metal screws and the air gap is ensured using five Nylon spacers of 2 mm height. The overall dimensions of the antenna are $L_g \times W_g = 19 \times 19\,\text{cm}^2$. To complete the array structure, ten 240 Ω resistors were soldered (one at each Wilkinson).

The array was simulated and optimized using the CST electromagnetic simulator, and its structure is shown in Fig.(4.9a).

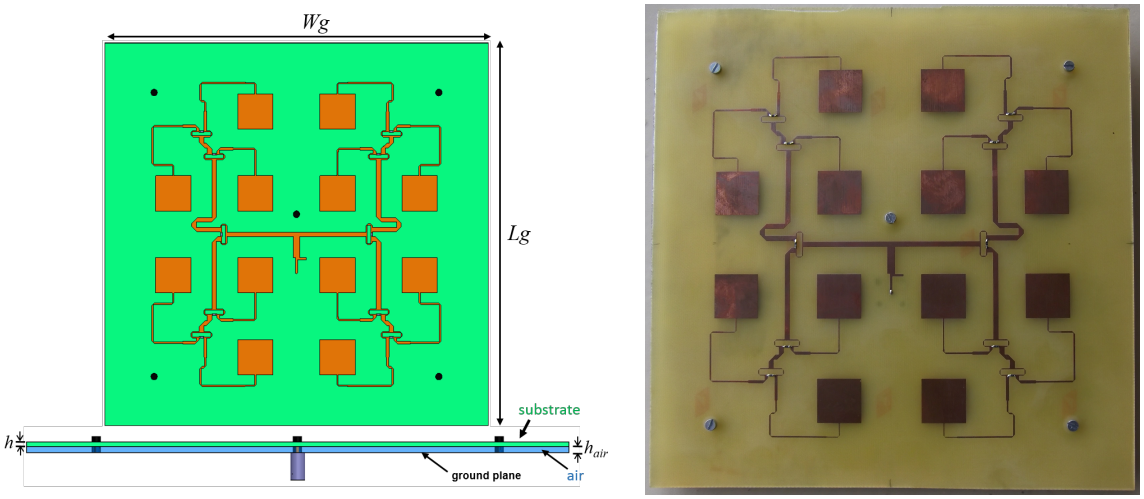

(a) Antenna array designed structure

(b) Photography of antenna array prototype

Figure 4.9: Wi-Fi 5.2 GHz antenna array

The array was fabricated and measured in an anechoic chamber, and the prototype is shown in Fig.(4.9b). It was characterized regarding its main parameters, reflection coefficient and radiation pattern, and the results were compared with those obtained by simulation, and are presented in the Figs.(4.10) and (4.11).

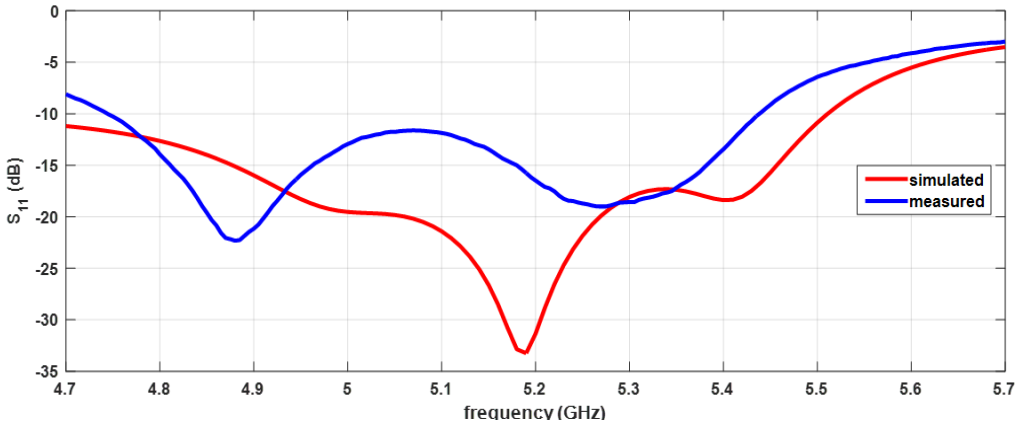

Figure 4.10: Simulated and measured S_{11} of the antenna

A comparison between the simulated and measured reflection coefficient of the proposed antenna is shown in Fig.(4.10). Assuming as criterion for a good impedance matching an $S_{11} < -10\,\text{dB}$, the antenna has an S_{11} of -16.5 dB at 5.2 GHz and a bandwidth of 700 MHz, between [4.75- 5.45]GHz, covering the frequency band of interest.

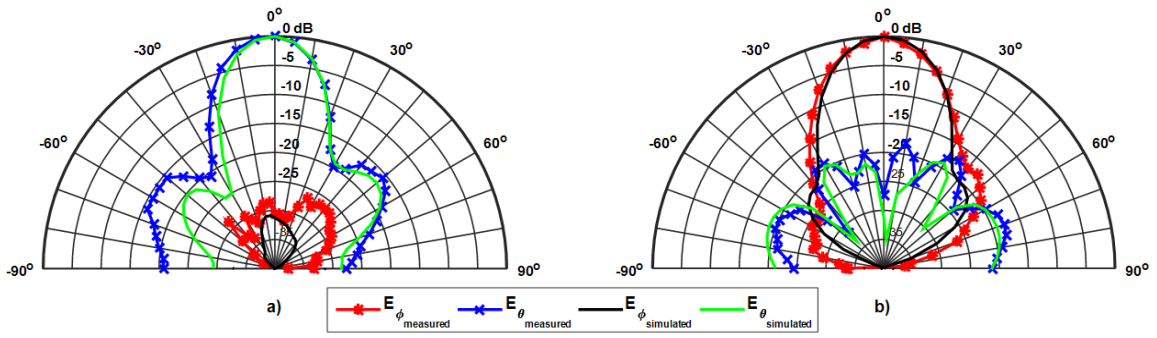

Figure 4.11: Normalized radiation pattern (5.2 GHz): a) plane $\phi = 0^o$ b) plane $\phi = 90^o$

Fig.(4.11) shows the normalized radiation pattern of the antenna array at 5.2 GHz, in terms of the two components of electric field, E_θ and E_ϕ, simulated and measured, in the two main planes a) $\phi = 0^o$ and b) $\phi = 90^o$. The main relevant properties are summarized in the Table (4.3).

Table 4.3: Radiation Pattern characteristics

Frequency (GHz)	5.2	
$Plane(\phi)$	0^o	90^o
$HPBW_{simulated}$	20^o	24^o
$HPBW_{measured}$	21.5^o	24^o
$SLL_{simulated}(dB)$	-17.05	-20
$SLL_{measured}(dB)$	-15.7	-17

First, it is important to note the good agreement between simulations and measurements results. The antenna has an HPBW of 22^o in the plane $\phi = 0^o$ with a simulated SLL of -17 dB and measured about -15.7 dB. The cross polar rejection is more than 25 dB at boresight. In the plane $\phi = 90^o$ the simulated and measured HPBW is equal to 24^o, with the simulated SLL of -20 dB and measured of -17 dB. In this plane, the cross polar rejection exceeds the 25 dB. The antenna gain is 15.9 dBi.

4.3 Concluding Remarks

The developed antenna arrays for the Wi-Fi 2.4/5.2 frequency bands were designed consisting of a 12 elements planar antenna array, using non-uniform excitation based on Dolph-Chebyshev polynomials distribution. This array presents low cost and a structure that simplifies the manufacturing process since the array is printed in a single layer of FR-4 substrate. Also, the design with desensitization to the FR-4 properties by introduction of an air layer enables another important characteristic of immunity to small variations in the substrate main properties.

The results of the 2.4 GHz antenna array are good, and the ones for the second array at 5.2 GHz are also promising, and can be improved in the detail of the SLL values. It is important to refer that while the first array was manufactured by a specialized company (it's noticeable in the figure prototype), the second array was made locally (by chemical process) showing naturally lower reliability in their physical dimensions, and possibly the reason for some difference with the simulations.

Overall, both antennas reveal relevant features that make them feasible to deploy in wireless network infrastructures in sports venues. Its directive radiation pattern combined with the reduced sidelobes that avoid adjacent sector interference, the wide bandwidth and the capability to accommodate large manufacturing tolerances, with easiness of manufacturing and low cost materials are important achievements.

Chapter 5

Adaptive Antennas

In recent decades we have witnessed a great progress in wireless communications, its use has grown, as well as the huge amount of traffic that users expect to consume, putting the capacity of wireless networks as the key factor in its development. Its main limitation is the increasingly interference between channels and multipath fading. To improve the performance of wireless networks, the smart antennas technology has emerged, opening new perspectives of increasing its capacity and the coverage.

5.1 Introduction

Adaptive antennas [63, 64], often referred as Smart antennas, have a great potential over all the future wireless communications and have been the subject of relevant study and development over the past years. While in the also known phased arrays the direction of maximum radiation is controlled by adjusting the phase of feeding of each element of the array, the adaptive antennas continuously adjust the feeding of its elements of the array, and therefore their radiation characteristics, to adapt to the changes in the environment around them, improving the communication.

This type of antennas attracted the attention in the past, mainly by the military branch, although it has had a greater progress in recent years, as the result of technological developments, especially in the processors and in the new signal processing techniques. Nowadays smart antennas are attractive for several areas including the military applications, software defined radio, satellites, mobile communications (especially in base stations), 4G MIMO and the emerging 5G MIMO.

Adaptive antennas consist, in a simple way, of an antenna array and a sophisticated signal processor, allowing automatically adjustment of its form of radiation. The dynamic and flexible adjustment of its radiation pattern, using a relevant signal processing capability allows to respond in real time, not only by detecting the directions of arrival (DOA) signals, but also, according with them, by applying beamforming techniques and using a proper excitation of each element of the array, shape and steer the radiation pattern of the array, adjusting the locations of its maximums and nulls, to achieve a better reception or transmission.

The increase of the coverage, since the signals from the elements are constructively combined in a specific direction of interest, and also the ability to reduce or eliminate the impact of interference signals, allowing frequency reuse and contributing to increase the capacity, are some of the principal advantages of adaptive antennas over the conventional arrays. Further-

more, it enables the reduction of delay spread effects and a greater ability to reduce the impact of multipath fading. Fig.(5.1) shows the simplified block diagram of an adaptive antenna, in the receiving mode, in which is noticeable some of the different elements that constitute an adaptive antenna.

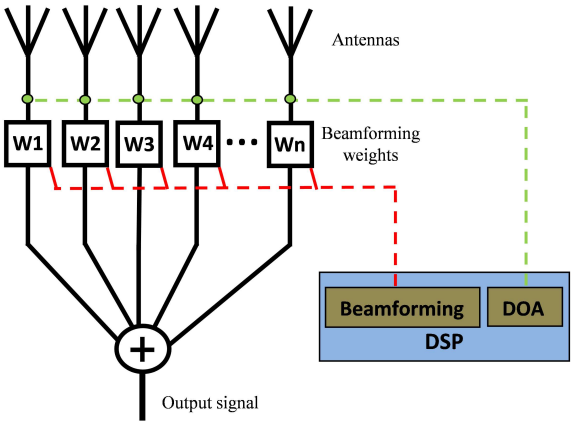

Figure 5.1: Adaptive antenna system

This antenna starts by the antenna array, and the entire subjacent RF chain, which includes the possible frequency down conversion and analog to digital conversion. Another key component is the DSP (Digital Signal Processor) unit that handles with all signal processing of the adaptive antenna.

Using samples of received signal from each array element, by applying DOA algorithms, the DSP estimates the arrival directions of the signal or signals that impinge on the adaptive antenna array. After using an auxiliary intelligence process, the detected signals are divided in terms of signals-of-interest (SOI) and signals-not-of-interest/interferences, and therefore beamforming algorithms are employed, using this information (DOA's and SOI's/SNOI's), computing the necessary weights $(W_1, W_2, \ldots, W_n)$, in terms of amplitude and phase delay, to apply to each array element, in order to obtain the desired radiation pattern, pointing the antenna to directions of interest signals, and reducing or even nulling the impact of the interferences.

This chapter reports the analysis of an adaptive antenna system composed by a planar array, with $M \times N$ elements, affected by a number of signals with different directions. A group of algorithms, DOA and Beamforming, applied to planar antenna arrays are discussed, implemented in a theoretical scenario, simulated and their performance are evaluated. This information was summarized in a state of the art review paper **[J5]** *published in a journal and also another contribution just focused on DOA algorithms was achieved* **[J6]**. *The analysis and obtained results were considered important findings, and a help for research in the topic, by the editor who have invited for a book chapter* **[Ch1]**. *Also, in this chapter a set of phase shifter technologies that allow to create the necessary phase delays in adaptive antennas are described, as well as, the contributions for a ongoing research project inserted in this topic are presented, where a 2×4 antenna array for Ka-band was designed, which resulted in an international conference paper* **[C10]**.

5.2 Planar Antenna Array System

The system consists of planar antenna array, as illustrated in the Fig.(5.2), which is affected by a group of signals including SOI's and SNOI's, resulting in an input signal $x(t)$ that is composed by contributions of all these arriving signals, and noise.

A sample of this signal $x(t)$ is then processed to estimate the angles of arrival of the various signals involved, and the respective weights W to apply to each element of the array are thereafter calculated to create a proper radiation pattern, pointing it to the direction of interest and reducing the influence of the signals from interfering directions.

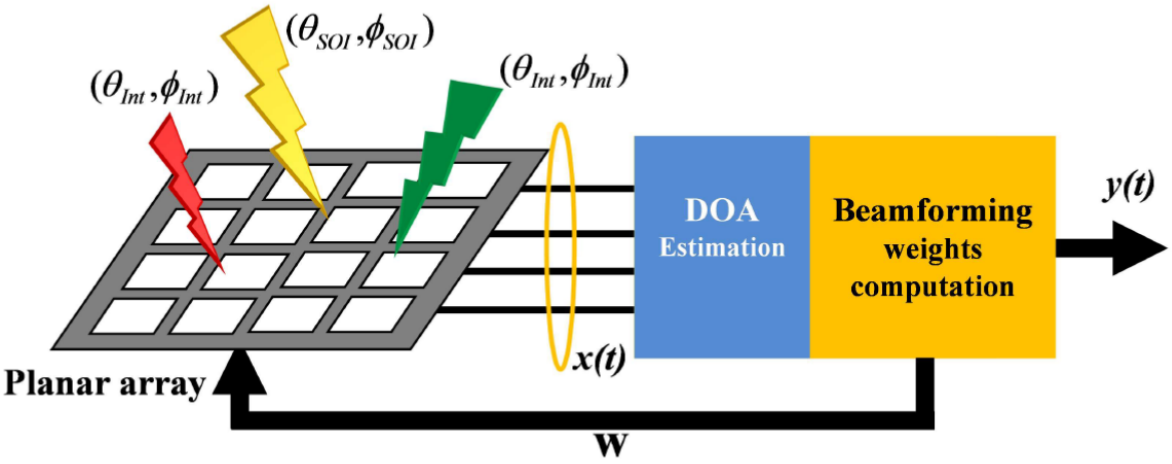

Figure 5.2: Planar Adaptive Array System

Considering a planar antenna array with $M \times N$ elements, spaced by d_1 in the rows and d_2 in the columns, in which impinge J different signals $s(t)$ of frequency with wavelength λ, coming from a direction (θ, ϕ), where θ is the elevation angle and ϕ the azimuth angle.

The input signal received by each element (m, n) of the array, has components from each of J arriving signals and noise $n(t)$, and is given by [65, 66]:

$$x_{mn} = \sum_{i=1}^{J} s_i(t)\, e^{j\frac{2\pi}{\lambda}[u_i\, d_1(m-1)+v_i\, d_2(n-1)]} + n(t) \tag{5.1}$$

with,

$$u_i = \sin\theta_i \quad v_i = \cos\theta_i \sin\phi_i \tag{5.2}$$

$$m = 1 \ldots M \quad n = 1 \ldots N \quad i = 1 \ldots J \tag{5.3}$$

The received data $x(t)$ and the noise $n(t)$ of the whole antenna array can be represented in a vector structure $X(t)$ and $N(t)$ as:

$$X(t) = [x_{11}(t)\ \ x_{21}(t)\ \ \cdots\ x_{M1}(t)\, x_{12}(t)\ \ \cdots\ x_{MN}(t)]^T \tag{5.4}$$

$$N(t) = [n_{11}(t)\ \ n_{21}(t)\ \ \cdots\ n_{M1}(t)\, n_{12}(t)\ \ \cdots\ n_{MN}(t)]^T \tag{5.5}$$

where T denotes the matrix transpose operation.

The total input signal $X(t)$ can be also expressed by the following formula:

$$X\left(t\right) = \sum_{i=1}^{J} s_i\left(t\right)\ A_i\ +\ N\left(t\right) \tag{5.6}$$

where A represents the steering matrix of the planar antenna array and is given by eq.(5.7), the operation $\otimes$ denotes the Kronecker product and C_u and C_v are the steering vectors in each direction of the planar array.

The steering vector [67] contains the set of phase delays that a wave will take, relating to each element of the array, and for a planar array can be represented by the eqs.(5.8) and (5.9) [65, 68].

$$A = C_u \otimes C_v \tag{5.7}$$

$$C_u = \left[1 \quad e^{j\frac{2\pi d_1}{\lambda}(2-1)u_i} \quad \ldots \quad e^{j\frac{2\pi d_1}{\lambda}(M-1)u_i}\right]^T \tag{5.8}$$

$$C_v = \left[1 \quad e^{j\frac{2\pi d_2}{\lambda}(2-1)v_i} \quad \ldots \quad e^{j\frac{2\pi d_2}{\lambda}(N-1)v_i}\right]^T \tag{5.9}$$

The output signal of the adaptive antenna is therefore, the product of the received signal $X(t)$ by the beamforming weights W estimated through the beamforming algorithms, applied to each array element, as the following,

$$y\left(t\right) = W^H\, X\left(t\right) \tag{5.10}$$

$$W = \left[w_{11}\ w_{21}\ \cdots\ w_{N1}\ w_{12}\ \cdots\ w_{MN}\right]^T \tag{5.11}$$

In the next sections such a system is implemented and studied using Matlab [69]. The signal $X(t)$, that consists of the sum of a number of generated signals from several directions (θ, ϕ), being some of these signals SOI and others SNOI, adding up some noise, is created. The locations of the generated incoming signals are totally unknown beyond this step. Then, $X(t)$ is sent as a single input parameter for DOA algorithm, which provides as output parameters the estimated number of signals that reach at the array, and their locations (θ, ϕ).

After the locations of all the signals impinging at the antenna are known, the identification and distinction between the SOI and interferences is mandatory, and then is applied a beamforming algorithm to determine the necessary weights to apply to each element of the array.

By simulation, using HFSS [37], with the ability to change the amplitude and phase of feeding of a simulated array structure, these set of estimated weights are applied to the array, and its radiation pattern is analyzed.

5.3 DOA Algorithms

The processor that estimates the DOAs of arriving signals to the antenna array is a crucial part of an adaptive antenna, allowing to understand the environment in which the antenna is inserted. By processing the electromagnetic waves that arrive to the antenna is possible to extract a number of information about them, particularly their arrival directions to the array.

This processing is done by using DOA algorithms. The arriving signals could be divided into SOI's, which are important and matter to steer the antenna toward them, and/or interfering signals (SNOI's), which impact on the system should be reduced.

There are three main classes of DOA estimation methods referred in the literature, differing mainly in the performance and its computational requirements [70, 71]: the classical, the maximum likelihood, and the subspace methods.

The classics are based in the beamforming, in which the central idea is to scan the antenna beam over the space and the peaks of received power are the DOAs. These methods are theoretically simple but involve a high computational effort and provide a poor performance and a low resolution. The maximum likelihood methods present higher performance than the others (especially with low SNR conditions), because they can take advantage of using better signal and noise models to provide better DOA estimation. However, due to the needs to solve nonlinear multidimensional optimization problems, it increases the required computational load, which makes these methods less popular.

Finally, there are several subspace methods for DOA estimation which have become popular and widely studied over the last decades due to their good trade-off between the computational complexity and good performance. These methods are based on the eigen decomposition of the estimated covariance matrix of the data received by antenna array, into a signal subspace and a noise subspace. The performance of these methods is essentially limited by the accuracy of distinguishing the signal and the noise subspaces in the presence of noise.

For a planar uniform antenna array the most applied algorithms are 2D MUSIC and the 2D ESPRIT, that are subspace based methods, and will be subject of a more detailed description below.

5.3.1 2D MUSIC algorithm

The Multiple Signal Classification (MUSIC) is perhaps the most popular DOA estimation algorithm, which assumes that the steering vectors of the incoming signals lie in signal subspace and are orthogonal to the noise subspace. The algorithm search in the all possible steering vectors those that are orthogonal to the noise subspace of the covariance matrix of the received data (R_{xx}) [71, 72, 73, 74].

The MUSIC algorithm, as illustrates the Fig.(5.3), uses the received information from each element of the array, and through eigenvalue or singular value decomposition of the R_{xx} matrix, estimates the noise subspace (U_N).

After identified the noise subspace U_N, the DOAs are the resulting peaks of the MUSIC spectrum $P_{\mathrm{MUSIC}}(\theta, \phi)$, given by eq.(5.12):

$$P_{\mathrm{MUSIC}}(\theta, \phi) = \frac{1}{s^{\mathrm{H}}(\theta, \phi) U_{\mathrm{N}} U_{\mathrm{N}}^{\mathrm{H}} s(\theta, \phi)} \tag{5.12}$$

where H represents the conjugate transpose matrix (Heremitian).

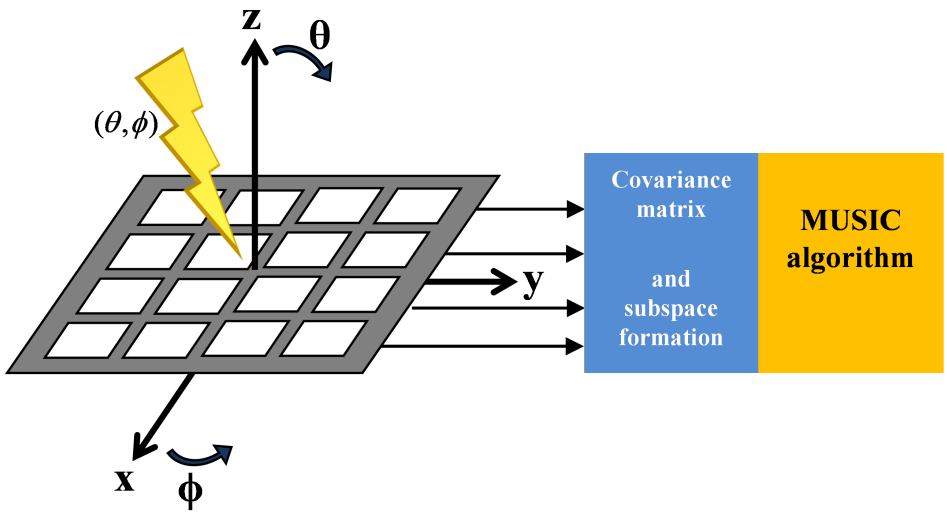

Figure 5.3: 2D MUSIC DOA Estimator

When a steering vector $s(\theta, \phi)$ is related to one arriving signal, the product of $s^{\mathrm{H}}(\theta, \phi)U_{\mathrm{N}} = 0$, ideally, the function assumes a high value (peak), and therefore (θ, ϕ) is the DOA. There might be several signals from different angles of arrival, creating several peaks in the MUSIC spectrum.

The MUSIC algorithm is simpler to understand and can be applied in all antenna array geometries, however, computationally requires a lot of resources, since it has to calculate the MUSIC spectrum, eq.(5.12), for all the possible steering vectors to estimate the expected peaks.

The error of estimation of the MUSIC algorithm is significantly influenced by the angle grid interval in which the eq.(5.12) is evaluated. In the presence of coherent signals, as in multipath environments, spatial smoothing schemes [75, 76] must be applied to suppress the correlations between the incoming signals.

5.3.2 2D ESPRIT algorithm

Estimation of Signal Parameters via Rotational Invariance Techniques (ESPRIT) algorithm is a different subspace based DOA estimator [77, 78, 79, 80, 81]. This algorithm solves some of drawbacks of the MUSIC, in terms of the high computational requirements, and the resulting effects of array calibration errors. The ESPRIT algorithm does not require a high level of calibration in the array since it employs the property of shift invariance of the antenna array. Also, the computational complexity of the ESPRIT is reduced in comparison to MUSIC because it imposes some constraints on array structure.

The ESPRIT algorithm assumes that the separation between equivalent elements in each sub-array is fixed, as shown in Fig.(5.4), and therefore, the array presents a translational invariance. This translational invariance leads to a rotational invariance of the signal subspace that will enable to estimate the DOAs.

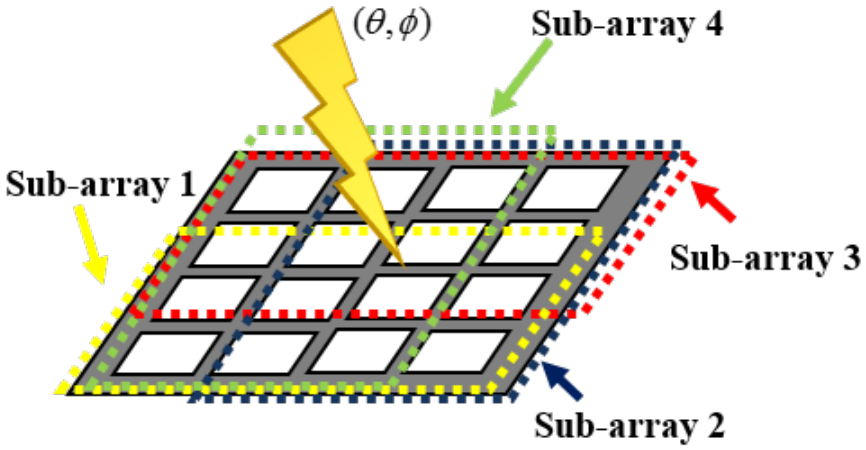

Figure 5.4: ESPRIT sub-array division with maximum overlap

This algorithm contemplates three main stages: the signal subspace estimation, the solution of the invariance equation, and the DOA estimation.

The algorithm procedure is [77, 78, 79]:

1) Signal subspace estimation

Computation of the U_S

2) Solve the invariance equation

$$K_{u_1} U_s Y_u = K_{u_2} U_s \tag{5.13}$$
$$K_{v_1} U_s Y_v = K_{v_2} U_s \tag{5.14}$$

where K_{u_1}, K_{u_2}, K_{v_1} and K_{v_2} represent the two pairs of transformed selection matrices, while Y_u and Y_v are the real-valued matrices.

3) DOA estimation

$$\lambda_i \quad i = 1 \ldots d \rightarrow eigen\ values\ of\ Y_u + j\, Y_v \tag{5.15}$$
$$u_i = 2 \tan\left(Re\left\{\lambda_i\right\}\right), \tag{5.16}$$
$$v_i = 2 \tan\left(Im\left\{\lambda_i\right\}\right), \tag{5.17}$$
$$\phi_i = arg(u_i - j\, v_i) \quad \theta_i = \sin^{-1}\left(\|u_i - j\, v_i\|\right) \tag{5.18}$$

where θ_i and ϕ_i are the DOA angular information.

5.3.3 Test and comparison of the DOA algorithms

A system composed by a signal generator (with signals of interest and interferences) followed by a DOA estimator and beamforming was implemented using the MATLAB [69]. The two DOA algorithms, 2D MUSIC and 2D ESPRIT, were implemented and applied to a planar array configuration.

To test the beamforming results, a planar antenna array of 16 square microstrip elements, arranged in a 4×4 planar structure with spacing between elements in both directions of $d = 0.5\lambda$, as shown in the Fig.(5.5) was designed (for a central frequency of 12 GHz) and simulated in HFSS [37].

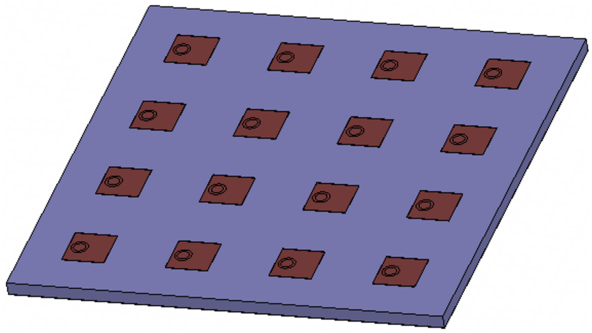

Figure 5.5: Simulated microstrip planar array

Several simulations were performed with good results. As an example, two signals with directions $(\theta, \phi) = (45^o, 45^o)$ and $(70^o, 0^o)$ were generated and 'received' by the 4×4 array. With the received signal from each element of the antenna array, given by (5.4), the DOAs were estimated using the 2D MUSIC algorithm.

The 2D MUSIC algorithm creates a two-dimensional grid, in the range which the angles vary $\theta \in [0, 90]$ and $\phi \in [0, 360]$, and then, evaluates the eq.(5.12) for each point of the grid.

The Fig.(5.6) illustrates the spatial graph of the MUSIC spectrum, resulting of the algorithm, which has peaks in the position of incident signals.

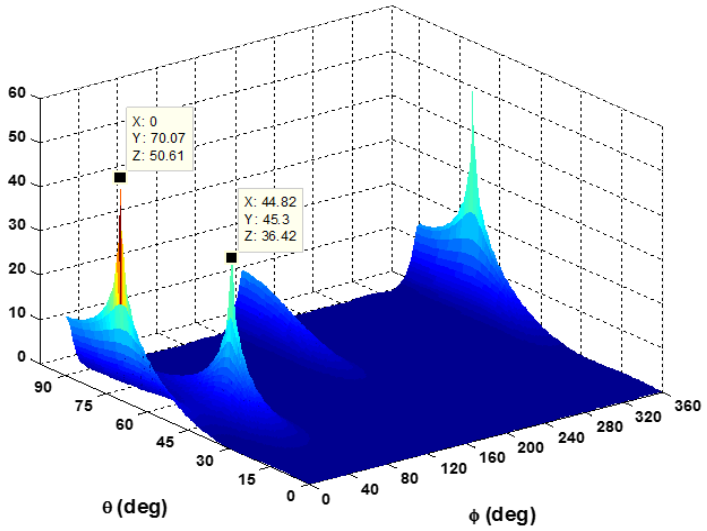

Figure 5.6: 2D MUSIC spectrum

According to the Fig.(5.6), the MUSIC spectrum contains two evidenced peaks. Note that there is another peak but is assumed to be repeated, since 0^o and 360^o is the same spatial location.

In order to simplify the definition and extraction the peaks of the 2D MUSIC spectrum, a function to correctly detect the N maximum values was implemented. This function provides the points of zero gradient, and its result is shown in the Fig.(5.7), with the two well defined peaks.

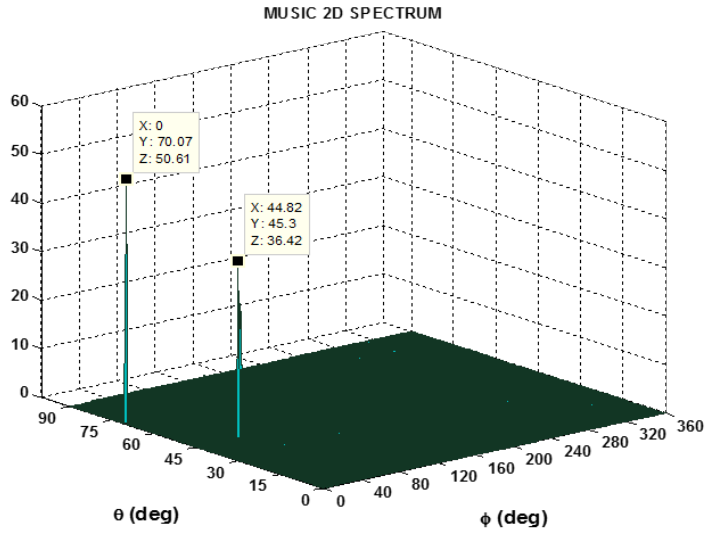

Figure 5.7: 2D MUSIC spectrum peaks

The output of the 2D MUSIC algorithm is that the incident signals arrive to antenna from (θ, ϕ) $(45.3^o, 44.82^o)$ and $(70.07^o, 0^o)$, which are quite close to the initially proposed angles.

Identical signal given to the 2D MUSIC algorithm was provided to the 2D ESPRIT algorithm, also implemented with MATLAB. The output of ESPRIT is just the pair (θ, ϕ) of estimated DOAs, since it does not have a grid to evaluate by a function. The ESPRIT algorithm was preformed and the output result estimates that the signals are arriving from $(45.02^o, 45.11^o)$ and $(69.82^o, 0.03^o)$.

The implemented DOA algorithms reveal estimated results very approximate to the original and expected values. These algorithms only receive the signal $X(t)$, and provides the spatial position of each incoming source that compose it.

The analysis of the performance of the 2D DOA algorithms was performed for a large number of experiments. In Fig.(5.8) are presented the runtimes of both subspace-based DOA algorithms for $n = 50$ experiences.

The upper part concerns the 2D MUSIC algorithm while the bottom is about the 2D ESPRIT algorithm. In both graphs there are identified the line of the average time of all samples. It is clear the huge difference in the time that MUSIC algorithm takes to perform compared with the ESPRIT. This runtime of the MUSIC is much higher than ESPRIT essentially because the MUSIC algorithm needs to calculate the MUSIC function to each possible steering vector.

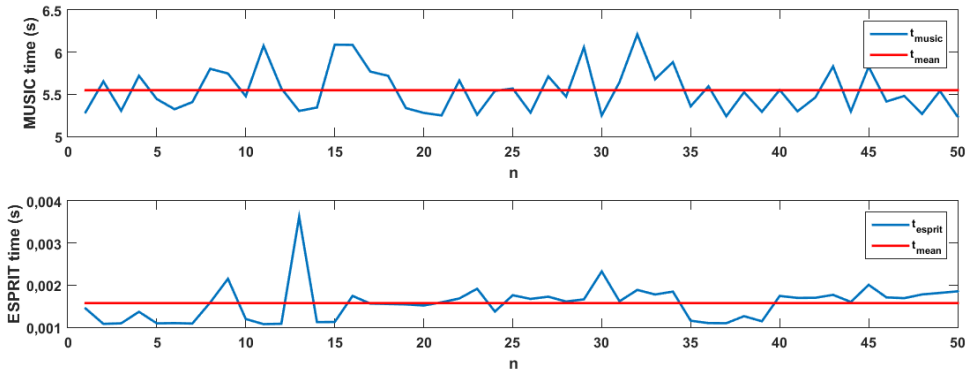

Figure 5.8: Runtime of DOA algorithms over n samples

The 2D MUSIC algorithm takes between 5 and 6 seconds to estimate the DOAs with an average time of 5.4 s, while 2D ESPRIT, in the majority of samples, varies between 1 and 2 milliseconds, with an average execution time of 1.57 ms.

Another property that can be analyzed is the estimation error, between the real location of the incoming waves, and the estimated DOAs from both algorithms. Fig.(5.9) shows the progress of the estimating error over the set of n experiences, using the two DOA algorithms. The upper graph is relating to the coordinate θ, while the bottom is about the ϕ, and are further presented the lines of the average error.

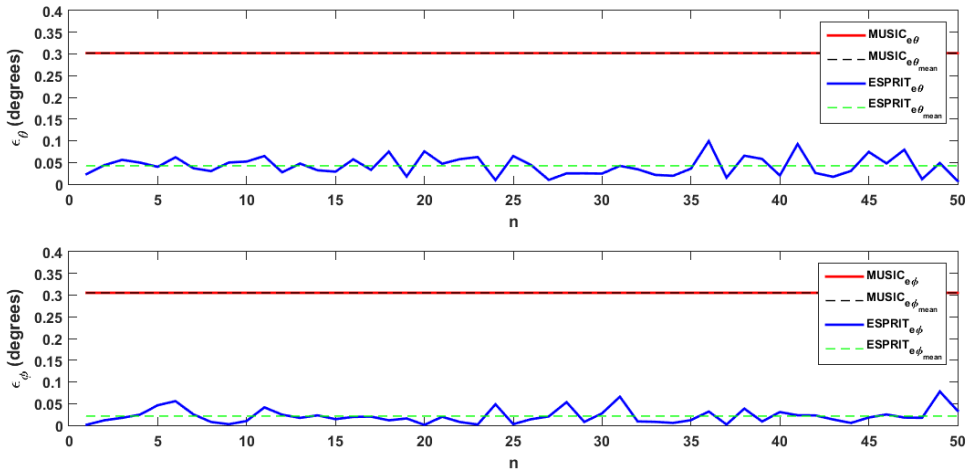

Figure 5.9: Estimation error in θ and ϕ coordinates for MUSIC and ESPRIT algorithms

According to the Fig.(5.9), it is possible to notice that the 2D MUSIC algorithm has a constant estimation error, with an average value of 0.302° in θ and 0.3052° in ϕ coordinate. The 2D ESPRIT algorithm has average errors extremely lower than 2D MUSIC, about 0.037° in θ and 0.015° in ϕ coordinates.

The 2D ESPRIT errors are mainly due to the mathematical process and the noise of the signal, however, in the 2D MUSIC, the errors are strongly affected by the evaluation interval, as in explained by the Fig.(5.10).

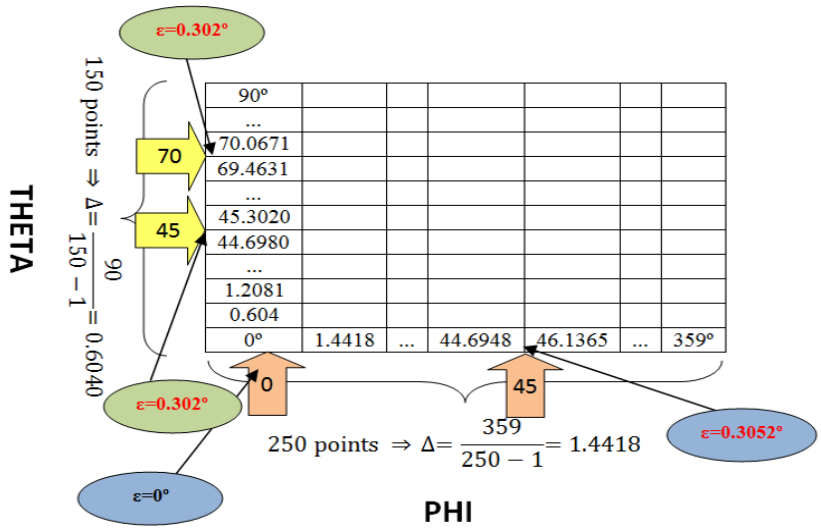

Figure 5.10: Evaluation grid of 2D MUSIC algorithm

The accuracy of the 2D MUSIC algorithm depends on the number of points of its angle grid in which the eq.(5.12) is evaluated. More points lead to longer computational times. The number of points of this evaluation grid is then the main issue of MUSIC algorithm, and this value should be an agreement between the required accuracy and computational load allowed.

The Fig.(5.10) shows how the MUSIC algorithm of error is consistent with the error estimates of the Fig.(5.9), and its relationship with the number of grid points, that in these simulations were 150 in θ and 250 in ϕ.

5.4 Beamforming algorithms

An antenna array, depending on the environment where it is inserted, is usually affected by several electromagnetic signals propagating there around, which some are desired to be received, and others, called interferences, are undesirable. Signals of interest and intrusive signals occupy the same frequency range, however, they are coming from different spatial locations. In order to improve system performance, the signals of interest must be received in the perfect way, while the impact of the unwanted interferences must be reduced or abolished.

In an adaptive antenna array, after identified the locations of arriving signals, it is essential to use spatial filtering techniques, also known as beamforming techniques. These techniques deal with the radiation pattern (or beam pattern) of an antenna array, shaping it according to a group of constraints, improving the performance of the communication system.

The beamforming process consists of, as is illustrated in the Fig.(5.11), adjusting the relative amplitude and phase of feeding of each element of the array, estimated through beamforming algorithms, in order to form the radiation pattern of the array, steering its mainlobe and putting nulls in interference directions. There are a number of developed algorithms to estimate the complex weights (amplitude and phase) to apply to an antenna array. These algorithms are classified as data independent or statistically optimum, according to the way how the weights are estimated [82, 83].

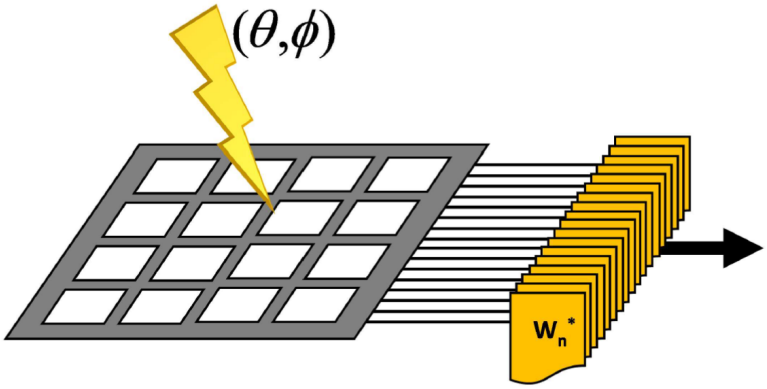

Figure 5.11: Beamformer System

In the data independent beamforming algorithms, the weights are estimated to provide a desired response independently of the data received through the antenna, while in the statistically optimum, the weights are estimated according to the statistics of the received data, to optimize its response.

Sometimes, the statistical information of the received data is not available or changes in time, therefore adaptive algorithms are usually applied to estimate the weights. In this situation, the calculated weights tend to a solution statistically optimum.

5.4.1 Data Independent algorithms

The data independent beamformers are characterized by the estimation of its weights be independent of the received data statistics from the array. One of the most used data independent algorithms is the classical beamformer [82].

Classical Beamformer

The operating principle of this method is similar to the phased array, since it estimates the necessary weights w in order that the maximum of radiation is steered to a desired direction θ_{SOI}. The vector w adjusts the phases to feed each element, in a way that the signals of all the elements are added constructively in a certain direction.

However, the main limitation is the impossibility of placing nulls, which is many times required to eliminate the impact of unwanted signals.

5.4.2 Statistically optimum algorithms

The statistically optimum beamformers are characterized by the calculation of its weights is based on data statistics of received signals. The weights are estimated to steer the radiation pattern in the direction of the SOI while reduces the influence of interfering signals and noise.

Some examples of statistically optimum algorithms mentioned in the literature [82] are the Multiple Side Lobe Canceller (MSC), Reference Signal, SNR Maximization and the Linearly constrained minimum variance (LCMV).

Multiple Side Lobe Canceller

The MSC beamformer [82] consists of a main channel and other auxiliary channels. The main idea of this algorithm is to estimate the appropriate weights to apply to the auxiliary channels to cancel or reduce the impact of interference signals in the main channel. In the main channel, a data independent beamformer can be used to steer the maximum of the array to the desired direction.

Although this method is simple and effective, when the signal of interest is weak relating to interferences, it presents some limitations since the weights are estimated with the absence of the desired signal.

Reference Signal

The use of Reference Signal beamformer [82] requires some knowledge about the desired signal to create a reference signal, and its objective is to minimize the mean square error between the output of the beamformer and the reference signal.

The main difficulty of this method is to generate a proper reference signal.

Maximum SNR

The maximum SNR [82] method requires the knowledge of the covariance matrix of the desired signal and of the noise, and the weights are estimated to maximize the SNR.

Linear Constrained Minimum Variance

One of the most important statistically optimum beamformers with higher applicability is the Linear Constrained Minimum Variance (LCMV) method [82], and a different approach of its formulation known as generalized sidelobe canceller (GSC).

Most of the times the desired reference signal is unknown or we do not have enough information about it, being necessary to impose some linear constraints in the weight vector to minimize the variance of beamformer output. The LCMV technique can overcome the main drawbacks of most of the techniques presented before [84].

The principal idea of the LCMV beamformer is that its output is constrained in a way that signals of interest are preserved and the undesired (noise and interfering signals) are minimized.

The LCMV formulation problem is to select the complex weights that are suitable to the multiple linearly independent constraints:

$$\min_{w} \; w^H R_x w \;\; \text{Subject to} \;\; C^H w = f \tag{5.19}$$

where w is the vector of weights, R_x the covariance matrix, C is the constraint matrix and f is the response vector.

The solution of the constrained minimization of LCMV problem can be obtained using the method of Lagrange multipliers [82] resulting in:

$$w_{opt} = R_x^{-1} C (C^H R_x C)^{-1} f \tag{5.20}$$

It is important to observe the dependence of the optimal weight vector of eq.(5.20) with the data correlation matrix, and therefore with the statistics of the input signal.

Generalized Sidelobe Canceller The generalized sidelobe canceller (GSC) is a different approach to solve the LCMV problem, providing a simple implementation of the beamformer, changing the constrained minimization problem to an unconstrained arrangement [66, 85]. The GSC method, illustrated in the Fig.(5.12), splits the LCMV problem into two parts, one data independent and other data dependent.

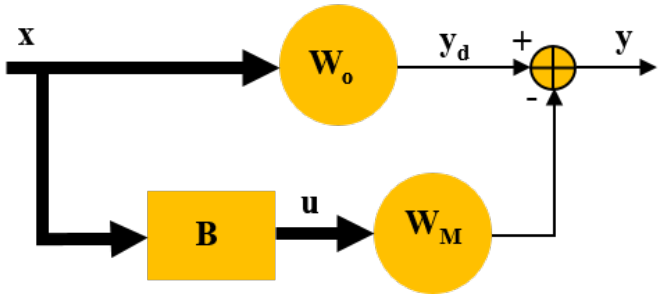

Figure 5.12: Generalized sidelobe canceller

This structure splits the optimum weight vector in two orthogonal components, that are in the range and in the null space of C, in such way that $w = w_0 - Bw_M$. The beamformer output is $y = w_0^H x - w_M^H B^H x$.

The vector w_0 is designed to comply with the imposed constraints, consisting in the quiescent part of w. This weight vector is also independent of the input data and represents the non-adaptive component of the LCMV solution. Then, w_0 must satisfy the linear constraints[66]:

$$C^H w_0 = f \;\Rightarrow\; w_0 = C(C^H C)^{-1} f \tag{5.21}$$

The bottom branch of GSC is the data dependent part, and consists of the blocking matrix B and w_M that will block influence of interfering signals, while minimizes the variance of the output signal y. The blocking matrix B must be orthogonal to the constraint matrix C, so $C^H B = 0$.

The GSC unconstrained problem is

$$\min_{w_M} \; (w_0 - Bw_M)^H R_x (w_0 - Bw_M) \;\text{ subject to }\; C^H w = f \tag{5.22}$$

and the optimal solution is

$$w_M = (B^H R_x B)^{-1} B^H R_x w_0 \tag{5.23}$$

This implementation of GSC beamformer enables important benefits, since the w_0 is data independent beamformer and w_M is an unconstrained beamformer.

5.4.3 Adaptive Algorithms

Adaptive algorithms [82] solve the problem of the statistics of the received data, that changes over the time or may not be available, and affects the statistically optimum beamformers. Examples of adaptive algorithms are the least mean square (LMS), the recursive least squares (RLS) or the Frost's algorithm.

Frost's Algorithm for LCMV Beamforming

The Frost's algorithm [83] belongs to the group of LCMV beamformers. Its weights are estimated based on the statistics of the received data, that sometimes are not available or are continually changing, being necessary the use of adaptive algorithms. The Frost's algorithm minimizes the mean square error while maintains the specified response to the desired signal. The weight vector starts with an initial value:

$$w = C(C^H C)^{-1} f \tag{5.24}$$

and at each iteration, the vector is updated on negative gradient direction with a factor μ, and the weights are defined by:

$$w(n+1) = C(C^H C)^{-1} f + P(w(n) - \mu e^*(n) x(n)) \tag{5.25}$$

$$P = I - C(C^H C)^{-1} C^H \tag{5.26}$$

Least Mean Square

Least mean square adaptive algorithm estimates the gradient vector from the available data [82, 83, 86, 87]. This method follows an iterative procedure that successively adjusts the weight vector in the direction of the negative of the gradient vector at each iteration, eventually leading to the minimum mean square error:

$$w_M(n) = w_M(n-1) + \mu u(n-1) y^*(n-1) \tag{5.27}$$

$$y(n) = y_d(n) - w_M^H(n) u(n) \tag{5.28}$$

$$0 < \mu < \frac{1}{\lambda_{max}} \tag{5.29}$$

where λ_{max} is the largest eigenvalue of the correlation matrix.

The gain μ ($0 < \mu < 1$) is the parameter that controls the convergence rate of the algorithm. Smaller values lead to slow convergence, but good approximation, while higher values result in a faster convergence and the stability around the minimum value isn't ensured.

This algorithm is simple since requires no matrix inversion and by choosing correctly the μ value, the weight vector tends to an optimum solution.

Recursive least squares

The recursive least squares algorithm has a faster convergence rate than the LMS, however it involves more complex mathematical operations and requires more computational resources [82, 83].

The RLS problem is:

$$\min_{w_M(k)} \sum_{n=0}^{N} \lambda^{N-n} \left| y_d(n) - w_M^H(n) u(n) \right|^2 \tag{5.30}$$

$$P(0) = \delta^{-1} I \tag{5.31}$$

$$v(n) = P(n-1)u(n) \tag{5.32}$$

$$k(n) = \frac{\lambda^{-1} v(n)}{1 + \lambda^{-1} u^H(n) v(n)} \tag{5.33}$$

$$\alpha(n) = y_d(n) - w_M^H(n-1)u(n) \tag{5.34}$$

$$w_M(n) = w_M(n-1) + k(n)\alpha^*(n) \tag{5.35}$$

$$P(n) = \lambda^{-1} P(n-1) - \lambda^{-1} k(n) v^H(n) \tag{5.36}$$

with $0 < \lambda < 1$ a constant called forgetting factor.

5.4.4 Test and comparison of the Beamforming algorithms

The beamforming weights can be exhibited in the exponential form $w = Ae^{\phi}$, and consists of a set of amplitude and phases, that are applied to each element of an antenna array, to combine its signals in such way that produces constructive interference for the desired locals and destructive in undesired.

With the MATLAB some beamforming algorithms were implemented, and the weights from each algorithm were computed. Then, their performance was analyzed when applied to the aforementioned planar antenna array, presented in the Fig.(5.5).

The system (DOA and Beamforming) simulation was tested using several groups of angles of arrival with excellent results. First by estimating the necessary weights, after, applying it to the simulated planar array to analyze its radiation pattern. In the simulations presented here, was considered that the signals were coming from: Signal of Interest: $(\theta, \phi) = (45^o, 45^o)$ and Interference signal: $(\theta, \phi) = (70^o, 0^o)$.

The LVCM algorithm was implemented, using as input parameters the two pair of angles considered, and with a response vector $f = [1\ 0]^H$ in order to assume the first pair of angles the SOI direction, and the second the SNOI. The output weights, given in terms of amplitude and phase, to apply to the corresponding element of the 4×4 array, are presented in Table (5.1a). The resultant radiation pattern when these weights are applied is shown in the Fig.(5.13a).

It is possible to observe the maximum of the radiation pattern pointed to the direction of the SOI $(45^o, 45^o)$, indicated by the green dashed arrow, while in the direction $(70^o, 0^o)$, identified with a red filled arrow, there is a low gain value, that reduces significantly the influence of the interference signal in this direction.

Table 5.1: Estimated weights resulting from beamforming algorithms

(a) Optimum LCMV

Amplitude $\angle$ *Phase*				
	1	2	3	4
1	$1.0\angle 0^o$	$1.0\angle -90^o$	$1.0\angle -180^o$	$1.0\angle 90^o$
2	$1.0\angle -90^o$	$1.0\angle 180^o$	$1.0\angle 90^o$	$1.0\angle 0^o$
3	$1.0\angle 180^o$	$1.0\angle 89^o$	$1.0\angle 0^o$	$1.0\angle -90^o$
4	$1.0\angle 90^o$	$1.0\angle 0^o$	$1.0\angle -91^o$	$1.0\angle 180^o$

(b) Adaptive Frost's LCMV

Amplitude $\angle$ *Phase*				
	1	2	3	4
1	$1.0\angle 0^o$	$1.0\angle -90^o$	$1.0\angle -180^o$	$1.0\angle 90^o$
2	$1.0\angle -90^o$	$1.0\angle -180^o$	$1.0\angle 90^o$	$1.0\angle 0^o$
3	$1.0\angle 180^o$	$1.0\angle 90^o$	$1.0\angle 0^o$	$1.0\angle -90^o$
4	$1.0\angle 90^o$	$1.0\angle 0^o$	$1.0\angle -90^o$	$1.0\angle -180^o$

(c) Adaptive LMS

Amplitude $\angle$ *Phase*				
	1	2	3	4
1	$1.0\angle 0^o$	$1.0\angle -83^o$	$0.9\angle 156^o$	$0.6\angle 83^o$
2	$0.7\angle -83^o$	$1.0\angle 179^o$	$1.0\angle 93^o$	$1.2\angle 2^o$
3	$0.9\angle -178^o$	$0.9\angle 61^o$	$0.9\angle 23^o$	$0.6\angle -78^o$
4	$0.9\angle 69^o$	$0.6\angle 13^o$	$0.6\angle -59^o$	$0.6\angle -169^o$

(d) Adaptive RLS

Amplitude $\angle$ *Phase*				
	1	2	3	4
1	$1.0\angle 0^o$	$0.7\angle -104^o$	$0.5\angle -161^o$	$0.9\angle 102^o$
2	$1.2\angle -92^o$	$1.2\angle 175^o$	$0.8\angle 107^o$	$0.9\angle -34^o$
3	$0.8\angle -163^o$	$0.3\angle 127^o$	$0.8\angle -100^o$	$0.8\angle -73^o$
4	$0.4\angle 101^o$	$0.6\angle -4^o$	$0.7\angle -114^o$	$0.5\angle -128^o$

The adaptive algorithms were also implemented because they are a more realistic approach, due to the environment changes.

The adaptive Frost's Algorithm was tested applying the considered pair of angles. This algorithm was processed with $n = 100$ samples of the input signal, iteratively. The output resulting weights are shown in the Table (5.1b), and the produced radiation pattern is presented in the Fig.(5.13b). The array points to the direction of interest (green dashed arrow) placing a null in the interference zone (red filled arrow), as desired.

The Least Mean Square algorithm was also performed in MATLAB using 100 samples of the received signal $X(t)$. The output of this algorithm is shown in the Table (5.1c), and the respective radiation pattern is presented in the Fig.(5.13c). It is possible to find out that using these weights, the antenna steers its mainlobe (green dashed arrow) in the direction of interest $(45^o, 45^o)$ and places a null (red filled arrow) in the SNOI zone $(70^o, 0^o)$.

Finally, the RLS algorithm was implemented and its weights for identical scenario were estimated. The output weights are shown in the Table (5.1d), leading to the radiation pattern

of the Fig.(5.13d). The array directs its maximum of radiation pattern to SOI direction (45°, 45°) indicated by green dashed arrow.

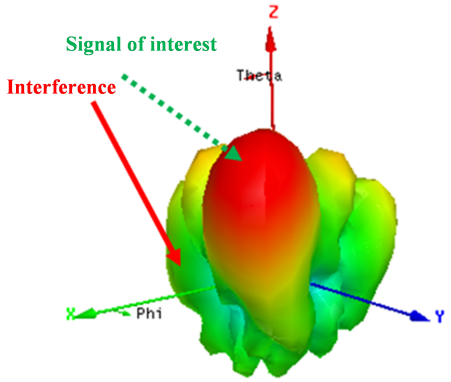

(a) The radiation pattern of the planar array with optimum LCMV weights applied

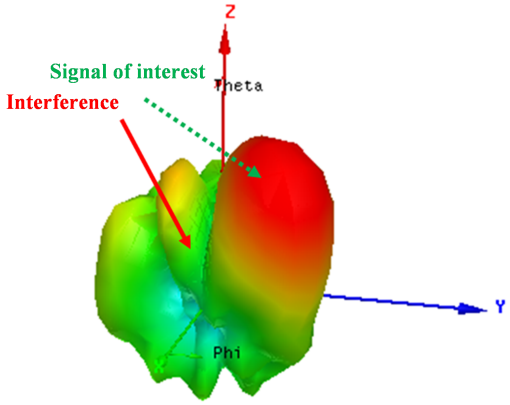

(b) The radiation pattern of the planar array with adaptive Frost's LCMV weights applied

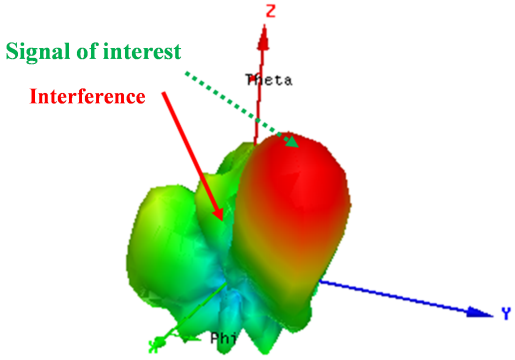

(c) The radiation pattern of the planar array with LMS adaptive weights applied

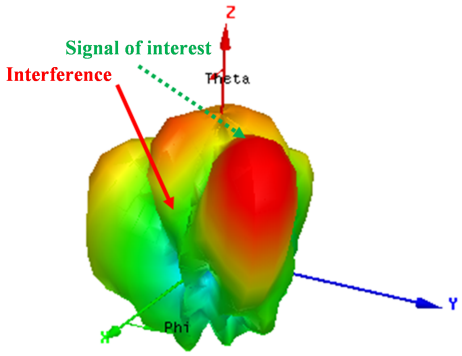

(d) The radiation pattern of the planar array with RLS adaptive weights applied

Figure 5.13: 3D radiation pattern of the planar array with the beamforming weights applied

Implemented and tested the four beamforming algorithms, a set of 50 consecutive experiments were done, performing a comparative statistical analysis, evaluating the runtime each iteration. Fig.(5.14) shows the progress of the execution time of each beamforming algorithm along the n experiences. In each sub-figure is presented also a straight line (red) corresponding to the average runtime of all the 50 samples.

According to the Fig.(5.14), there are a couple of samples with a more accentuated discrepancy, observed by a couple of peaks in the runtime compared to the average value, property that is common in all beamforming algorithms.

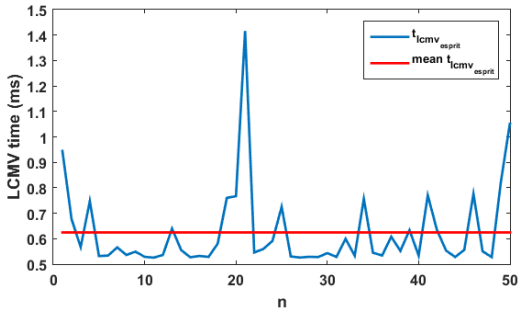

(a) Runtime time of LCMV algorithm

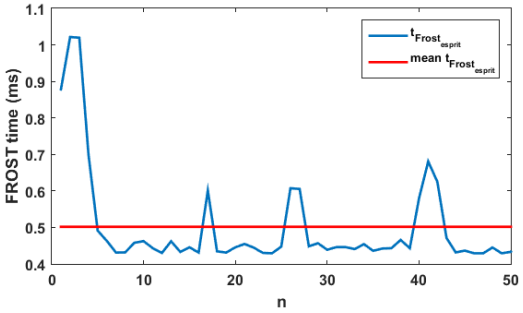

(b) Runtime time of Frost's adaptive algorithm

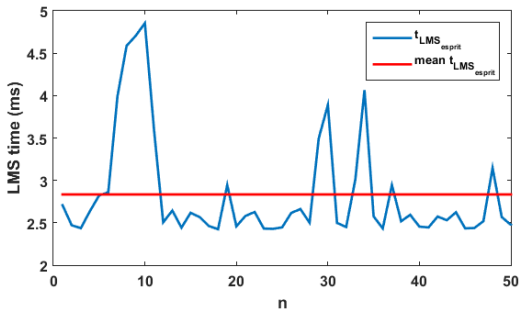

(c) Runtime time of LMS adaptive algorithm

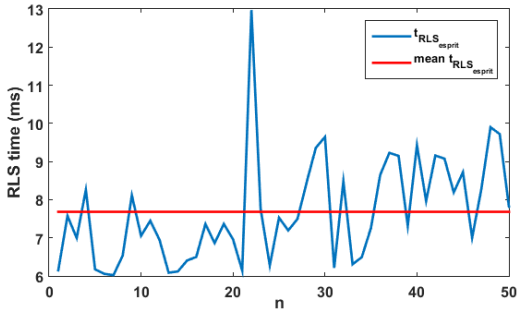

(d) Runtime time of RLS adaptive algorithm

Figure 5.14: Runtime time of the beamforming algorithms

The LCMV algorithm, Fig.(5.14a), has an average runtime of about 0.62 ms. Concerning the adaptive algorithms, the Frost's shown in Fig.(5.14b) presents a mean value of 0.5 ms, that even being an adaptive presents a better result than the LCMV (but similar).

The LMS and RLS algorithms, presented in the Fig.(5.14c) and Fig.(5.14d), have an average runtime over all the 50 experiences, of about 2.8 ms and 7.6 ms, with the RLS, as expected, requiring more computational resources than LMS.

After the evaluation of the DOA and beamforming algorithms independently, a comparative analysis about their performance in the system was made, operating together as an adaptive antenna array. The system consists of DOA estimation followed by beamforming weights computation. It was evaluated in terms of total runtime (for all algorithms), the changeability of its results when the noise level modifies, and in terms of estimation errors. The results are presented in the Tables (5.2) to (5.5), for each beamforming algorithm.

According to the Table (5.2), the runtime of LCMV algorithm is similar using both DOA algorithms (MUSIC or ESPRIT), and its variation with SNR is not significantly noted when SNR changes from 10 to 15 dB. However, it almost doubles when SNR changes from 10 to 5 dB. Another important and already referred characteristic, is that the MUSIC algorithm is heavier than the ESPRIT in terms of runtime, and while the τ_{MUSIC} doesn't show a significant variation, the τ_{ESPRIT} tends to reduce with the increase of SNR. In terms of DOA estimation errors, they tend to reduce with the increasing of the SNR.

Table 5.2: Variation of the runtime and estimation error, using LCMV beamforming algorithm

Algorithms		SNR(dB)		
DOA	Performance	5	10	15
MUSIC	$\tau_{MUSIC}(s)$	5.92	6.03	5.34
	$\tau_{LCMV}(s)$	0.0199	0.00089	0.00098
	$\epsilon_\theta(^o)$	0.302	0.302	0.302
	$\epsilon_\phi(^o)$	0.305	0.305	0.305
ESPRIT	$\tau_{ESPRIT}(s)$	0.052	0.038	0.013
	$\tau_{LCMV}(s)$	0.0013	0.0011	0.0009
	$\epsilon_\theta(^o)$	0.08	0.04	0.02
	$\epsilon_\phi(^o)$	0.167	0.141	0.0275

Regarding to ESPRIT algorithm, it is observed a reduction of the estimation errors, however, using the MUSIC algorithm this error maintains constant. This fact is due to the choice of the angle grid for evaluation of music function P_{MUSIC}, eq.(5.12), as was previously referred. Its interval must be an agreement between runtime and estimation error.

Using the Frost's algorithm, Table (5.3), its runtime reduces with the SNR. The performance of DOA algorithms maintains with the already described characteristics, in terms of execution time and estimation errors.

Table 5.3: Variation of the runtime and estimation error, using Frost's beamforming algorithm

Algorithms		SNR(dB)		
DOA	Performance	5	10	15
MUSIC	$\tau_{MUSIC}(s)$	5.67	5.15	5.53
	$\tau_{Frost's}(s)$	0.0118	0.0047	0.0007
	$\epsilon_\theta(^o)$	0.302	0.302	0.302
	$\epsilon_\phi(^o)$	0.305	0.305	0.305
ESPRIT	$\tau_{ESPRIT}(s)$	0.015	0.0018	0.0077
	$\tau_{Frost's}(s)$	0.013	0.001	0.00086
	$\epsilon_\theta(^o)$	0.140	0.042	0.042
	$\epsilon_\phi(^o)$	0.0188	0.014	0.010

The performance using LMS algorithm is presented in Table (5.4). The runtime decreases when the SNR increases, whereas the MUSIC and ESPRIT algorithms keep with similar characteristics to the preceding cases. Finally, using the RLS algorithm, Table (5.5), it is possible to observe a high reduction of the runtime when SNR increases from 5 dB to 10 dB. The error follows the expected behavior, reducing when SNR increases, using the DOA ESPRIT algorithm, and with the DOA MUSIC algorithm the estimation error holds up constant.

Table 5.4: Variation of the runtime and estimation error, using LMS beamforming algorithm

Algorithms		SNR(dB)		
DOA	Performance	5	10	15
MUSIC	$\tau_{MUSIC}(s)$	5.35	5.37	5.46
	$\tau_{LMS}(s)$	0.020	0.007	0.002
	$\epsilon_{\theta}(^{o})$	0.302	0.302	0.302
	$\epsilon_{\phi}(^{o})$	0.305	0.305	0.305
ESPRIT	$\tau_{ESPRIT}(s)$	0.0095	0.0012	0.0011
	$\tau_{LMS}(s)$	0.0054	0.0050	0.0046
	$\epsilon_{\theta}(^{o})$	0.203	0.042	0.02
	$\epsilon_{\phi}(^{o})$	0.090	0.045	0.024

Table 5.5: Variation of the runtime and estimation error, using RLS beamforming algorithm

Algorithms		SNR(dB)		
DOA	Performance	5	10	15
MUSIC	$\tau_{MUSIC}(s)$	5.82	5.75	5.71
	$\tau_{RLS}(s)$	0.0163	0.0070	0.0161
	$\epsilon_{\theta}(^{o})$	0.302	0.302	0.302
	$\epsilon_{\phi}(^{o})$	0.305	0.305	0.305
ESPRIT	$\tau_{ESPRIT}(s)$	0.00181	0.00180	0.0015
	$\tau_{RLS}(s)$	0.0101	0.01	0.01
	$\epsilon_{\theta}(^{o})$	0.2294	0.0378	0.0972
	$\epsilon_{\phi}(^{o})$	0.156	0.031	0.01

5.5 Phase Shifters

An essential component in an adaptive antenna array system, that enables the control of its radiation pattern and is the principal element in the antenna feed network is the Phase Shifter (PS). This device represents the main challenge in the phased array or adaptive antenna design and takes the highest portion of the antenna cost. The performance of any phase shifter can be evaluated by a group of factors, such as the range of phase shift, the loss/gain, bandwidth, linearity, power consumption or even the size [88].

The literature describes that the principal advances in phase shifter technology achieved over the last decades are divided into three main categories [89], MMIC (monolithic microwave integrated circuit), MEMS (micro-electromechanical systems) and thin film ferroelectric-based devices.

Monolithic microwave integrated circuit The MMIC phase shifters offers reduced size components with low control voltage and high speed tuning, however with considerable losses and low power handling capability [89].

Micro-electromechanical systems The MEMs phase shifters have reduced insertion losses and broad range of phase shift, but present a limited resolution [89].

Barium Strontium Titanate The category of thin films ferroelectric phase shifters [89, 90], have received particular attention and have a big potential to explore. The variation of the high permittivity of the ferroelectric materials with the applied electric field allows the development of RF phase shifters. The most used ferroelectric material is the BST - Barium Strontium Titanate (BaxSr1-xTiO3) [91, 92, 93, 94, 95]. This BST technology provides high tenability and high tuning speed phase shifters, maintaining the low losses and high power handling capabilities, which makes them suitable to apply in phase array antennas. However, high voltage bias is required to control this phase shifter [90, 96]. Some examples of phased arrays using such phase shifters are reported in the literature.

In [91] a low-cost phased-array antenna at 10 GHz is presented using a continuously tunable printed BST thick-film ceramic phase shifters. The phase-shifter has a very compact size combined with a 342° of total phase shift. However the bias applied has been increased to a maximum of 150 V to achieve the proposed phase shift.

A low loss phase shifter based on a hybrid thin ferroelectric film that combines an analog ferroelectric section and a digital switch is found in [92]. The maximum phase shift achieved was 320 degrees using voltages up to 300 V. In [93] a BST phase shifter is developed, printed with a drop-on-demand inkjet printer. The phase shifter was designed to operate in the frequency range from 8-10 GHz. In this phase shifter, changing the bias voltage from 0 V to 200 V, a phase shift of 175 at 10 GHz is achieved, and the permittivity of the material changes from 220 in untuned state to 140 at 200 V. A low cost ferroelectric phase shifter for a higher microwave power level using the conventional scheme of a transmission type phase shifter is used in [94]. The phase shift achieved is about 360° when a voltage bias of 200 V is applied.

In [95] is demonstrated a 1:4 distribution network for phased-array antenna applications, that consists of Wilkinson dividers, BST phase shifters, dc blocks, and CPW-to-MS transitions based on CPW configuration. The beam steering of the antenna array is accomplished with external bias voltages applied to the BST phase shifters. The 0, 80, 150, and 300 V corresponds to the phase shifts of 0°, 30°, 60°, and 90° at 15 GHz, respectively.

Photonic Phase Shifter Recently, there was a start research to use optical technology in phase shifter development for beamformer systems. Advantages of optical systems such as the small size devices, high time bandwidth, light weight, immunity to electromagnetic interference and low losses can bring to the phased array antennas new perspectives to improve the performance [97, 98].

The optical beamforming can be categorized into two true-time delay schemes that are the switched delay lines and the variable propagation velocity lines. The SDL corresponds to different fibers with multiple lengths resulting into several delay times. The number of optical components required, and the quantity of fibers needed leads to bulky systems [99]. In the VPVL, Long fibers and temperature control are important aspects to achieve the needed phase shift and guarantee of absence of instabilities, once the refractive index of fibers changes with the temperature [99]. Integrated photonic beamforming is the object of research, since their tuning mechanisms are thermo-optical tuning that do not accomplish a fast scanning applications [97, 100]. In [98] presents a new technique for ultrafast tunable true time delay beamforming, avoiding the thermo-optic tuning problems, consuming less power and reduced size.

5.6 BEACON project application

ScalaBle & Low Power Microwave Photonics for FlexiblE, TerAbit Telecom Payloads & High speed Coherent Inter Satellite LiNks (BEACON) is an ongoing FP7 research project, in which the Instituto de Telecomunicações is a collaborating partner, and for which I have contributed.

The use of satellites in communication systems has received a greater attention over the years, and nowadays reveals a great potential for development, offering a wide range of services, fixed and mobile, with several applications such as data transfer and video, internet access, earth observation, global positioning system, military applications, and others.

In this regard, the size and weight of current telecom satellites are increasing to comply with new necessities, employing multiple beams technology to provide high speed broadband connectivity and broad coverage. New technologies for satellite communications have to be developed to deliver practical, low-power and scalable components with high performance under harsh environment conditions.

Photonic systems provide a high-capacity and the ability to reduce power consumption, the weight and volume of satellite systems, improving the performance and reducing the costs. BEACON will enable the entrance of photonic technology in satellites, incorporating the system with photonic beamformer. An antenna array will demonstrate that the technology can be scaled to high capacities with considerable savings in size/power against current systems.

The growing needs of higher transmission rates lead to the use of the Ka frequency bands and multi-beam technology, in the satellite communications, allowing more coverage. Also, the use of multi-beam technology increases the capacity and coverage, by pointing several beams to a particular area, whereby is required the use of highly directive antennas and beamforming techniques to achieve a precise control of radiation pattern. The BEACON expects to create hundreds of beams to cope with multi-beam capability, each beam with between 0.19^o and 0.21^o of beamwidth.

The contribution to the project has been on the development of an antenna array for the Ka-band that allow to test and prove the concept of the new beamforming technology for satellite communications.

This section presents the design of a 2×4 planar circularly polarized microstrip antenna array, for Ka-band (at 29 GHz), suitable to satellite communications. The array will be a module part to develop an ample antenna array suitable to fulfill the satellite requirements. This antenna will be coupled at a beamforming feed network, based on photonic technology, integrated with the collaboration research project BEACON. A study was also done, predicting the necessary number of modules to get a 0.2^o beamwidth.

The part that has been carried out about this work already culminated in a scientific contribution **[C10]**, accepted and presented in an international conference.

5.6.1 Array Design

The number of envisaged outputs for the optical phase shifter device under development by the BEACON is eight, so the purpose was to design an array with 8 elements to connect to this device, as shown in the Fig.(5.15).

Taking this array as part of a module, a higher number of modules (array + phase shifter) is going to be combined (in the satellite arm) in such way, to obtain an array with the global

radiation pattern with the desired HPBW, about 0.21^{o}.

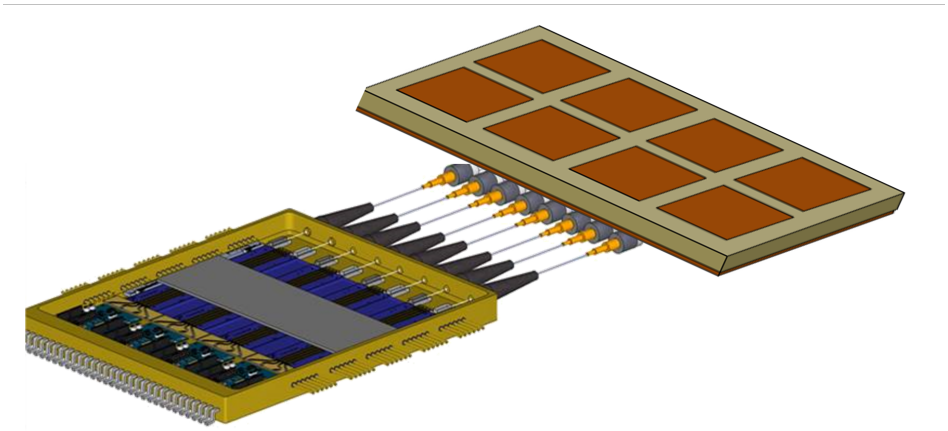

Figure 5.15: Schematic diagram of the integrated subsystem with the beamforming control, (the optical chip and the 2×4 antenna array module.)

The satellites operate at Ka-band, in the frequencies [27.5-31]GHz for uplink and at [17.7-21.2]GHz for downlink. This work presents the design of the array for uplink band, however, considering that the structure is preserved for the downlink band, just changing the operating frequency and the respective dimentions. Therefore, the antenna array was designed to a central frequency of 29 GHz using LHCP.

The array elements were considered as microstrip elements due to the benefits of this type of antennas, especially regarding to the simplicity, small size and light weight.

In order to design an array with the aforementioned number of elements (N=8), a planar structure 2×4 was adopted, since it is a compact structure, easily scalable, and its radiation diagram allows some tests using the phase shifter in order to steer easily its main beam in two directions, ϕ and θ, i.e. in a semi-spherical space. The distance between elements selected, in both directions of the array, was $d = 0.7\lambda$. This option is a compromise between some factors, such as the HPBW and the global dimension of the module.

Each microstrip patch is fed by the aperture coupling technique [101], the more suitable feeding technique, due to the reduced dimensions of the microstrip structures at this frequency range. The most significant advantages of this feeding technique compared with other common techniques such as microstrip line feed or coaxial feed, are the high antenna impedance bandwidth, the possibility to choose different substrates for the feed and for the patches, shielding between the feed and the antenna radiation and, finally, an increase of space for the feed network. Thick substrates with lower permittivity are more suitable for radiation because they provide better efficiency and larger bandwidth. However, a larger element size is required. Conversely, thin substrates with higher dielectric constants are desirable for microstrip lines because they require tightly confined fields to minimize undesired radiation and coupling, and results in reduced element sizes. However, such substrates have higher losses, lower efficiency and result in lower bandwidths.

Aperture coupling method requires two substrate layers, separated by a ground plane, as illustrated in the Figs.(5.16a) and (5.16b). The upper layer is dedicated to enhance the radiation characteristics of the antenna, whereas the lower should have characteristics to

improve the feed network of the antenna. In the upper side of the structure, above the SUB1 (see Fig.(5.16c)) are placed the radiation elements, while in the bottom, below SUB2, are inserted the microstrip feed lines. The connection between the microstrip lines and the radiating elements is performed by direct coupling, through cutting a slot in the ground plane that separates the two substrates.

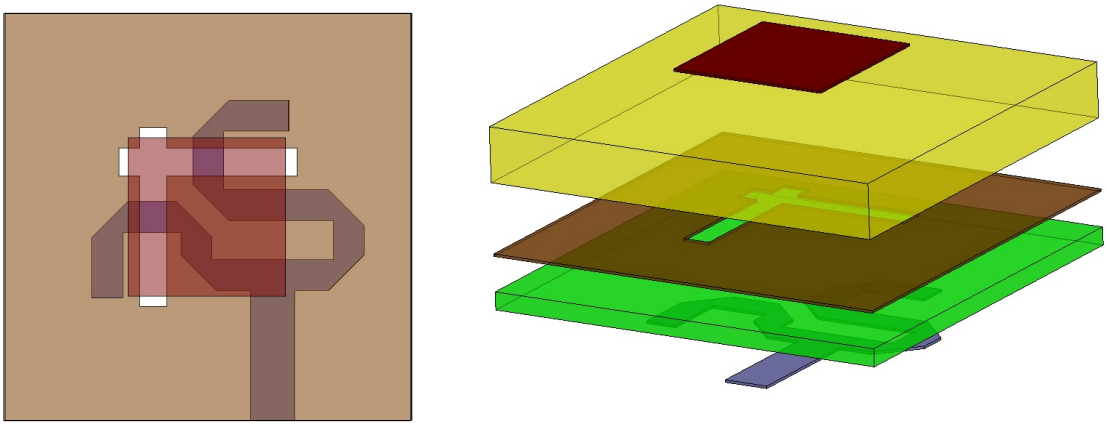

(a) Upper view

(b) Planar view

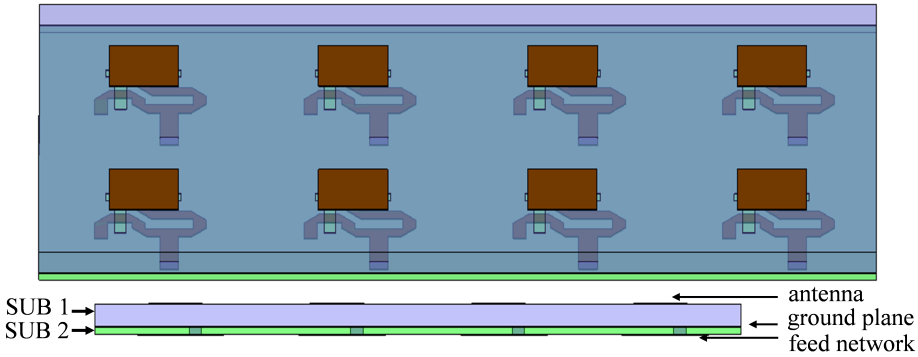

(c) Antenna array structure

Figure 5.16: Microstrip array structure

To create the circular polarization, the dual feed method was used in two orthogonal directions with a 90° phase shift between them, creating two orthogonal slots. Due to the high frequency, the antenna dimensions are quite small, which in turn implies that the slots must intersect. Consequently, a painstaking impedance adaptation was required.

The dielectric substrate used for the two substrate layers is the RT/duroid®5880 High Frequency Laminates, suitable for the present application, with good performance at the Ka band, whose main characteristics are an relative dielectric constant, $\epsilon_r = 2.2$, and a loss tangent, $\tan\delta = 0.0009$. The selected standard thickness for the upper substrate layer corresponding to the antenna radiation is $h_1 = 0.787\,\text{mm}$ for SUB1, whereas for the bottom layer SUB2, devoted to the feed network was chosen a thickness of $h_2 = 0.254\,\text{mm}$.

5.6.2 Simulated Results

The designed array, shown in Fig.(5.16c), was simulated using an electromagnetic simulator, CST [48], and evaluated in its main parameters: impedance adaptation, polarization and radiation pattern. The dimensions of the 2×4 antenna array module are $14.5 \times 28.9\,\text{mm}^2$.

The Fig.(5.17) shows the simulated S_{11} of each element of the array. Assuming as a good impedance matching the commonly accepted condition, $S_{11} < -10\,\text{dB}$, the array has a bandwidth over 5 GHz [27.7-33.3GHz] in which is correctly matched.

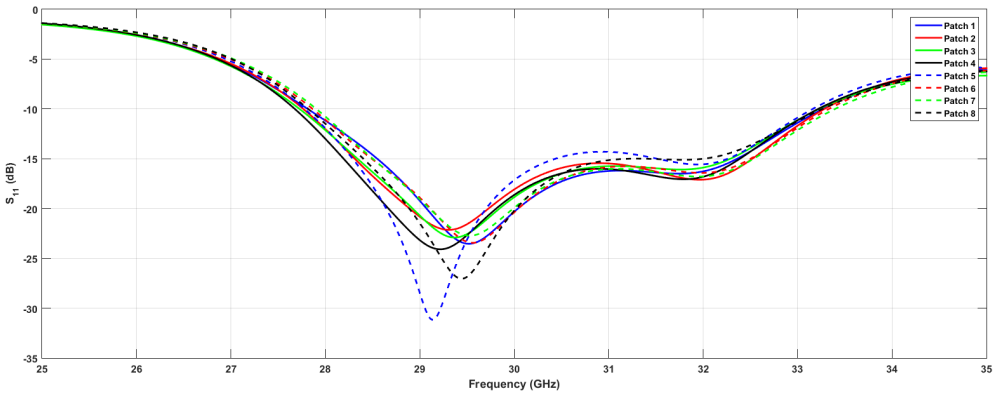

Figure 5.17: Simulated S_{11} of each element

The Fig.(5.18) exhibits the simulated axial ratio of the array, which qualifies the quality of the circular polarization, in this case over the frequency band. An acceptable circular polarization implies an axial ratio below 3 dB, so that the array presents a circular polarization bandwidth close to 800 MHz.

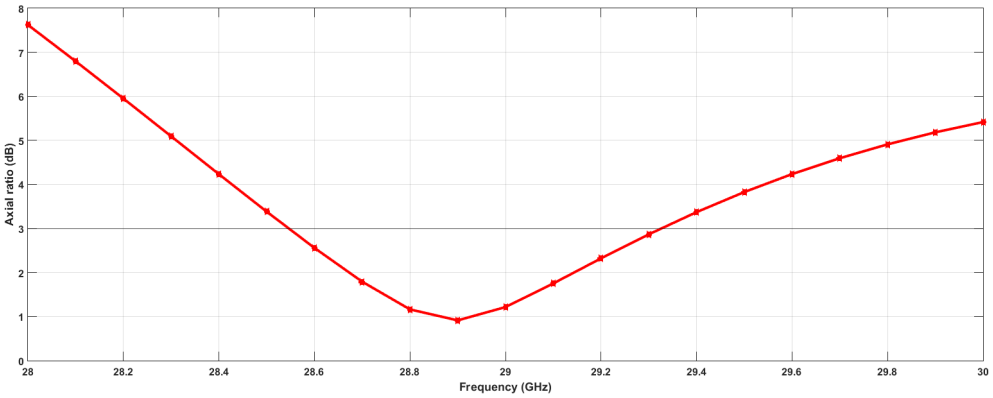

Figure 5.18: Axial ratio of the antenna array

The simulated radiation pattern of the antenna array is presented in the Fig.(5.19), in terms of left and right components of the electric field, in both main planes. As expected, the antenna operates correctly only for left-hand circular polarization, as at boresight the rejection of the right-hand component is higher than 22 dB. In the plane $\phi = 0^o$, the antenna shows an HPBW around 35^o, while in the plane $\phi = 90^o$, the HPBW is 18^o.

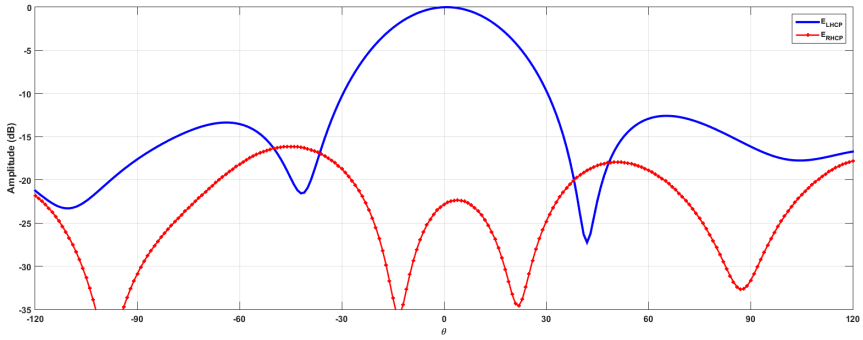

(a) Plane $\phi = 0^{o}$

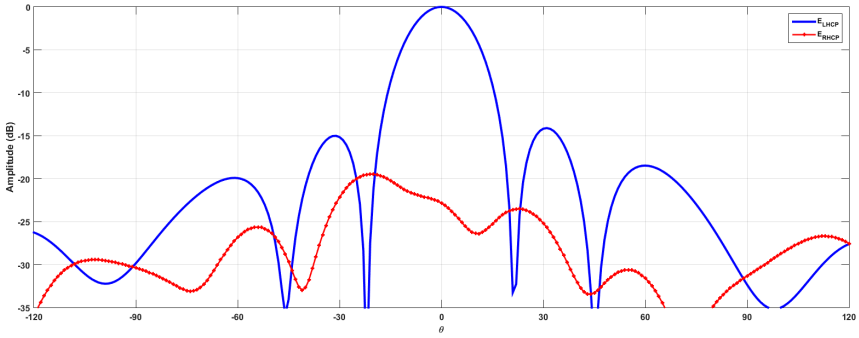

(b) Plane $\phi = 90^{o}$

Figure 5.19: Radiation pattern of the antenna array

Once characterized the 2×4 array module, using a potentiality provided by the CST MWS simulator tool "Farfield Calculation of Antenna Arrays" [48], which using as element factor the radiation pattern of the simulated 2×4 array structure, estimates the radiation pattern of an array $X \times Y$, (or in this case $N \times M$), also inserting the distances between elements in each direction and the feeding.

Four different 2×4 array modules were simulated with distances between elements of 0.65λ, 0.7λ, 0.75λ and 0.8λ respectively. Using each of the obtained radiation patterns, and using the CST tool, the number of elements in each direction $N \times M$ that would enable a radiation pattern with HPBW of 0.2^{o}, as intended by the project, was searched for. These results are summarized in the Table (5.6). The dimensions $L_g \times W_g$ of the 4 arrays are also provided in the Table (5.6), as well as the predicted global dimension of the array for the satellite, by using the number of elements estimated in each direction.

Table 5.6: Variation of the number of 2×4 array modules predicted, and its global dimensions, for the satellite array, with the distance between elements

d	$L_g \times W_g$ (mm^2)	$N \times M$	N^{o} *modules*	*Global Dimensions* (m^2)
0.65λ	13.45×26.90	156×78	12168	2.10×2.10
0.70λ	14.48×28.97	146×73	10658	2.11×2.11
0.75λ	15.52×31.03	136×68	9248	2.11×2.11
0.80λ	16.55×33.10	128×64	8192	2.12×2.12

As can be seen from Table (5.6), it is estimated an antenna for the satellite with global dimensions around $2 \times 2\,\mathrm{m}^2$. In the procedure of selection of the final structure to be used, it should be an agreement between the total number of modules and the respective size of each module, as well as some possible benefits or disadvantages that each module can provide.

The Fig.(5.20) shows the simulated radiation pattern using the simulator tool, achieved using a planar structure of 146×73 modules, with a distance between elements of $d = 0.7\lambda$. Each module corresponds to the planar 2×4 structure present in Fig.(5.16c) whose radiation pattern is given in Fig.(5.19). Using this arrangement, a HPBW of 0.2^o is obtained.

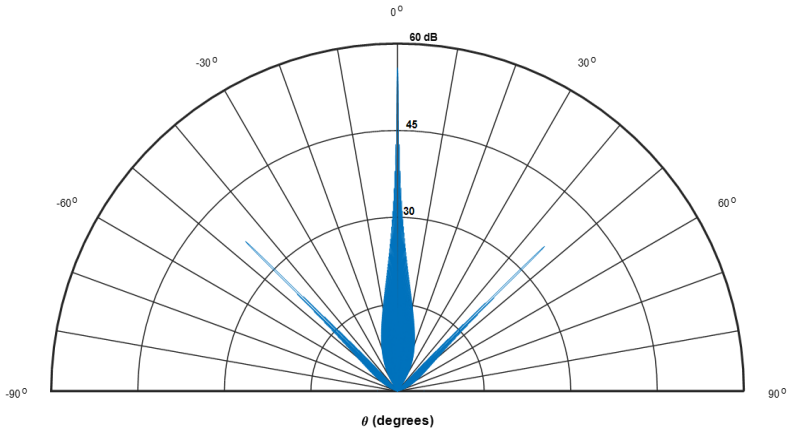

Figure 5.20: Radiation pattern using a large array of $M \times N$ antenna modules ($d = 0.70\lambda$) predicted using CST tools

The following step in the design of the antenna array is the inclusion of connectors. As shown in Fig.(5.21), a careful adjustment must be given to the phase of each element since the top and bottom elements have a phase difference of 180^o. The connectors drawn in Fig.(5.21) are compatible with SMP technology, which in turn are suitable to the used at high frequencies and have very small dimensions, suitable with the dimensions of the array.

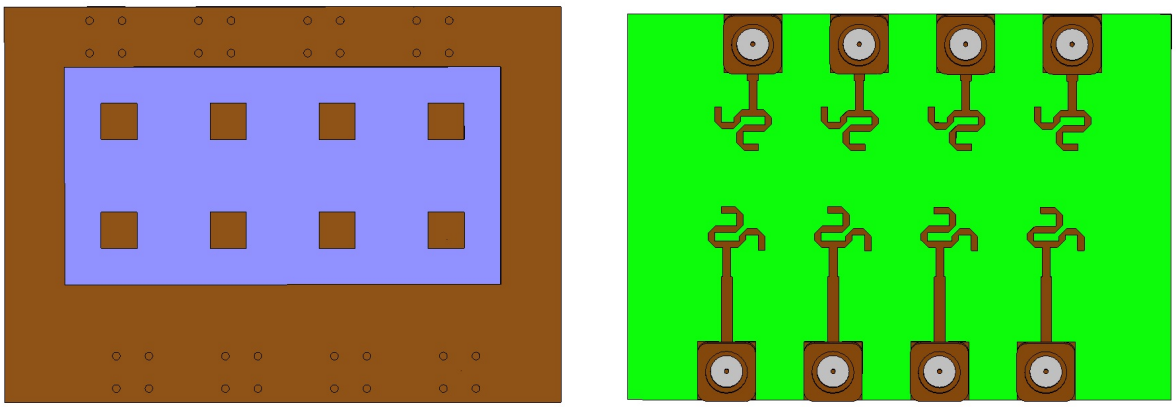

(a) Top view (b) Bottom view

Figure 5.21: Dual-feed microstrip antenna array structure for fabrication and test, using SMP connectors

The array is awaiting for fabrication and characterization by measurements, to implement any necessary adjustments.

5.7 Concluding Remarks

In this chapter were studied and implemented a set of DOA and beamforming algorithms. Furthermore, an analysis of each algorithm were carried out, allowing to understand and consolidate the differences between the various algorithms.

Regarding the DOA algorithms, both have good estimates in all the simulations performed. It was possible to conclude the reason why the MUSIC algorithm has much larger runtimes and estimation errors, this is due to the grid in which the algorithm is applied. However, it was also concluded that it is a simpler algorithm to implement compared to the ESPRIT.

In terms of beamforming algorithms, four algorithms have been implemented and tested and the main notes retained are that all of them present good estimations of weights and the radiation patterns obtained point to the desired direction. It is also possible to remark the reduction of the runtime of the algorithms with increase of SNR.

Finally, the contribution for ongoing research project is presented, in which the design of a modular 2×4 planar antenna array is developed, and which is going to be part of a larger array for satellite, using beamforming. The array has dual feed by coupling, allowing to achieve circular polarization, and shows promising simulated results. A study was also carried out that allowed to realize the number of modules necessary to meet the project requirements, and its variation with the distance between array elements.

Chapter 6

Conclusions and Future Work

This PhD thesis was devoted essentially to work with nonuniform techniques applied to planar antenna arrays in order to comply with a given set of specific requirements of different applications of wireless communications. It should be noted that all the developed antennas were subject to a scrutiny of the scientific community, with their revisions, through published papers in relevant journals and international conferences.

In this sense, is highlighted the high level of cooperation with companies, their practical needs, and the applicability of most of the presented arrays in areas with great relevance and interest for research in which these works are inserted, such as the vehicular communications, Wi-Fi in densely populated spaces, and smart antennas.

With respect to the topic of vehicular communications, a number of antennas for both the elements that belong to a DSRC system (OBU and RSU) were developed in compliance with the requirements that rule these communications. The developed antennas consist of printed antennas on a dielectric substrate, due to the important features they enable to the system in terms of light weight, low volume, reduced manufacturing cost, and also the compatibility with microwave circuits.

For the OBU module, three different versions of a printed monopole antenna were presented with the aim of enabling the best V2V and V2I communication, operating in all the DSRC bands.

Starting with a linear monopole, it presents an omnidirectional radiation, the known *donut*, with a simulated 4 GHz bandwidth. However, since it has linear polarization and the RSU uses circular polarization, there is a 3 dB loss in the communication. Given this result and attempting to overcome these losses in the communication, another printed monopole with a structure that allows for circular polarization was designed, keeping the omnidirectional radiation characteristic. This property was obtained by detaching simulated axial ratio bandwidth about 900 MHz. However, regarding to the radiation pattern, it was concluded that the sense of circular polarization was left (LHCP) to one side of the radiation pattern on the road plane, and right (RHCP) on the opposite side. This solution was considered unsuitable because it prevents the communication to one side. The last solution presented consists of a structure using the previous described monopole, as well as an absorbent material board, allowing to take the best of each structure (the LHCP radiation part) while the absorbent blocks the unwanted radiation (RHCP), enabling to obtain an omnidirectional LHCP radiation pattern. This solution was verified by simulation, but still needs the practical confirmation, by characterizing

a ferrite board and applying it to a prototype.

Regarding the RSU module, a group of nonuniform antenna arrays were developed, both for transmission and for receiving part. The first approach designed to TX was a 2×4 array of microstrip patches in which was applied the sequential rotation technique for circular polarization generation. This array has about 300 MHz of LHCP bandwidth, complying with DSRC standards regarding to the beamwidths, only with a small limitation on the measured SLL. The array was tested in a practical toll system on the road, and a set of practical characteristics were reported as feedback, which could be improved to ensure a better communication, particularly in terms of the beamwidth at 15 dB below the maximum.

A new 12-elements nonuniform planar array was developed using a more complex structure to meet to the DSRC standards as well as the reported practical issues, also improving the SLL. Its structure was properly described, theoretically analysed and proved with simulations. The unusual adopted structure, that removes the four corner elements in a 4×4 array using nonuniform excitation, enables a vast number of benefits in the array design, which has also led to be applied to other array designs. The increase of free space in the board which enables the design of the AFN in the plane of antenna elements by minimizing its interference with the radiation, the reduction of the number of elements to feed and the simplification of the AFN were important achievements. This array presents as main characteristics the wide operating bandwidth, exceeding 1 GHz, covering the DSRC bands, and the design of the AFN in the plane of the array elements, allowing a single dielectric layer structure, which greatly reduces the manufacturing costs.

A nonuniform array of five elements devoted to the receiving part was designed, with features that fit to the DSRC requirements, and allowing to obtain a smaller size array (than the designed for TX), enabling a more compact RSU system, but keeping its functionality intact. It was also developed a nonuniform planar array of 18 elements for the new approach presented, which consists in placing toll gates on access roads, simplifying the whole system. In this case, the new developed antenna presents as main new characteristics the negligible SLL and radiation pattern with a wide main lobe beamwidth with an almost uniform amplitude, adjusted to the new application.

Regarding the application of wireless networks in densely populated sports arenas, two antenna arrays were developed for both Wi-Fi bands, at 2.4 GHz and 5.2 GHz. These arrays will be part of an AP that covers a particular area of the stadium. The two arrays are identical to each other, changing mainly in their dimensions. The structure consists of a nonuniform planar array of 12 elements, similar to the structure shown for the array of 12 elements designed for RSU-TX. However, in terms of feeding, it is modified to a power distribution based on a Dolph-Chebyshev polynomials. To promote mass production, since a huge number of sectors (and antennas) are necessary to entirely cover a stadium, these arrays had to be designed using low cost dielectric materials, and the cheapest is the FR-4. It was crucial to desensitize the FR-4 due to its variations, by inserting an air layer between the FR-4 and the ground plane. Both antennas have good results despite some small deviations in the 5.2 GHz array, which I think are due to the quality of its manufacture. However, both arrays fulfill the constraints applied, showing a directive radiation pattern, as intended, with reduced sidelobes, a good quality of linear polarization, and an operation bandwidth which is much wider than the respective Wi-Fi bands.

In the context of adaptive antennas, a number of DOA and beamforming algorithms applied to planar arrays were studied, implemented, and applied to a group of different scenarios in order to evaluate their comparative performance between the various algorithms. In terms

of DOA algorithms, the main conclusions that can be taken are the simplicity in terms of implementation of the MUSIC algorithm compared to ESPRIT, although in terms of runtime, MUSIC is much heavier than the ESPRIT. In terms of estimation errors, the MUSIC depends on the grid in which the algorithm is evaluated. In this algorithm, a trade-off between estimation error and runtime must be taken, since a smaller estimation errors involves evaluating the MUSIC function in a huge number of points, which leads, naturally, to higher runtimes. In terms of beamforming algorithms, they all have good estimates of weights and their runtimes decrease with increasing of SNR. The application of the estimated weights to a simulated array allows to conclude, visually in terms of 3D radiation patterns, that the direction to which the array is steered is the desired local.

The participation in an ongoing research project was also presented, with the design of a modular 2×4 array, for the Ka band (freq. 29 GHz) using circularly polarized microstrip elements, through dual feed by aperture coupling. A study was also carried out in order to comprehend the number (estimated) of modules needed to fulfill with the requirements of the radiation pattern for the satellite arm. This number of modules depends, of course, on the radiation pattern of the basic module, which in turn depends on the distance between the elements of the module. This parameter must be decided according to the project's priorities.

In terms of future work, there is always room for improvement, in order to achieve better and more accurate results. Concerning to the antenna arrays designed for vehicular applications, the manufacture by specialized companies of the presented monopoles, also due to their reduced dimensions, allows for more reliable prototypes and certainly better measured results. Furthermore, and as already mentioned, the practical implementation and test of the monopole structure using an absorbent material obtained by simulation will be important. This implies to use an already characterized ferrite material or characterize one. This solution, if predicted results are verified, allows to obtain a LHCP omnidirectional radiation pattern, which will certainly be a major breakthrough in the DSRC communications, specifically in the OBU module. Also in the array of 18 elements for the access lane of highway, it shows a measured frequency shift so that a better characterization of substrate used and a more reliable manufacturing can be carried out.

In terms of Wi-Fi communications in sports stadiums, the fabrication of the designed array to 5.2 GHz by a suitable company, as was done in the array at 2.4 GHz, and using a better characterized material (simulated), closer to the real value of the FR-4, can lead to better results in terms of central frequency of operation. However, in these arrays which use an air layer, the bandwidth and the stability of the parameter to variations is fairly improved.

In terms of adaptive antennas algorithms, it is possible to extend the study to other DOA and beamforming algorithms, using larger antenna arrays or with other more complex array structures, and by using other scenarios.

Also, I have expectations about the successful conclusion of the research project BEACON, and its knowledge will allow to propose the application of photonic phase shifter in the design of a feed network with the aim to develop a smart antenna using fully electronic beamforming.

References

[1] C. A. Balanis, *Antenna theory: analysis and design*, vol. 1. John Wiley & Sons, 2005.

[2] J. Kraus, *Antennas*. Electrical Engineering Series, McGraw-Hill, 1988.

[3] T. A. Milligan, *Properties of Antennas*, pp. 1–41. John Wiley & Sons, Inc., 2005.

[4] Y. Lo, *Antenna Handbook VOLUME I: Antenna Fundamentals and Mathematical Techniques*. Springer US, 1993.

[5] "Ieee standard definitions of terms for antennas," *IEEE Std 145-1993*, pp. 1–32, July 1993.

[6] J. Huang, *Microstrip Antennas: Analysis, Design, and Application*, pp. 157–200. John Wiley & Sons, Inc., 2007.

[7] R. Garg, *Microstrip Antenna Design Handbook*. Antennas and Propagation Library, Artech House, 2001.

[8] Y. Lo, *Antenna Handbook VOLUME II: Antenna Theory*. Springer US, 1993.

[9] A. Derneryd, "Linearly polarized microstrip antennas," *IEEE Transactions on Antennas and Propagation*, vol. 24, pp. 846–851, Nov 1976.

[10] R. L. Haupt, *Linear and Planar Array Factor Synthesis*, pp. 115–215. John Wiley & Sons, Inc., 2010.

[11] G. V. Tsoulos and C. G. Christodoulou, *Arrays and Smart Antennas*, pp. 529–580. John Wiley & Sons, Inc., 2007.

[12] C. L. Dolph, "A current distribution for broadside arrays which optimizes the relationship between beam width and side-lobe level," *Proceedings of the IRE*, vol. 34, pp. 335–348, June 1946.

[13] T. A. Milligan, *Aperture Distributions and Array Synthesis*, pp. 136–216. John Wiley & Sons, Inc., 2005.

[14] R. C. Hansen, *Linear Array Pattern Synthesis*, pp. 49–107. John Wiley & Sons, Inc., 2009.

[15] R. C. Hansen, "Array pattern control and synthesis," *Proceedings of the IEEE*, vol. 80, pp. 141–151, Jan 1992.

[16] J. Huang, "A technique for an array to generate circular polarization with linearly polarized elements," *IEEE Transactions on Antennas and Propagation*, vol. 34, pp. 1113–1124, Sep 1986.

[17] G. Kumar and K. Ray, *Broadband Microstrip Antennas*. Artech House antennas and propagation library, Artech House, 2003.

[18] C. Cseh, "Architecture of the dedicated short-range communications (dsrc) protocol," vol. 3, pp. 2095–2099 vol.3, May 1998.

[19] Y. J. Li, *An Overview of the DSRC/WAVE Technology*, pp. 544–558. Berlin, Heidelberg: Springer Berlin Heidelberg, 2012.

[20] IEEE802.11P, "Ieee standard for information technology– local and metropolitan area networks– specific requirements– part 11: Wireless lan medium access control (mac) and physical layer (phy) specifications amendment 6: Wireless access in vehicular environments," 2010.

[21] ETSI-ES202-663, "Intelligent transport systems (its); european profile standard for the physical and medium access control layer of intelligent transport systems operating in the 5 ghz frequency band," *European Telecommunications Standards Institute*, 2010.

[22] ETSI-ES302-571, "Intelligent transport systems (its); radiocommunications equipment operating in the 5 855 mhz to 5 925 mhz frequency band; harmonized en covering the essential requirements of article 3.2 of the r&tte directive," *European Telecommunications Standards Institute*, 2013.

[23] EN12253, "Road transport and traffic telematics. dedicated short-range communication. physical layer using microwave at 5.8 ghz," *Comité Européen de Normalisation*, July 2004.

[24] C. Y. D. Sim and B. H. Yang, "A single layer dual-band cp microstrip antenna for gps and dsrc applications," *Journal of Electromagnetic Waves and Applications*, vol. 22, no. 4, pp. 529–539, 2008.

[25] C.-W. Su, C.-M. Su, and K.-L. Wong, "Compact dual-band circularly polarized antenna for gps/etc operation on vehicles," *Microwave and Optical Technology Letters*, vol. 40, no. 6, pp. 509–511, 2004.

[26] A. Malarky, G. Z. Rafi, S. Safavi-Naeini, and L. Delgrossi, "A planar dual band gps and dsrc antenna for road vehicles," *2007 IEEE 66th Vehicular Technology Conference*, pp. 2096–2100, Sept 2007.

[27] T. Fujimoto and K. Tanaka, "Stacked rectangular microstrip antenna with a shorting plate for dual band (vics/etc) operation in its," *IEICE Transactions*, vol. 90-B, pp. 3307–3310, 2007.

[28] H. Aissat, L. Cirio, M. Grzeskowiak, J. M. Laheurte, and O. Picon, "Reconfigurable circularly polarized antenna for short-range communication systems," *IEEE Transactions on Microwave Theory and Techniques*, vol. 54, pp. 2856–2863, June 2006.

[29] S. Zhang, Y. Zhuang, and S. Zhu, "Slot-coupled circularly polarized square patch antenna for electronic toll collection system," *Microwave and Millimeter Wave Technology, 2008. ICMMT 2008. International Conference on*, vol. 3, pp. 1210–1213, April 2008.

[30] D. Megnet and H. Mathis, "Circular polarized patch antenna for 5.8 ghz dedicated short-range communication," *Microwave Conference, 2009. EuMC 2009. European*, pp. 638–641, Sept 2009.

[31] Y. Xia and J. Luo, "Rhcp patch antenna for automotive dsrc system," *2010 6th International Conference on Wireless Communications Networking and Mobile Computing (WiCOM)*, pp. 1–3, Sept 2010.

[32] K. P. Ray, P. V. Anob, R. Kapur, and G. Kumar, "Broadband planar rectangular monopole antennas," *Microwave and Optical Technology Letters*, vol. 28, no. 1, pp. 55–59, 2001.

[33] K. P. Ray, "Design aspects of printed monopole antennas for ultra-wide band applications," *International Journal of Antennas and Propagation*, pp. 1–8, Jan 2008.

[34] M. Ojaroudi, C. Ghobadi, and J. Nourinia, "Small square monopole antenna with inverted t-shaped notch in the ground plane for uwb application," *IEEE Antennas and Wireless Propagation Letters*, vol. 8, pp. 728–731, 2009.

[35] K. P. Ray, Y. Ranga, and P. Gabhale, "Printed square monopole antenna with semi-circular base for ultra-wide bandwidth," *Electronics Letters*, vol. 43, pp. 13–14, March 2007.

[36] W. Wang, W. Hong, Z. Kuai, and J. Wu, "Printed omni-directional wide-band monopole antenna with compact size," vol. 1, pp. 1–4, Sept 2010.

[37] AnsoftCorporation, "user's guide – high frequency structure simulator," *Edition: REV 1.0, Software Version 10.0*, June 2005.

[38] J. W. Wu, J. Y. Ke, C. F. Jou, and C. J. Wang, "Microstrip-fed broadband circularly polarised monopole antenna," *IET Microwaves, Antennas Propagation*, vol. 4, pp. 518–525, April 2010.

[39] A. Ghobadi and M. Dehmollaian, "A printed circularly polarized y-shaped monopole antenna," *IEEE Antennas and Wireless Propagation Letters*, vol. 11, pp. 22–25, 2012.

[40] W. Grabow, T. Wixforth, and H. Ziegler, "5.8 ghz phased array antenna for electronic toll collection in road traffic applications," vol. 1, pp. 325–328 vol.1, June 1996.

[41] G. Villino, C. Passmann, D. Mansen, C. Brenzel, and T. Wixforth, "Integrated 5.8 ghz phased array antenna, for electronic toll collection," vol. 3, pp. 1215–1218 vol.3, June 1998.

[42] Y. Kim, C. Song, I. Koo, H. Choi, and S. Lee, "Design of a double-looped monopole array antenna for a dsrc system roadside base station," *Microwave and Optical Technology Letters*, vol. 37, no. 1, pp. 74–77, 2003.

[43] B. R. Franciscatto, T. P. Vuong, T. T. Trang, and C. Defay, "Microstrip-fed quasi-yagi antenna array for a different dsrc system," pp. 1–5, June 2012.

[44] B. R. Franciscatto, A. C. Souza, C. Defay, T. T. Trang, and T. P. Vuong, "High gain microstrip patch antenna array using multiple superstrate layers for dsrc applications," pp. 736–739, Sept 2012.

[45] M. T. Le, Q. C. Nguyen, T. P. Vuong, and C. Defay, "Design of a high gain antenna at 5.8ghz using a new metamaterials structure," pp. 411–416, Aug 2012.

[46] B. S.-H. Choi, H.-C. Lee, and K.-S. Kwak, "Circularly polarized h-shaped microstrip-array antenna with a t-slot for dsrc system roadside equipment," *Microwave and Optical Technology Letters*, vol. 51, no. 6, pp. 1545–1548, 2009.

[47] J. Yoon and K. Kwak, "Fabrication and measurement of a microstrip-array antenna for the electronic toll collection system (etcs)," *Microwave and Optical Technology Letters*, vol. 36, no. 2, pp. 77–79, 2003.

[48] CST, "Cst microwave studio," *3D EM Simulation Software. Computer Simulation Technology, Framingham, MA, [Online]. Available: http://www.cst.com.*

[49] E. J. Wilkinson, "An n-way hybrid power divider," *IRE Transactions on Microwave Theory and Techniques*, vol. 8, pp. 116–118, January 1960.

[50] L. Parad and R. Moynihan, "Split-tee power divider," *Microwave Theory and Techniques, IEEE Transactions on*, vol. 13, pp. 91–95, Jan 1965.

[51] B.-H. Z. Dau-Chyrh Chang and J.-C. Liu, "High performance antenna array with patch antenna elements," in *PIERS Proceedings,Xi'an, China,*, pp. 710–713, March 2010.

[52] N. Li, W. Chen, and Z. Feng, "A switched sector beam planar antenna," in *Antennas and Propagation Society International Symposium, 2005 IEEE*, vol. 1A, pp. 230–233 Vol. 1A, July 2005.

[53] W. S. Kaswiati and J. Suryana, "Design and realization of planar bow-tie dipole array antenna with dual-polarization at 2.4 ghz frequency for wi-fi access point application," in *Telecommunication Systems, Services, and Applications (TSSA), 2012 7th International Conference on*, pp. 218–222, Oct 2012.

[54] K. K. Chan, H. C. Chin, W. L. Lim, and H. K. Oh, "A very low profile and high efficiency antenna array for wlan at s-band," in *2008 Asia-Pacific Microwave Conference*, pp. 1–4, Dec 2008.

[55] M. Bemani and S. Nikmehr, "A novel wide-band microstrip yagi-uda array antenna for wlan applications," *Progress In Electromagnetics Research B*, vol. 16, no. 1, pp. 389–406, 2009.

[56] O. K. K. Sarkodie, "A wideband rectangular-slot microstrip array antenna for wireless applications," in *2nd Intl' Conference on Advances in Engineering Sciences and Applied Mathematics (ICAESAM'2014)*, pp. 80–83, May 4-5 2014.

[57] Y.-Z. Yin, J.-P. Ma, Y.-J. Zhao, H.-L. Zheng, and Y.-M. Guo, "Wideband printed dipole antenna for wireless lan," in *Antennas and Propagation Society International Symposium, 2005 IEEE*, vol. 2B, pp. 568–571 vol. 2B, July 2005.

[58] Y. h. He and J. s. Li, "A novel multi-band array antenna for wlan/wimax applications," in *Microwave, Antenna, Propagation, and EMC Technologies for Wireless Communications (MAPE), 2011 IEEE 4th International Symposium on*, pp. 246–248, Nov 2011.

[59] W. K. Toh, X. Qing, and Z. N. Chen, "A planar dualband antenna array," *IEEE Transactions on Antennas and Propagation*, vol. 59, pp. 833–838, March 2011.

[60] M. Sonkki, D. Pfeil, V. Hovinen, and K. R. Dandekar, "Wideband planar four-element linear antenna array," *IEEE Antennas and Wireless Propagation Letters*, vol. 13, pp. 1663–1666, 2014.

[61] K. S. Bialkowski and S. Zagriatski, "A dual band 2.4/5.2 ghz antenna including a radial line slot array and a patch," in *Antennas and Propagation Society International Symposium, 2004. IEEE*, vol. 3, pp. 3095–3098 Vol.3, June 2004.

[62] Y. J. Yoon and B. Kim, "A new formula for effective dielectric constant in multi-dielectric layer microstrip structure," in *Electrical Performance of Electronic Packaging, 2000, IEEE Conference on.*, pp. 163–167, 2000.

[63] C. Balanis and P. Ioannides, *Introduction to Smart Antennas*. Synthesis lectures on antennas, Morgan & Claypool Publishers, 2007.

[64] B. Widrow, P. E. Mantey, L. J. Griffiths, and B. B. Goode, "Adaptive antenna systems," *Proceedings of the IEEE*, vol. 55, pp. 2143–2159, Dec 1967.

[65] S.-J. Yu and J.-H. Lee, "Design of two-dimensional rectangular array beamformers with partial adaptivity," *IEEE Transactions on Antennas and Propagation*, vol. 45, pp. 157–167, Jan 1997.

[66] J.-H. Lee and Y.-H. Lee, "Two-dimensional adaptive array beamforming with multiple beam constraints using a generalized sidelobe canceller," *IEEE Transactions on Signal Processing*, vol. 53, pp. 3517–3529, Sept 2005.

[67] L. C. Godara, "Applications of antenna arrays to mobile communications. i. performance improvement, feasibility, and system considerations," *Proceedings of the IEEE*, vol. 85, pp. 1031–1060, Jul 1997.

[68] R. Li, C. Rao, L. Dai, and S. Zhao, "Adaptive-adaptive beamforming algorithm of planar array based on one-dimensional auxiliary beam," in *Image and Signal Processing (CISP), 2010 3rd International Congress on*, vol. 7, pp. 3300–3303, Oct 2010.

[69] MATLAB, *version 7.10.0 (R2010a)*. Natick, Massachusetts: The MathWorks Inc., 2010.

[70] J. Foutz, A. Spanias, and M. Banavar, *Narrowband Direction of Arrival Estimation for Antenna Arrays*. Synthesis Lectures on Antennas, Morgan & Claypool Publishers, 2008.

[71] L. C. Godara, "Application of antenna arrays to mobile communications. ii. beamforming and direction-of-arrival considerations," *Proceedings of the IEEE*, vol. 85, pp. 1195–1245, Aug 1997.

[72] R. Schmidt, "Multiple emitter location and signal parameter estimation," *IEEE Transactions on Antennas and Propagation*, vol. 34, pp. 276–280, Mar 1986.

[73] S. Sekizawa, "Estimation of arrival directions using music algorithm with a planar array," in *Universal Personal Communications, 1998. ICUPC '98. IEEE 1998 International Conference on*, vol. 1, pp. 555–559 vol.1, Oct 1998.

[74] K. V. Rangarao and S. Venkatanarasimhan, "gold-music: A variation on music to accurately determine peaks of the spectrum," *IEEE Transactions on Antennas and Propagation*, vol. 61, pp. 2263–2268, April 2013.

[75] C. C. Yeh, J. H. Lee, and Y. M. Chen, "Estimating two-dimensional angles of arrival in coherent source environment," *IEEE Transactions on Acoustics, Speech, and Signal Processing*, vol. 37, pp. 153–155, Jan 1989.

[76] Y.-M. Chen, "On spatial smoothing for two-dimensional direction-of-arrival estimation of coherent signals," *IEEE Transactions on Signal Processing*, vol. 45, pp. 1689–1696, Jul 1997.

[77] Z. Chen, G. Gokeda, and Y. Yu, *Introduction to Direction-of-Arrival Estimation*. Artech House signal processing library, Artech House, 2010.

[78] M. Haardt, M. D. Zoltowski, C. P. Mathews, and J. Nossek, "2d unitary esprit for efficient 2d parameter estimation," in *Acoustics, Speech, and Signal Processing, 1995. ICASSP-95., 1995 International Conference on*, vol. 3, pp. 2096–2099 vol.3, May 1995.

[79] M. D. Zoltowski, M. Haardt, and C. P. Mathews, "Closed-form 2-d angle estimation with rectangular arrays in element space or beamspace via unitary esprit," *IEEE Transactions on Signal Processing*, vol. 44, pp. 316–328, Feb 1996.

[80] Y. Y. Wang and W. W. Chen, "A low complexity 2d-doa estimation algorithm using signal decomposition," in *High Speed Intelligent Communication Forum (HSIC), 2012 4th International*, pp. 1–4, May 2012.

[81] J. Hui and Y. Gang, "An improved algorithm of esprit for signal doa estimation," in *Industrial Control and Electronics Engineering (ICICEE), 2012 International Conference on*, pp. 317–320, Aug 2012.

[82] B. D. V. Veen and K. M. Buckley, "Beamforming: a versatile approach to spatial filtering," *IEEE ASSP Magazine*, vol. 5, pp. 4–24, April 1988.

[83] W. Liu and S. Weiss, *Wideband Beamforming: Concepts and Techniques*. Wireless Communications and Mobile Computing, Wiley, 2010.

[84] F. Huang, W. xing Sheng, and X. feng Ma, "Efficient parallel adaptive beamforming algorithm for planar array system," in *Antennas, Propagation and EM Theory, 2008. ISAPE 2008. 8th International Symposium on*, pp. 282–285, Nov 2008.

[85] A. M. G. Guerreiro, A. D. D. Neto, and F. A. Lisboa, "Beamforming applied to an adaptive planar array," in *Radio and Wireless Conference, 1998. RAWCON 98. 1998 IEEE*, pp. 209–212, Aug 1998.

[86] S. Razia, T. Hossain, and M. A. Matin, "Performance analysis of adaptive beamforming algorithm for smart antenna system," in *Informatics, Electronics Vision (ICIEV), 2012 International Conference on*, pp. 946–949, May 2012.

[87] S. K. Imtiaj, I. S. Misra, and R. Biswas, "Performance comparison of different adaptive beamforming algorithm in smart antennas," in *Computers and Devices for Communication (CODEC), 2012 5th International Conference on*, pp. 1–4, Dec 2012.

[88] *Phase Shifters*, pp. 459–480. Berlin, Heidelberg: Springer Berlin Heidelberg, 2007.

[89] R. R. Romanofsky, "Array phase shifters: Theory and technology," in *NASA Glenn Research Center, Cleveland, OH, United States*, July 2007.

[90] *Circuit and System Applications of Tunable Ferroelectric Devices*. Springer London, 2009.

[91] M. Sazegar, Y. Zheng, H. Maune, C. Damm, X. Zhou, J. Binder, and R. Jakoby, "Low-cost phased-array antenna using compact tunable phase shifters based on ferroelectric ceramics," *IEEE Transactions on Microwave Theory and Techniques*, vol. 59, pp. 1265–1273, May 2011.

[92] R. Romanofsky, C. Mueller, and C. V. Chandrasekar, "Concept for a low cost, high efficiency precipitation radar system based on ferroelectric reflectarray antenna," in *2009 IEEE Radar Conference*, pp. 1–6, May 2009.

[93] M. Nikfalazar, M. Sazegar, A. Friederich, C. Kohler, Y. Zheng, A. Wiens, J. R. Binder, and R. Jakoby, "Inkjet printed bst thick-films for x-band phase shifter and phased array applications," in *Antenna Technology (iWAT), 2013 International Workshop on*, pp. 121–124, March 2013.

[94] O. Vendik, A. Vasiliev, and M. Parnes, "Low cost ferroelectric phase shifter for a higher microwave power level," in *Microwaves, Communications, Antennas and Electronics Systems, 2009. COMCAS 2009. IEEE International Conference on*, pp. 1–4, Nov 2009.

[95] T. Ji, H. Yoon, J. K. Abraham, and V. K. Varadan, "Ku-band antenna array feed distribution network with ferroelectric phase shifters on silicon," *IEEE Transactions on Microwave Theory and Techniques*, vol. 54, pp. 1131–1138, March 2006.

[96] V. K. Palukuru, "Electrically tunable microwave devices using bstltcc thick films," 2010.

[97] L. Zhuang, C. G. H. Roeloffzen, A. Meijerink, M. Burla, D. A. I. Marpaung, A. Leinse, M. Hoekman, R. G. Heideman, and W. van Etten, "Novel ring resonator-based integrated photonic beamformer for broadband phased array receive antennas;part ii: Experimental prototype," *Journal of Lightwave Technology*, vol. 28, pp. 19–31, Jan 2010.

[98] M. V. Drummond, P. P. Monteiro, and R. N. Nogueira, "Photonic true-time delay beamforming based on polarization-domain interferometers," *Journal of Lightwave Technology*, vol. 28, pp. 2492–2498, Sept 2010.

[99] A. Capozzoli, C. Curcio, and G. D'Elia, "A flexible integrated photonic true time delay phaser for phased array antennas," *Progress In Electromagnetics Research B*, vol. 38, pp. 261–279, 2012.

[100] L. Zhuang, D. Marpaung, M. Burla, C. Roeloffzen, W. Beeker, A. Leinse, and P. van Dijk, "Low-loss and programmable integrated photonic beamformer for electronically-steered broadband phased array antennas," in *IEEE Photonic Society 24th Annual Meeting*, pp. 137–138, Oct 2011.

[101] M. Himdi, J. P. Daniel, and C. Terret, "Transmission line analysis of aperture-coupled microstrip antenna," *Electronics Letters*, vol. 25, pp. 1229–1230, Aug 1989.